EXPERIMENTAL AND NUMERICAL EVALUATION OF CONTINUOUS COMPOSITE GIRDERS USING UHPC SLAB AT HOGGING MOMENT REGION

BY

NIZAR ABDUL-HAMID YOUSEF ASSI

A Dissertation Presented to the

DEANSHIP OF GRADUATE STUDIES

KING FAHD UNIVERSITY OF PETROLEUM & MINERALS

DHAHRAN, SAUDI ARABIA

In Partial Fulfillment of the

Requirements for the Degree of

DOCTOR OF PHILOSOPHY

In

CIVIL ENGINEERING

DECEMBER 2018

KING FAHD UNIVERSITY OF PETROLEUM & MINERALS

DHAHRAN- 31261, SAUDI ARABIA

DEANSHIP OF GRADUATE STUDIES

This dissertation, written by **NIZAR ABDUL-HAMID YOUSEF ASSI** under the direction of his thesis advisor and approved by his thesis committee, has been presented and accepted by the Dean of Graduate Studies, in partial fulfillment of the requirements for the degree of **DOCTOR OF PHILOSOPHY IN CIVIL ENGINEERING.**

Dr. Alfarabi M. Sharif
(Advisor)

Dr. Husain J. Al-Gahtani
(Member)

Dr. Ali Algadhib
(Member)

Dr. Shamsad Ahmad
(Member)

Dr. Salah U. Al-Dulaijan
(Member)

Dr. Salah U. Al-Dulaijan
Department Chairman

Dr. Salam A. Zummo
Dean of Graduate Studies

14/1/09
Date

Dedicated To

My Beloved Parents, Brothers and Sisters

My Holy Homeland Palestine

ACKNOWLEDGMENTS

All praise and thanks be to Allah for guiding me through my life especially in this dissertation. Thanks to Allah for the blessing of health, education and everything to complete this work.

I would like to express my deep gratitude and respect to my dear parents, brothers and sisters for their sincere prayers, encouragement, motivation and guidance in my life. Their continuous emotional and moral support helped me to complete my Ph.D. and made my happiness and success.

Also, I would like to thank KFUPM in particularly Civil Engineering Department for giving me the opportunity to complete my Ph.D. program. Thanks to the Deanship of Scientific Research for providing the financial support to complete the experimental work.

Foremost, I would like to thank my dissertation advisor Dr. Alfarabi Sharif for the guidance and insightful comments throughout my Ph.D. program. I have benefited a lot from his distinguished teaching and academic skills. Also, thanks to my thesis committee members, Dr. Husain Al-Gahtani, Dr. Ali Algadhib, Dr. Shamsad Ahmad and Dr. Salah Al-Dulaijan for their comments and guidance. In addition, special thanks to Dr. Mohammed Al-Osta for his help and support during my Ph.D. research work.

Finally, I would like to acknowledge my friends and everybody who helped me throughout my life.

TABLE OF CONTENTS

LIST OF TABLES

LIST OF FIGURES

LIST OF ABBREVIATIONS

NC	:	Normal Concrete
UHPC	:	Ultra-High Performance Concrete
FE	:	Finite Element
ASTM	:	American Society for Testing and Materials
AISC	:	American Institute of Steel Construction
LRFD	:	Load and Resistance Factor Design
LVDT	:	Linear Variable Displacement Transducer
CFRP	:	Carbon-Fiber Reinforced Polymer
f_c'	:	Concrete compressive strength at 28-days
f_r	:	Modulus of rupture for concrete
f_t	:	Tensile strength of UHPC
f_y	:	Yielding strength of steel
E	:	Modulus of elasticity
Q_n	:	Stud's shear strength
A_{sc}	:	Stud's cross sectional area
C	:	Compressive force

T	:	Tensile force
$T_{S.R}$	:	Tensile force in reinforcement steel
T_S	:	Tensile force in steel section
T_c	:	Tensile force in UHPC
P_u	:	Ultimate failure load
P_{cr}	:	Cracking load
P_y	:	Yielding load
M_{+ve}	:	Sagging moment
M_{-ve}	:	Hogging moment
M_p	:	Plastic moment capacity
M_{cr}	:	Cracking moment capacity
α	:	Ratio of sagging to hogging moment capacity
n	:	Modular ratio
I	:	Second moment of area or moment of inertia

ABSTRACT

Full Name : NIZAR ABDUL-HAMID YOUSEF ASSI

Thesis Title : Experimental and Numerical Evaluation of Continuous Composite Girders Using UHPC Slab at Hogging Moment Region

Major Field : Civil Engineering

Date of Degree : December 2018

The concrete slab at the hogging moment zone of continuous composite steel-concrete girders is subject to tension and consequently loses its contribution to the composite action. The American Institute of Steel Construction (AISC) code either ignores the contribution of concrete slab at hogging moment zone for continuous composite girders or considers the steel reinforcements of concrete slab to act compositely with the steel section. For both options of the AISC code, the section capacity at the hogging moment zone is greatly reduced.

The loss of composite action at the hogging moment zone for a continuous composite girder reduces the girder stiffness and strength. This work presents an experimental investigation of the use of an ultra-high performance concrete (UHPC) slab at the hogging moment zone and a normal concrete (NC) slab at the sagging moment zone. The testing was conducted to verify the level of loading at which composite action is maintained at the hogging moment zone. Four two-span continuous composite girders were tested. The thickness of the UHPC varied between a half and a full depth of slab. The degree of shear connection at the hogging moment zone varied between full and partial. The experimental results confirmed the effectiveness of the UHPC slab to enhance the girder stiffness and

maintain the composite action at the hogging moment zone at a load level much higher than the upper service load limit. To a lesser degree enhanced performance was also noted for the smaller thickness of the UHPC slab and partial shear connection at the hogging moment zone. Plastic analysis was conducted to evaluate the ultimate capacity of the girder which yielded a conservative estimation.

In addition, finite element (FE) modeling evaluated the girder performance numerically and yielded satisfactory results. The developed model was employed to conduct a parametric study to investigate the effects of the degree of shear connection, the thickness and length of UHPC slab at hogging moment zone on the behavior of the continuous composite girders. The results indicated that composite action at the hogging moment zone is maintained for the degree of shear connection taken as 50% of the full composite action and use of UHPC as half-depth of slab thickness and length of 20% of the span length. Besides, a simplified analytical approach was developed to evaluate the capacity of composite girders at service and ultimate stages. It yields a conservative prediction compared to the experimental and numerical approaches.

ABSTRACT (ARABIC)

الاسم الكامل : نزار عبد الحميد يوسف عاصي

عنوان الرسالة : دراسة تجريبية وعددية للكمرات المستمرة والمركبة باستخدام البلاطات الخرسانة فائقة الأداء في منطقة عزم الدوران السالب

التخصص : هندسة مدنية (إنشاءات)

تاريخ الدرجة العلمية : كانون الأول 2018 م

تكون البلاطة الخرسانية في منطقة عزم الدوران السالب في الكمرات المستمرة والمركبة من الخرسانة والمقطع الفولاذي تحت تأثير اجهادات الشد وبالتالي تفقد البلاطة الخرسانية مساهمتها في العمل كجزء من المقطع المركب. يتجاهل المعهد الأمريكي للإنشاءات الفولاذية (AISC) مساهمة البلاطة الخرسانية في منطقة عزم الدوران السالب في الكمرات المركبة والمستمرة أو يعتبر ان المقطع الفولاذي وحديد التسليح داخل البلاطة الخرسانية يعملان معاً بشكل مركب. لكلا الخيارين المقترحين من قِبل المعهد الأمريكي للإنشاءات الفولاذية، فإن قدرة تحمل المقطع المركب تنخفض إلى حد كبير في منطقة عزم الدوران السالب.

إن فقدان البلاطة الخرسانية لمساهمتها في منطقة عزم الدوران السالب في الكمرات المركبة والمستمرة يُقلل من صلابة وقوة الكمرات المركبة والمستمرة. يقدم هذا العمل بحثًا تجريبيًا عن استخدام البلاطة الخرسانية فائقة الأداء (UHPC) في منطقة عزم الدوران السالب والخرسانية العادية (NC) في منطقة عزم الدوران الموجب. تم إجراء الاختبار للتحقق من مدى مستوى التحميل الذي يتم فيه الحفاظ على دور المقطع المركب في منطقة عزم الدوران السالب. تم اختبار أربعة كمرات مركبة ومستمرة ذات بحرين فقط. تفاوت سمك الخرسانية فائقة الأداء (UHPC) بين نصف وعمق كامل للبلاطة. تفاوتت درجة الاتصال/الترابط ما بين البلاطة الخرسانية والمقطع الفولاذي في منطقة عزم الدوران السالب بين الاتصال الكامل والجزئي. أكدت النتائج التجريبية فعالية الخرسانية فائقة الأداء (UHPC) في تعزيز صلابة الكمرات المركبة والمستمرة والمحافظة على تحمل المقطع المركب في منطقة عزم الدوران السالب عند مستوى حمولة أعلى بكثير من الحد الأقصى لحمولة الخدمة. ولوحظ كذلك أداء مُحسَّن بدرجة أقل لسمك أصغر للبلاطة الخرسانية فائقة الأداء (UHPC) واتصال جزئي في منطقة عزم الدوران السالب. تم أيضا إجراء تحليل بلاستيكي لتقييم قدرة

تحمل الكمرات المركبة والمستمرة لحظة الانهيار. حيث وُجد أن التحليل البلاستيكي يُقلل من قدرة تحمل الكمرات المركبة والمستمرة.

علاوة على ذلك، تم عمل تقييم عددي لسلوك الكمرات المركبة والمستمرة باستخدام أحد البرامج المتوفرة لتحليل العناصر المحدودة (ABAQUS) وتم التحقق من صحة ودقة النتائج العددية بمقارنتها مع النتائج العملية، حيث اظهرت المقارنة مدى دقة التحليل العددي في التنبؤ بسلوك الكمرات المركبة والمستمرة. بالإضافة الى ذلك، تم إجراء دراسة بارا مترية لتقييم بشكل عميق مدى تأثير بعض المتغيرات على سلوك الكمرات المركبة والمستمرة. حيث تتضمن هذه المتغيرات المسافة بين مسامير القص، سماكة وطول البلاطة الخرسانة فائقة الأداء (UHPC) في منطقة عزم الدوران السالب. أشارت النتائج إلى أنه يتم المحافظة على اداء المقطع المركب في منطقة عزم الدوران السالب من خلال استخدام مسافة بين مسامير القص ما يعادل 50٪ من تلك المسافة للمقطع المركب بشكل كامل واستخدام الخرسانة فائقة الأداء (UHPC) بعمق يعادل نصف السمك الكامل للبلاطة وبطول يعادل 20% من طول البحر. وأخيرا، تم تطوير حل تحليلي لتقييم قوة تحمل الكمرات المركبة تحت تأثير الاحمال الخدماتية واحمال الانهيار.

CHAPTER ONE

INTRODUCTION

1.1 General

Composite steel-concrete construction has been extensively used in buildings and bridges in recent years to combine these two construction materials [1-4]. This construction scheme was developed since 1930s by utilizing the steel framing system in supporting cast-in-place slab. It was used by neglecting the connection between concrete slab and steel beam. With the advent of welding, shear connectors were used to connect the steel beam with cast-in-place concrete slab. The shear connector is the key component that assures shear connection between the steel girder and the concrete slab, which enables the composite action to contribute to the shear transfer and prevent uplift [5, 6]. Therefore, the shear connection can be obtained by reducing or preventing the relative displacement of the concrete and steel sections at their interfaces [7, 8].

The use of composite steel-concrete construction provides an efficient and cost-effective form of construction due to a reduction in member depth, savings in steel weight and its rapid construction process. In addition, it increases the floor stiffness allowing to an increase in the length of the span of structural members. Therefore, composite construction

became more practical and economical to be utilized in building construction since early 1960s.

For continuous composite steel-concrete girders, optimal use of the composite action will be at the sagging moment where the concrete and the steel are under compression and tension, respectively. However, at the hogging moment zone, the concrete slab will be under tension and consequently loses its contribution to the composite action leading to a reduction in stiffness and strength. Therefore, standard codes such as the American Institute of Steel Construction (AISC) [9] ignores the contribution of a normal concrete (NC) slab in the evaluation of the moment capacity at the hogging moment zones where NC is under tension, or considers only the steel reinforcements of concrete slab to act compositely with steel section. For both options, the section capacity at the hogging moment zone greatly reduced.

The aim of this work is to investigate the use of ultra-high performance concrete (UHPC) [10] slab at hogging moment zone for the two-span continuous composite girders to maintain the composite action at service load. The new construction scheme will maintain the composite action at the hogging moment zone and consequently enhances the elastic stiffness and strength of the continuous composite girders. This work will be performed in three different stages, including the experimental, numerical and the simplified analytical approaches.

1.2 Shear Connection

The longitudinal shear connection between the steel section and the concrete slab is provided by shear connectors, which normally take the form of headed studs welded to the top of the steel section. The degree of shear connection is mainly characterized by the number of shear connectors required to transfer the compressive force developed in the slab to the steel beam. With different degrees of shear connection, composite action can be either partial or full composite action [11-15]. Thus, full composite action occurs when the strength of shear connectors is greater than the minimum between the maximum force developed either in concrete (C_{max}) or steel (T_{max}). In addition, partial composite action occurs when the strength of shear connection does not fulfill the previous criterion.

The nominal shear transfer strength at maximum moment cannot exceed the maximum force developed either in concrete (C_{max}) or steel (T_{max}). The forces (C_{max}) and (T_{max}) are evaluated using Eq. (1.1) & Eq. (1.2), respectively.

$$C_{max} = 0.85\, f'_c b_e\, t_s \tag{1.1}$$

$$T_{max} = A_s\, f_y \tag{1.2}$$

The total number (N) of shear connectors required between the points of maximum and zero moment to transfer the minimum force between (C_{max}) and (T_{max}) is evaluated utilizing Eq. (1.3). These studs are uniformly distributed between the points of maximum and zero moment.

$$N = \frac{C_{max}}{Q_n} \quad or \quad \frac{T_{max}}{Q_n}, \quad whichever\ is\ smaller \tag{1.3}$$

where f'_c = the compressive strength of concrete at 28-days;

b_e = the effective width of concrete slab;

t_s = the thickness of slab;

A_s = the cross sectional area of the structural steel section;

f_y = the yielding strength of structural steel; and

Q_n = the strength of a shear connector.

According to AISC specifications [9], the capacity of a shear connector (Q_n) embedded in NC slab is evaluated using Eq. (1.4). This equation predicts the capacity of the stud as long as bearing failure in NC slab is the limit state of the stud capacity.

$$Q_n = 0.5\, A_{sc}\sqrt{f_c'\, E_c} \qquad (1.4)$$

where A_{sc} = the cross sectional area of a shear stud;

f_c' = the compressive strength of concrete at 28-days; and

E_c = the modulus of elasticity of concrete.

For the studs embedded in UHPC slab, shear failure in the welding material becomes more critical than bearing failure in UHPC slab, and consequently Eq. (1.4) overestimates stud capacity. Therefore, the capacity of a shear connector can be evaluated experimentally using push-out test according to Eurocode-4 [16]. The details of push-out test are provided in section 4.2.3.

In continuous composite steel-concrete girders, NC slab at hogging moment zone is neglected since it resists no tensile stress and consequently only the slab reinforcements

act compositely with steel beam. Therefore, the maximum longitudinal shear transfer is given by Eq. (1.5).

$$T_{max} = A_{S.R} * F_{y\ S.R} \quad (1.5)$$

where $A_{S.R}$ = the total area of reinforcement steel at hogging moment zone; and

$F_{y.S.R}$ = the yielding strength of reinforcement steel.

When UHPC is utilized to maintain the composite action at hogging moment zone, the developed tensile stress in UHPC slab will also be transferred by the shear connectors. Therefore, the maximum longitudinal shear transfer will be evaluated, as given by Eq. (1.6).

$$T_{max} = A_{S.R}\ F_{y\ S.R} + A_{UHPC}\ * F_{UHPC} \quad (1.6)$$

Where A_{UHPC} = the cross sectional area of UHPC at the hogging moment zone; and

F_{UHPC} = the tensile strength of UHPC.

In this work, shear connection was designed to develop full composite action at hogging and sagging moment zones. Section 3.3 demonstrates the details of the design of shear connection.

1.3 Need for the Research

The use of composite construction provides an efficient and cost-effective form of construction. It reduces the construction cost, weight of materials and depth of the members. In simple spans or sagging moment zones, the composite action between the

steel and concrete is optimal because the concrete slab is under compression, where the compressive capacity of the concrete is high. This optimal use of composite action significantly enhances the stiffness and the strength of composite girders. However, for hogging moment zones of continuous composite girders, the concrete slab is under tension and consequently loses its contribution to the composite action leading to a great reduction in stiffness and strength of composite girders. Maintaining the composite action at the hogging moment zones leads to more economical girders with longer spans and less depth.

Researches have tried different construction approaches to improve the composite action at hogging moment zone. In view of the limited work done on the use of UHPC slab at the hogging moment zone, an experimental investigation will be conducted to evaluate the effectiveness of the UHPC slab in maintaining the composite action at hogging moment zone for the service load. The structural behavior of the two-span continuous composite girders with UHPC slab at hogging moment zone will be evaluated up to flexural failure. Furthermore, numerical investigation will be performed utilizing the commercially available software (ABAQUS) [17]. A three dimensional FE model of the composite girder will be developed using ABAQUS software and verified with the experimental results. The verified model will be employed to conduct a parametric study to investigate the effects of the degree of shear connection, thickness and length of UHPC slab at hogging moment zone on the performance of composite girders. Finally, a simplified analytical approach will be developed to evaluate the load carrying capacity of the composite girders at service and ultimate stages.

Four continuous composite girders will be prepared with adequate number of shear connectors to insure full composite action between the concrete slab and steel section. The

steel section will be proportioned to eliminate all secondary failure modes. UHPC will be used to cast the concrete slab at the hogging moment zone. Composite girders will be tested to fail in flexure and the obtained data will be compiled and analyzed to prepare the experimental results.

1.4 Research Objectives

The main objectives of this research is to investigate experimentally and numerically the behavior of a two-span continuous composite girder with UHPC slab at hogging moment zone. The specific objectives are to:

1. Conduct an experimental program to investigate the effectiveness of the UHPC slab at hogging moment zone of continuous composite girders to maintain composite action at service load;
2. Develop a three dimensional finite element model for the continuous composite girder with UHPC slab at hogging moment zone using ABAQUS software;
3. Validate the numerical results with the experimental results and conduct a parametric study to evaluate the effects of the degree of shear connection, thickness and length UHPC slab at the hogging moment zone, on the performance of continuous composite girders; and
4. Evaluate analytically the girder capacity at service and ultimate conditions.

1.5 Research Program

This work evaluates the behavior of the two-span continuous composite girders with UHPC slab at hogging moment zone. It consists of three main parts including the experimental investigation, numerical investigation and the simplified analytical approach.

1. Experimental investigation of a two-span continuous composite steel-concrete girder with UHPC slab at hogging moment zone to assess the effectiveness of UHPC in maintaining the composite action at service load. A total of four composite girders were fabricated and constructed to study the effects of the degree of shear connection and the UHPC slab thickness at the hogging moment zone on the behavior of composite girders.

   Furthermore, the mechanical properties of materials were measured experimentally for NC, UHPC, structural steel and reinforcement steel according to ASTM specifications [18, 19]. In addition, the capacity of a shear connector embedded in UHPC slab was evaluated through the push-out test according to Eurocode-4 specifications [16].

2. Numerical investigation of the behavior of a two-span continuous composite steel-concrete girder with UHPC slab at hogging moment zone. A three dimensional FE model was developed for the composite girder with UHPC slab at hogging moment zone. The obtained FE results were validated against the experimental results. The FE results showed a good agreement with the experimental ones. The verified model was employed to perform a parametric study on the effect of the degree of shear connection, thickness and length of UHPC slab at hogging moment zone on the behavior of the continuous composite girder.

3. A simplified analytical approach was developed to evaluate the capacity of the continuous composite girders at service and ultimate conditions. This approach was developed based on strain compatibility and equilibrium of forces.

1.6 Organization of the Dissertation

The content of this work is divided into three main parts: experimental investigation, numerical investigation and the simplified analytical approach. This dissertation consists of 8 chapters. Chapter 1 contains the introductory part, shear connection, need of the research, objectives of the research and the research program. Chapter 2 gives a comprehensive literature review about the experimental and numerical evaluation of continuous composite girders using UHPC slab at hogging moment region. The review includes: high strength concrete, maintaining composite action for continuous composite girders and behavior of partially composite beams under hogging moment.

Chapter 3 is devoted to the design of continuous composite girder according to the standard specifications. This chapter contains the design of shear connection, transverse stiffeners and slab reinforcements. All secondary failures are also included in this chapter.

Chapter 4 focuses on the experimental program of the four continuous composite girders and material testing. It contains the mechanical properties of all materials tested experimentally and the preparation and instrumentation of the composite girders.

Chapter 5 illustrates the results and discussion obtained from the experimental investigation. It includes the general behavior, strain distribution, plastic analysis, and service and ultimate loads.

Chapter 6 demonstrates the numerical investigation of the two-span continuous composite girders with UHPC slab at hogging moment zone utilizing ABAQUS software. It contains the FE modeling, the validation of the developed model with experimental results and the conducted parametric study.

Chapter 7 contains the simplified analytical approach for the continuous composite steel-concrete girders with UHPC slab at hogging zone. It includes the evaluation of the capacity of composite girders at service and ultimate stages.

The dissertation is concluded with chapter 8 which contains the conclusions and recommendations followed by the references.

CHAPTER TWO

LITERATURE REVIEW

Review of previous research conducted on ultra-high performance concrete (UHPC), maintaining the composite action for continuous composite girders over the interior support and behavior of partially composite beams under hogging moment are presented in the following sections.

2.1 High Strength Concrete

Researchers in the last two decays tried to improve the tensile strength of NC by using additives such as silica-fume and super-plasticizer with steel fibers. UHPC is a modern generated material developed in the early 1990s [20]. The tensile strength for UHPC improved substantially, it ranges between 15 to 25 times that of NC. UHPC has been extensively used for strengthening and repair of concrete structures.

Dugat et al. (1996) [21] noted that the average flexural tensile strength of UHPC reached up to 32 MPa and the compressive strength 200 MPa. These high strength values give the designers more options and choices of structural dimensions.

Gao et al. (1997) [22] evaluated experimentally the mechanical properties of high strength lightweight concrete with steel fibers. Steel fibers percentages used were 0%, 0.6%, 1%, 1.5% and 2% with 46, 58 and 70 aspect ratios. The splitting tensile strength, compressive strength and flexural strength increase as steel fibers percentage increase.

Lubbers (2003) [23] reported that the compressive and flexural strength of UHPFC could be 2 to 3 times and 2 to 6 times greater than high performance concrete (HPC), respectively.

Perry and Zakariasen (2004) [24] indicated that flexural tensile strength of UHPC ranges from 34 MPa to 48MPa and the compressive strength ranges between 158 MPa and 228 MPa. The results of the compressive strength greatly influenced by the heat treatment.

Song et al. (2004) [25] studied high strength concrete properties with different percentages of steel fibers. Flexural strength and splitting tensile strength increase with the increase in fibers percentage.

Graybeal (2005) [26] conducted an experimental work to test 71 specimens made with UHPC according to ASTM (C 1018). Prism samples used with span lengths of 6, 9, 12 and 15 inches. The flexural strength was 35.4 MPa for steam-cured specimen and 29.9 MPa for untreated specimens.

Lukasik, (2005) [27] presented the typical flexural tensile strength of ductal UHPC and another three concrete types. The highest flexural stress recorded was 47 MPa for UHPC with highest steel fibers content.

Brühwiler and Denarié, 2008 [28] presented the idea of using (UHPC) for strengthening of concrete structures at regions where the concrete structures is subjected to harsh environmental and high applied loading.

Kanga et al. (2010) [29] investigated experimentally the effect of fiber content on the tensile fracture properties of UHPC. A notched 3-point bending tests were performed with volume ratio of the fiber that were varied from 0% to 5%. The results demonstrated that the flexural tensile strength of UHPC linearly increased with increasing the volume ratio

of fiber. After that an inverse analysis was conducted to evaluate the tensile fracture model of UHPC and a tri-linear tensile softening model was recommended.

Kang and Kim, (2011) [30] investigated the orientation distribution of the fiber on the tensile behavior of UHPC. The results demonstrated that the effect of orientation distribution of the fiber was very small on the pre-cracking behavior of the UHPC, but it was imperative on post-cracking behavior.

Shende et al. (2012) [31] studied the effects of percentage of steel fibers on the mechanical properties of UHPC. The percentages of steel fibers were 0%, 1%, 2% and 3% and the aspect ratios were 50, 60 and 67. The obtained results indicated the highest splitting tensile strength and flexural strength are for 3% fibers percentage and 50 aspect ratio.

Hassan et al. (2012) [32] stated that the use of steel fibers in UHPC is almost doubled the tensile strength of this concrete. While the influence on the elasticity modulus and compressive strength is not significant.

Doo et al. (2013) [33] verified that the use of steel fibers enhances the tensile strength of UHPC. This enhancement depends mainly on the fiber content, aspect ratio, shape, distribution and orientation. Increasing steel fibers content is the best way to improve tensile strength of concrete.

Hakeem (2011) [10] studied experimentally the physical and mechanical properties of UHPC using local materials from the eastern province of Saudi Arabia. The flexural strength of UHPC with 6.3% fiber content is approximately 31.0 MPa and compressive strength exceeded 160 MPa. The mix design for UHPC developed by Hakeem is given in

Table 2.1. This mix design will be adopted for casting UHPC slab at hogging moment zone for the continuous composite girders.

Table 2.1: UHPC mix design [10].

Mix component	Weight (Kg/m^3)
Portland Cement	900
Water	168
Fine Sand	980
Superplasticizer	40.3
Steel Fibers	157
Micro-Silica	220

Yoo et al. (2014) [34, 35] investigated the effect of the length of fiber and the method of casting on the flexural behavior and tension-softening curve of UHPC. In this study four different lengths of fiber used (L_f = 13, 16.3, 19.5 and 30 mm) and two different methods of casting of UHPC were considered. The results showed that increasing the length of fiber resulted into increasing the ultimate flexural strength of UHPC up to 19.5 mm but using fiber with length of 30 mm in UHPC deteriorated the flexural performance of UHPC. Furthermore, the results showed that casting the UHPC in the center at the maximum moment gave higher strength flexural than that with UHPC in the corner.

Wu et al. (2016) [36] studied the effect of using three shaped of steel fibers with different quantities of fiber on the behavior of UHPC. It was shown that the compressive strength of concrete and flexural strength can reach over 150 and 35 MPa, respectively by incorporating of 3% straight steel fibers. However, using 3% hooked-end and corrugated

fibers in the UHPC results into increasing the compressive strengths at 28-day by 48% and 59%, respectively compared to those with the same quantity of straight fiber.

2.2 Maintaining Composite Action for Continuous Composite Girders

Researchers tried different construction schemes to maintain the composite action at the hogging moment zone for continuous composite girders. Basu et al. (1987) evaluated analytically [37] and experimentally [38] the behavior of two-span continuous composite steel-concrete beams with concrete slab prestressed at the hogging moment zone. Prestress was applied directly to the concrete slab at the hogging moment zone. This study evaluated the effect of using prestressing tendons on controlling concrete cracks at the hogging moment zone. The results indicated that cracks in concrete slab were eliminated at service load while the load carrying capacity was increased by 20%.

Elremaily and Yehia (2006) [39] conducted an experimental investigation for continuous composite concrete-steel girders by externally prestressing the composite girder to study the behavior of composite sections at the hogging moment zone. The results indicated an improvement in elastic limit and ultimate load capacity.

Chen et al. (2009) [40] investigated the external prestressing for two and three-spans continuous composite girders both experimentally and numerically. The continuous composite girders prestressed by external tendons attached externally to the steel girders. The results indicated a significant increase in the cracking moment resistance and the failure load of the prestressed continuous composite girders. Also, the prestressing technique maintained the composite action at hogging moment zone for the service load and enhanced stiffness and strength of composite girders.

Nie et al. (2011) [41] carried out experimental and numerical evaluation of prestressed continuous composite steel-concrete girders. Cracking, yielding and the ultimate loads of the two-span composite girder were evaluated and extended to a general cases of loading. The analytical results were verified with the experimental results, and numerical results suggested that the analytical procedure is reliable and appropriate for design purposes.

Lin et al. (2013) [42-44] investigated the mechanical properties of composite steel concrete girders under hogging moment. Eight inverted simply supported beams were prepared and tested to study the effect of three different variables including type of loading, steel fiber-reinforced concrete and rubber-latex mortar coating on the behavior of the composite girders. The study showed that the steel fiber-reinforced concrete controls the initiation and propagation of cracks. Also, the rigidity and capacity of the composite girders with Perfo-Bond Strips (PBLs) are much greater than that with headed shear studs.

Sharif et al. (2016) [45] investigated experimentally the use of a carbon fiber–reinforced polymer (CFRP) to maintain the composite action at the hogging moment zone of continuous composite girders. CFRP sheet was bonded to the top of concrete slab at hogging moment zone. The results indicated that composite action at the hogging moment zone was maintained and initiation of cracks was prevented in a concrete slab for service loads.

Samaaneh et al. (2016) [46] conducted numerical investigation of two-span continuous composite steel-concrete girders strengthened with CFRP sheet at hogging moment zone by using ABAQUS software. The results obtained from the model were validated experimentally. A parametric study was conducted to evaluate the effects of the CFRP thickness and degree of shear connection at hogging moment zone on the behavior of the

continuous composite girder. The results demonstrated that the thickness of the CFRP sheet depends on adhesive strength and the capacity of the girder at the sagging moment.

2.3 Behavior of Partially Composite Beams under Hogging Moment

Fabbrocino & Pecce (2000) [47] investigated experimentally the behavior of composite steel-concrete simply supported beams. The inverted beams were tested such that the concrete slab is under tension. The influence of slab-profile shear connection on the behaviors of the beams was investigated. Beams were tested with different degrees of shear connection, as shown in Figure 2.1. Beams of type A & B have the same composite action level with different arrangements while beams of Type C have partial composite action level. It was observed that beams of type A and B failed due to local buckling in the compression flange, while beam of type C failed due to the fracture in the headed shear studs. Load-deflection curves are similar up to yielding for the three types of beams, after that the curves are affected by the degree of shear connection. On the other hand, the load capacity of the beams reduces as the deformation increases. The stiffness of the beams got reduced once the concrete slab cracked and it increased with higher degree of shear connection between the slab and steel beam.

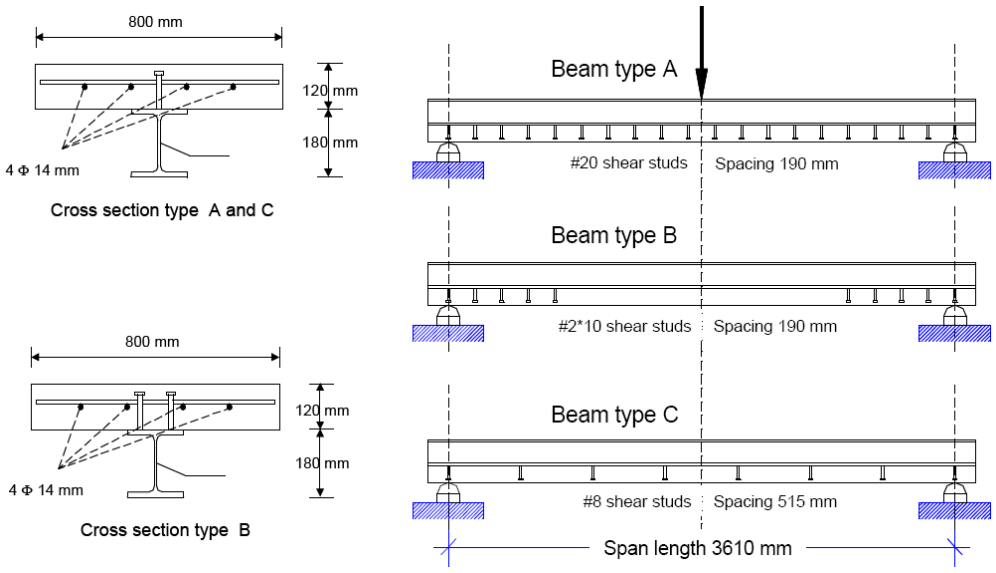

Figure 2.1: Cross sections with the corresponding arrangement of shear studs, Fabbrocino & Pecce (2000) [47].

Experimental and analytical investigations of the behavior of composite steel-concrete simply supported beams were conducted by Loh et al. (2004) [48, 49]. Eight-inverted simply supported beams are investigated under hogging moment. Three specimens were tested under monotonic loading and the others under cyclic loading. The three specimens which were tested under monotonic loading were designed with different spacing between shear connectors (83%, 50% and 33% shear connection) with similar reinforcement ratio. A concentrated force was applied on the top flange of steel beam at the mid-span. Lateral-torsional buckling was prevented by providing adequate lateral bracing to prevent any out-of-plane movement of the compression flange. It was observed that the beams which were tested under monotonic loading and with a degree of shear connection higher that 50% failed due to local buckling in the compression flange, while the beams with a degree of shear connection less than 50% failed due to fracture in shear connectors. The moment capacity and stiffness of the beams with a higher degree of shear connection are higher than those with lower shear connection. Moreover, a reduction in stiffness and an increase

in the slip between concrete slab and bottom flange were noticed due to the partial degree of shear connection.

Nie et al. (2008) [50] investigated experimentally the behavior of a thirteen-composite steel-concrete beams with different degrees of shear connection varied from 25 to 185%. Three different series (A, B, C) of beams, shown in Figure 2.2, were considered. Series A and B were simply supported and investigated experimentally under sagging and hogging moments, respectively. While, series C was continuous girders with two & three spans. The considered variables are shear studs spacing, longitudinal reinforcement, profiled sheeting and the loading conditions. It was concluded the following results: for series A, failure took place due to crushing of concrete slab for the specimens with a shear connection higher than 50% and due to studs' fracture for the specimens with a shear connection lower than 50%. For Series B, a reduction in the stiffness of beams took place due to developed cracks in the concrete slab. Also, a significant increase in the curvature and deflection of the beams was observed once the applied load exceeded 80% of ultimate load. Capacity and ductility of beams were reduced by the decrease of shear connection. Cracks initiated at the mid-span and extended toward the ends of beam as the applied load increased. For Series C, a linear behavior was observed up to the initiation of the first crack then the crack width and length increased with the increase of load. Cracks reduced beams stiffness and load capacity. Failure was governed by the fracture of shear connector because series C was designed with a partial degree of shear connection (50%).

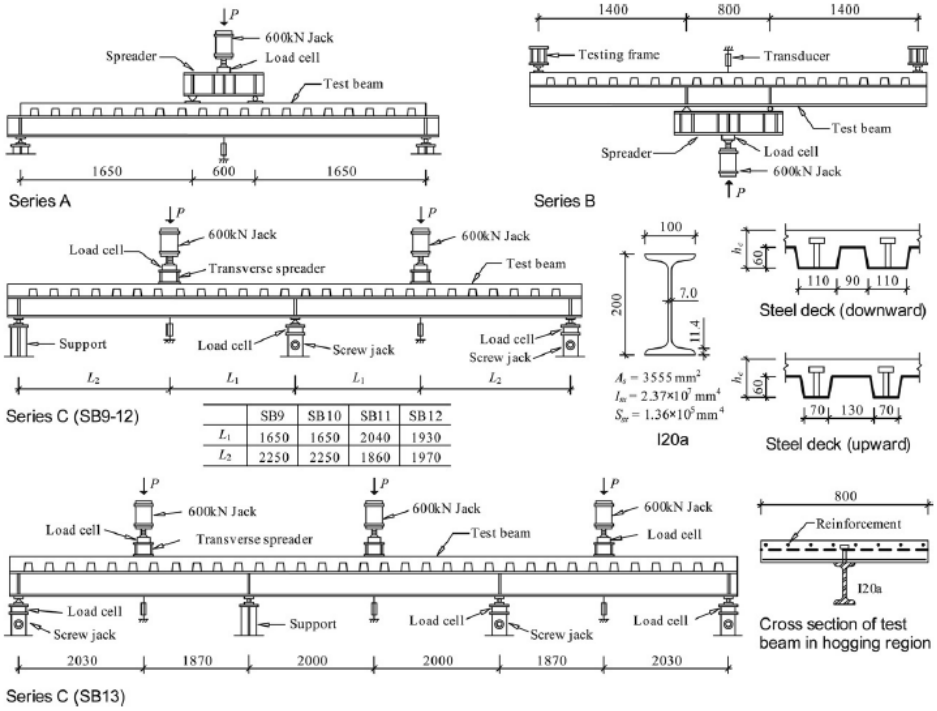

Figure 2.2: Test Set-up, Nie et al. (2008) [50].

Husain et al. (2009) [51] investigated numerically the behavior of composite steel-concrete beams subjected to hogging bending utilizing ANSYS software. A three dimensional FE model was developed to simulate the full flexural behavior of the composite steel-concrete beams including load-deflection behavior, concrete-steel interface slip and shear studs' distribution. The reliability of the developed model was validated with the experimental data provided by Fabbrocino & Pecce (2000) [47]. The validation showed a good agreement between the numerical and the experimental results.

Lin, W. and T. Yoda (2011) [52] evaluated experimentally the behavior of composite steel-concrete beams in hogging moment region. A total of four inverted-simply supported beams were tested under point load at the mid-span. Two of the composite beams with headed studs as the shear connectors, while the other two specimens are using Perfo-Bond Strips (PBLs) as the connection devices between the steel girder and the concrete slab. Ultimate load capacity of composite sections of composite sections in negative moment

region was evaluated and compared with experimental values. Crack formation, crack widths development process and strain distribution of the composite section before and after cracking were observed. Results indicated that the current specifications such as AASHTO, JSCE and Eurocode-4 can provide appropriate values for ultimate strength of composite girder under negative bending moment.

A review of the previous research has not uncovered any work on the use of ultra-high performance concrete (UHPC) slab at hogging moment zone for continuous composite girders to maintain the composite action at service load. Therefore, experimental and numerical evaluation on the behavior of continuous composite girders with partial length of UHPC slab at hogging moment zone is warranted.

CHAPTER THREE

DESIGN OF CONTINUOUS COMPOSITE GIRDERS

This chapter presents the design of a two-span continuous composite steel-concrete girder with UHPC slab at hogging moment zone. The design of continuous composite girder was conducted according to AISC specifications [9] and based on several assumptions, as shown in this chapter.

3.1 Design Criteria

The two-span continuous composite steel-concrete girder was designed following these criteria to satisfy research objectives:

I. The composite girders were designed to fail in flexure.

II. Shear failure of steel beam was eliminated utilizing the proper thickness of web.

III. Local buckling in flanges and web of steel section was eliminated by satisfying width/thickness ratio.

IV. Lateral-torsional buckling was eliminated using proper cross section and providing lateral support to the bottom flange at the interior support.

V. Local web yielding and local web crippling were eliminated by using the steel plates under the concentrated forces.

VI. The highest ultimate load carrying capacity of all girders with UHPC at hogging moment zone should not exceed the ultimate capacity of lab facilities (Loading cells, loading jack, Frame).

3.2 Materials and Geometry

The design of the continuous composite girder, shown in Figure 3.1, was conducted according AISC specifications [9] and using the material mechanical properties shown in Table 3.1. The composite girder's cross sections at mid-span and interior support are shown in Figure 3.2.

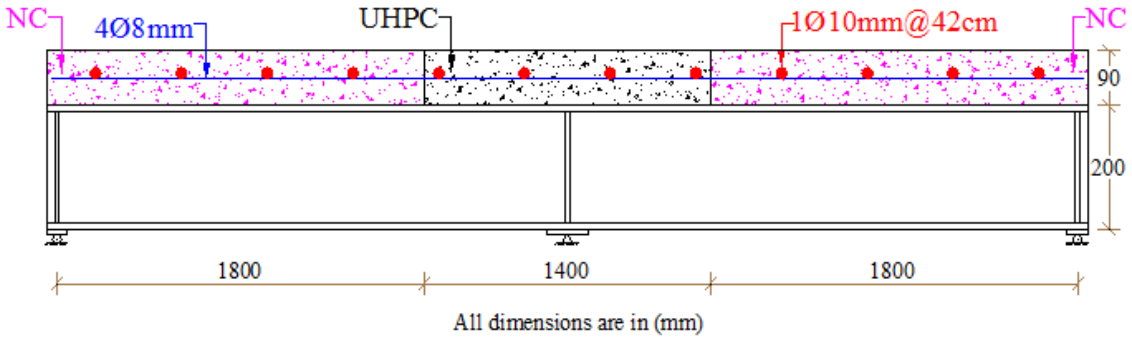

Figure 3.1: Detailed dimensions of the composite steel-concrete girder.

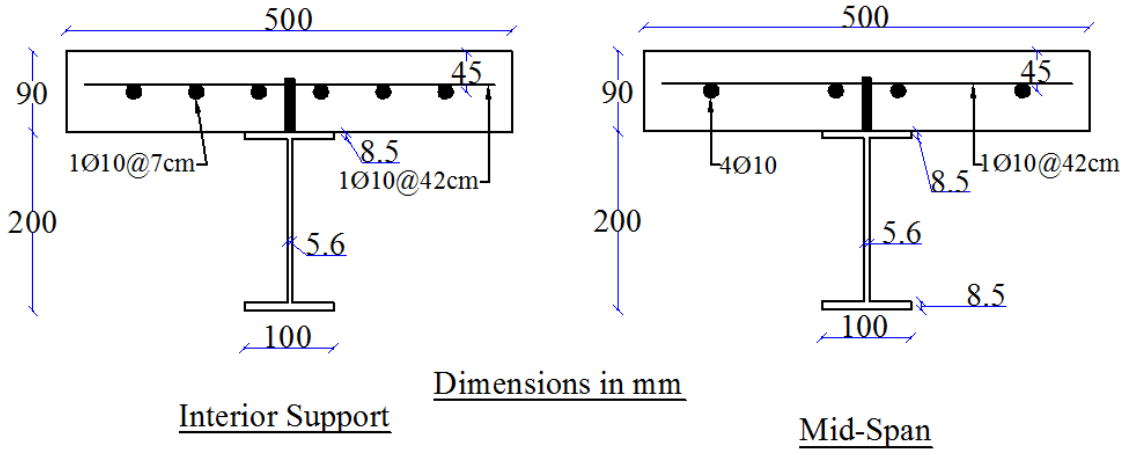

Figure 3.2: Composite girder's cross sections at both mid-span and interior support.

Table 3.1: Assumed mechanical properties of materials.

NC	Compressive strength fc'(MPa)	28
UHPC	fc'(MPa)	150
	f_t (MPa)	11
Yielding strength of structural steel fy (MPa)		248
Yielding strength of steel reinforcement $f_{yS.R}$ (MPa)		420

3.3 Design of Shear Connection

Shear connection was designed to develop full composite action between the concrete slab and the steel section at both sagging and hogging moment zones according to AISC specifications [9]. Section 3.3.1 shows the design of shear connection based on assumed mechanical properties of materials shown in Table 3.1. While, section 3.3.2 illustrates the revised design based on the actual mechanical properties obtained from experimental testing (Section 4.2) to check the degree of composite action at both sagging and hogging moment zones.

3.3.1 Assumed Mechanical Properties of Materials

A 19-mm-diameter shear studs were used to form the composite action between the concrete slab and the steel beam. The spacing between studs was evaluated to develop full composite action based on the assumed material properties given in Table 3.1. Sections 3.3.1.1 and 3.3.1.2 show the detailed design of shear studs spacing at sagging and hogging moment zones, respectively.

3.3.1.1 Sagging Moment Zone

Minimum shrinkage and temperature reinforcements are used within the concrete slab in the longitudinal and transverse directions according to ACI code [53]:

$f_y = 420\ MPa \rightarrow\rightarrow \rho_{min} = 0.0018 \rightarrow\rightarrow As_{min} = 0.0018 \times 500 \times 90 = 81\ mm^2$

The smallest steel bar diameter is 6 mm $\rightarrow\rightarrow As = \frac{\pi}{4}(6)^2 = 28.3\ mm^2$

$Number\ of\ bars = \frac{81}{28.3} = 2.9 \rightarrow\rightarrow use\ 4\ Ø\ 6\ mm$

$Spacing = \frac{50}{4} = 12.5\ cm < S_{max} = 2\text{h} = 2(9) = 18\ cm$

The number of shear studs and the spacing between shear studs are evaluated at the ultimate condition following the procedures shown below.

Assume the neutral axis N.A in the concrete slab, $a \leq t_s = 90\ mm$, as shown in Figure 3.3.

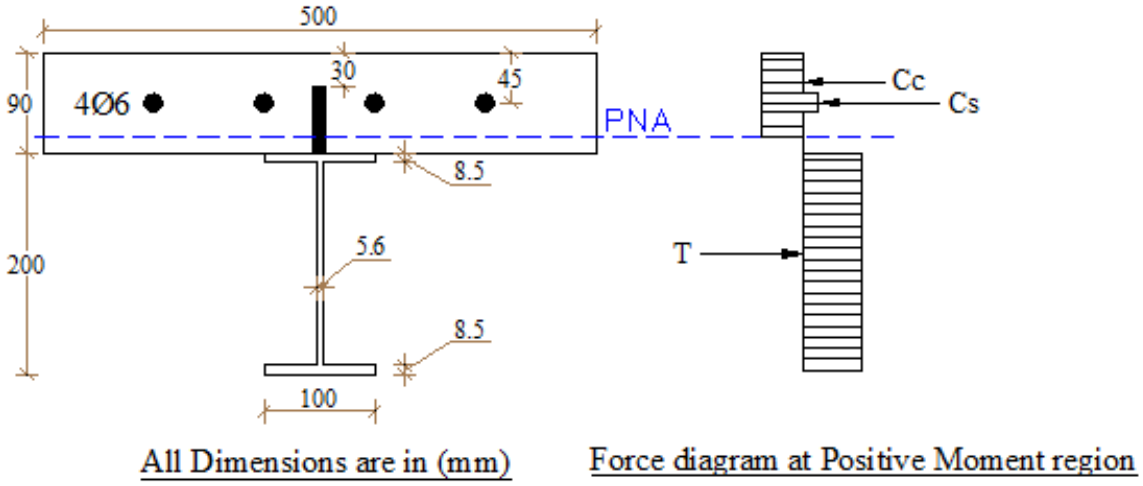

Figure 3.3: Composite girder's cross section at sagging moment zone.

Depth of neutral axis (a)

$C = 0.85\ f_c' b_E\ a\ +\ A_{SR} f_{y\,SR}$

$= 0.85 \times 28 \times 500 \times (a) + 113.2 \times 420$

$= 11900a + 47544 \quad N$

$T = f_y(2b_f t_f + b_w t_w)$

$= 248(2 \times 100 \times 8.5 + 5.6 \times 183)$

$= 675750.4 \quad N$

From equilibrium equation: $C = T$

$a = 52.8 \ mm < t_s = 90mm \rightarrow\rightarrow Assumption\ is\ correct$

The tangential shear force which will be resisted by the shear studs is 675.8 kN.

According to AISC specifications [9], the capacity of a shear stud is,

$Q_n = 0.5\ A_{sc}\sqrt{f_c' E_c}$

$E_c = 4700\sqrt{f_c'} = 4700\sqrt{28} = 24870\ MPa$

$A_{sc} = \frac{\pi}{4} D_{stud}^2 = \frac{\pi}{4}(19)^2 = 283.5\ mm^2$

$Q_n = 0.5\ A_{sc}\sqrt{f_c' E_c} = 0.5 \times 283.5 \times \sqrt{28 \times 24870} = 118287\ N = 118\ KN$

Number of shear studs $= \frac{675.8}{118} = 5.7$ studs $\rightarrow\rightarrow$ use 6 studs

Based on assumed material properties, 6 studs of a 19-mm-diameters are required to develop full composite action at sagging moment zone. These studs are uniformly distributed between the points of maximum and zero moments.

For the ultimate moment capacity of the composite section, take sum of moments of all forces about the center of the concrete slab:

$M_{+ve} = 2724.8 \times 248\left(\frac{200}{2} + 45\right) + 0.85 \times 28 \times 500 \times 52.8 \times \left(45 - \frac{52.8}{2}\right)$

$= 109.7\ kN.m$

3.3.1.2 Hogging Moment Zone

The number of shear studs and the spacing between shear studs are evaluated at the ultimate condition following the procedures shown below.

Assume the neutral axis N.A is located within the top flange, as shown Figure 3.4

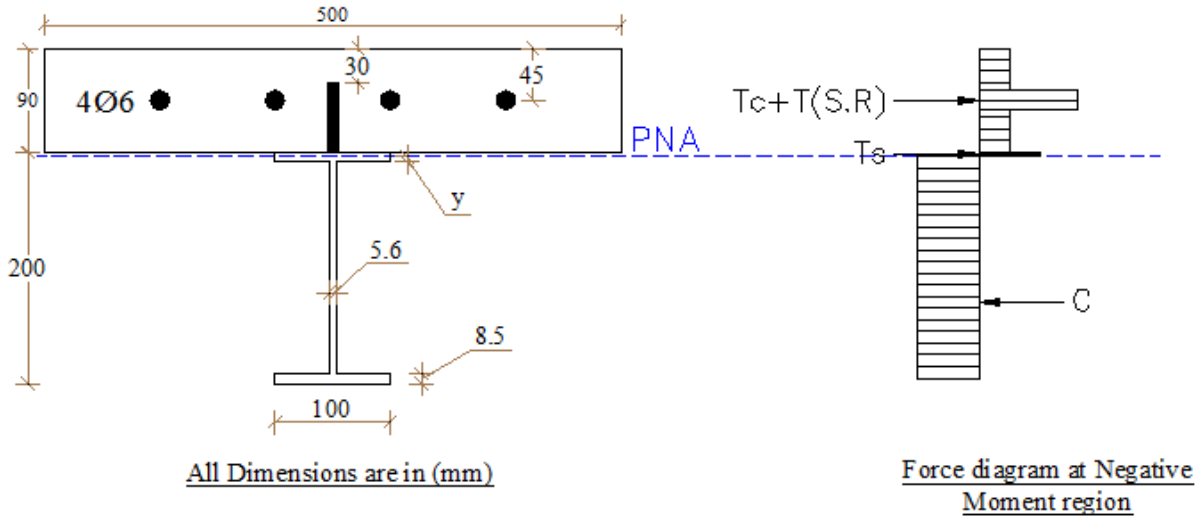

Figure 3.4: Stress distribution at hogging moment section.

$T_{S.R} = 113.2 \times 420 = 47544\ N = 47.5\ \ KN$

$T_c = 500 \times 90 \times 11 = 495000\ N = 495\ KN$

$T_s = \big(100 \times (8.5 - y)\big) \times 248 = 210800 - 24800\ y = 210.8 - 24.8\ y\ \ \ KN$

$T = T_{S.R} + T_c + T_s = 753.3 - 24.8\ y$

$C = (100 \times 8.5 + 183 \times 5.6 + 100 \times y) \times 248 = 464950.4 + 24800\ y$

$= 464.95 + 24.8\ y\ \ \ KN$

$C = T \rightarrow\rightarrow\rightarrow 753.3 - 24.8\ y = 464.95 + 24.8\ y$

$y = 5.81\ mm\ < 8.5\ mm \rightarrow\rightarrow OK$

Assume the capacity of a shear stud embedded in UHPC slab at hogging moment zone equals to that at sagging moment zone. Although this assumption reduces the capacity of a

shear stud at hogging zone, it was made to insure that the number of shear studs which will be identified can develop full composite action at hogging zone.

$$Number\ of\ shear\ studs = \frac{47.5 + 495}{118} = 4.6\ studs \rightarrow\rightarrow use\ 5\ studs$$

Based on assumed material properties, 5 studs of a 19-mm-diameters are required to develop full composite action at hogging moment zone. These studs are uniformly distributed between the points of maximum and zero moments.

For the ultimate moment capacity of the composite section, take sum of moments of all forces about the center of the concrete slab:

$$M_{-ve} = (248 \times 100 \times 8.5) \times 240.75 + (248 \times 183 \times 5.6) \times 145$$
$$+ (248 \times 100 \times 5.81\ ) \times 50.6 - (248 \times 100 \times 2.69) \times 46.34$$
$$= 91801326.7\ N.mm = 91.8\ \text{kN.m}$$

Define sagging and hogging moment zones and spacing between shear connectors

Using linear interpolation to specify hogging and sagging moment zones, as shown in Figure 3.5.

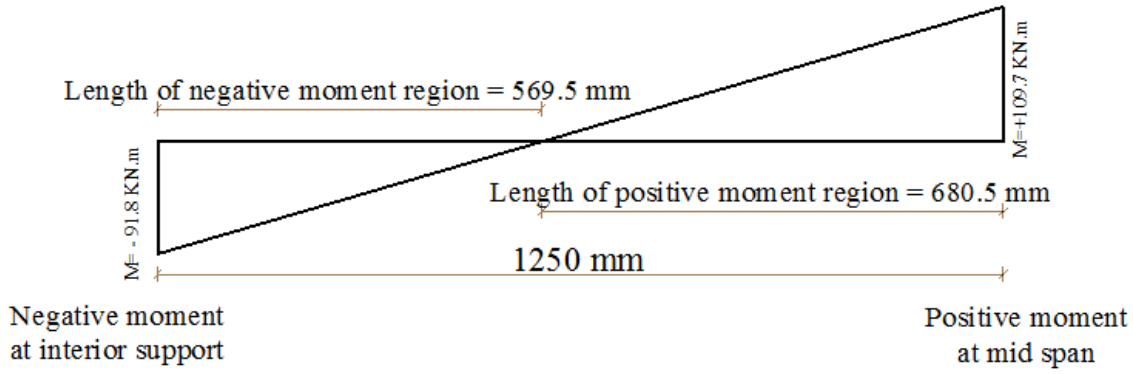

Figure 3.5: Bending moment diagram between mid-span and interior support.

$$Location\ of\ inflection\ point\ from\ mid\ span\ = \left(\frac{109.7}{91.8 + 109.7}\right) \times 1250$$

$$= 680.5\ mm$$

- Shear studs spacing between mid-span and exterior support $= \frac{1250}{5} = 250\ mm$
- Shear studs spacing between mid-span and inflection point $= \frac{680.5}{5} = 136.1\ mm$
- Shear studs spacing in the hogging moment zone $= \frac{569.5}{4} = 126.55\ mm$

Total required number of shear studs =30 stud

3.3.2 Actual Mechanical Properties of Materials

The design of shear connection is revised based on the actual mechanical properties of materials shown in section 4.2. Summary of the actual mechanical properties is given by Table 3.2. Sections 3.3.2.1 and 3.3.2.2 show the detailed design of shear studs spacing at both sagging and hogging moment zones, respectively.

Table 3.2: Actual mechanical properties of materials.

NC	Compressive strength fc'(MPa)	25
UHPC	fc'(MPa)	134
	f_t (MPa)	7.7
Yielding strength of structural steel fy (MPa)		306
Yielding strength of steel reinforcement $f_{yS.R}$ (MPa)		555
Stud's capacity at hogging moment zone (kN)		151.3

3.3.2.1 Sagging Moment Zone

Assume the neutral axis N.A in the concrete slab, $a \leq t_s = 90\ mm$, as shown in Figure 3.6.

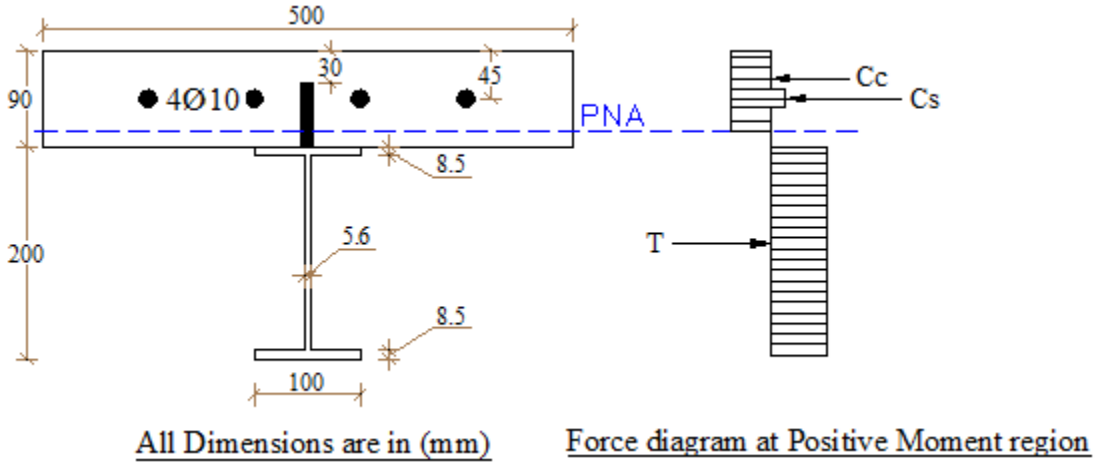

Figure 3.6: Composite girder's cross section at sagging moment zone.

Shrinkage and temperature reinforcements are used in concrete slab according to ACI code [53]:

$Use\ 4\ Ø\ 10\ mm$

Depth of neutral axis (a)

$C = 0.85\ f_c' b_E\ a\ +\ A_{SR} f_{y\,SR}$

$= 0.85 \times 25 \times 500 \times (a) + 314.2 \times 555$

$= 10625a + 174381 \quad N$

$T = f_y(2b_f t_f + b_w t_w)$

$= 306 * (2 \times 100 \times 8.5 + 5.6 \times 183)$

$= 833788.8 \quad N$

From equilibrium equation: $C = T$

$a = 62.1\ mm < t_s = 90mm \rightarrow\rightarrow Assumption\ is\ correct$

The tangential shear force which will be resisted by the shear studs is 833.8 KN.

Based on AISC specifications [9], shear strength capacity of shear stud is,

$Q_n = 0.5\, A_{sc} \sqrt{f_c' E_c}$

$E_c = 20283\ MPa$

$A_{sc} = \frac{\pi}{4} D_{stud}^2 = \frac{\pi}{4}(19)^2 = 283.5\ mm^2$

$Q_n = 0.5\, A_{sc} \sqrt{f_c' E_c} = 0.5 \times 283.5 \times \sqrt{25 \times 20283} = 100939\ N = 101\ kN$

$\text{Number of shear studs} = \frac{833.8}{101} = 8.3\ \text{studs} \rightarrow\rightarrow \text{use } 9\ \text{studs}$

The used number of shear studs (6 studs) based on assumed material properties is not adequate to develop full composite action at the sagging moment zone. Therefore, partial composite action at mid-span is obtained. The degree of shear connection is 67%.

For the ultimate moment capacity of the composite section, take sum of moments of all forces about the center of the concrete slab:

$$M_{+ve} = 2724.8 \times 306 \times \left(\frac{200}{2} + 45\right) + 0.85 \times 25 \times 500 \times 62.1 \times \left(45 - \frac{62.1}{2}\right)$$

$$= 130.1\ kN.m$$

3.3.2.2 Hogging Moment Zone

According to AASHTO specifications [54], the percentage of steel reinforcements at hogging moment section should be at least 1%. Therefore, it is required to use 6Φ10 bars at hogging moment section.

Assume the neutral axis N.A is located within the top flange, as shown Figure 3.7.

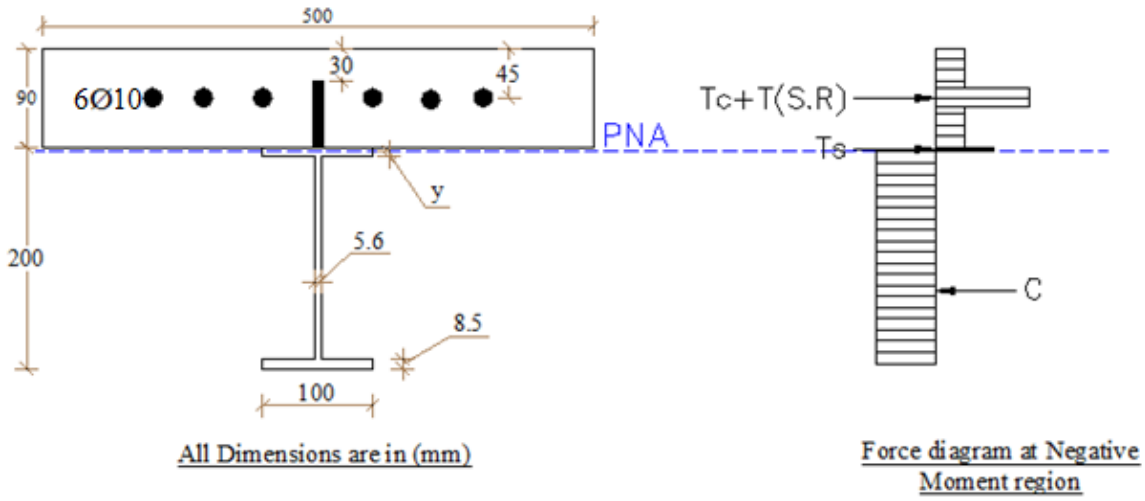

Figure 3.7: Stress distribution at the hogging moment section.

$T_{S.R} = 471.2 \times 555 = 261516\ N = 261.5\ \ kN$

$T_c = 500 \times 90 \times 7.7 = 346500\ N = 346.5\ kN$

$T_s = \big(100 \times (8.5 - y)\big) \times 306 = 260100 - 30600\ y = 260.1 - 30.6\ y\ \ \ kN$

$T = T_{S.R} + T_c + T_s = 868.1 - 30.6\ y$

$C = (100 \times 8.5 + 183 \times 5.6 + 100 \times y) \times 306 = 573688.8 + 30600\ y$

$= 573.7 + 30.6\ y\ \ \ KN$

$C = T \rightarrow\rightarrow\rightarrow 573.7 + 30.6\ y\ = 868.1 - 30.6\ y$

$y = 4.81\ mm\ < 8.5\ mm \rightarrow\rightarrow OK$

The tangential shear force which will be resisted by the shear studs is 608 kN.

The capacity of shear stud embedded in UHPC slab at hogging moment zone was evaluated experimentally through the push-out test according to Eurocode-4, as shown in section 4.2.3. The obtained capacity of a shear stud is 150 kN.

$$Number\ of\ shear\ studs = \frac{261.5 + 346.5}{150} = 4.07\ studs \rightarrow\rightarrow use\ 5\ studs$$

The used number of shear studs (5 studs) based on assumed material properties is adequate to develop full composite action at the hogging moment zone. Therefore, full composite action at interior support is obtained. The degree of shear connection is 100%.

For the ultimate moment capacity of the composite section, take sum of moments of all forces about the center of the concrete slab:

$$M_{-ve} = (306 \times 100 \times 8.5) \times 240.75 + (306 \times 183 \times 5.6) \times 145$$
$$+ (306 \times 100 \times 4.81\ ) \times 51.1 - (306 \times 100 \times 3.69) \times 46.84$$
$$= 110321763\ N.mm = 110.3\ \text{kN. m}$$

Define sagging and hogging moment zones and spacing between shear connectors

Using linear interpolation to specify sagging and hogging moment zones, as shown in Figure 3.8.

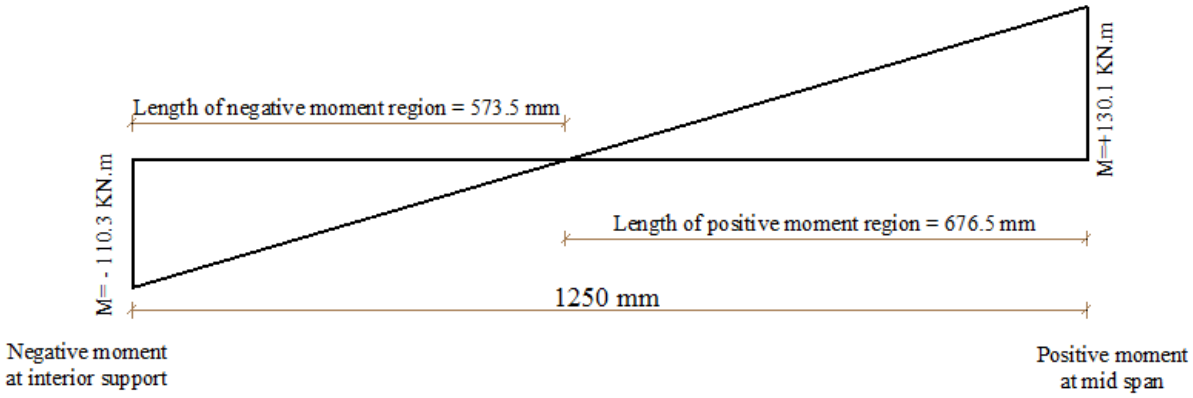

Figure 3.8: Bending moment diagram between mid-span and interior support.

$$Location\ of\ inflection\ point\ from\ mid\ span\ = \left(\frac{130.1}{130.1 + 110.3}\right) \times 1250$$
$$= 676.5\ mm$$

- Shear studs spacing between mid-span and exterior support $= \frac{1250}{8} = 156.25\ mm$
- Shear studs spacing between mid-span and inflection point $= \frac{676.5}{8} = 84.56\ mm$

- Shear studs spacing at the hogging moment zone $= \frac{573.5}{4} = 143\ mm$

3.4 Shear Capacity

The shear capacity of the composite steel-concrete section for shear force is evaluated based on the web of steel beam as per AISC specifications [9]. It was noticed that the section capacity is higher than the maximum shear force.

$\Phi V_n = 0.6 F_y A_w = 0.6 \times 248 \times 5.6 \times 200 = 166.6\ kN \geq 161.2\ kN$

3.5 Check Local Buckling in Flanges and Web

Local buckling is a stability mode of failure which may take place in the flanges or web of steel sections. Following the AISC specifications [9], the steel section, shown in Figure 3.9, will be checked for local buckling as follow:

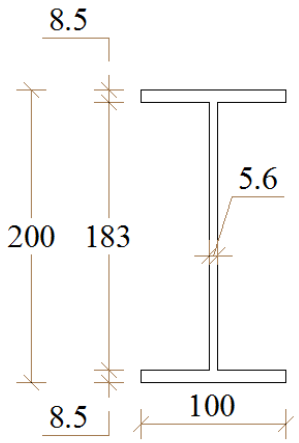

Figure 3.9: Dimensions of steel-beam's section.

- Flanges of doubly symmetric I-shape built-up sections:

Width to thickness ratio $\rightarrow\rightarrow \frac{b}{t} = \frac{50}{8.5} = 5.88$

Limiting width to thickness ratio $\rightarrow\rightarrow \lambda_p = 0.38\sqrt{\frac{E}{f_y}} = 0.38\sqrt{\frac{200 \times 1000}{248}}$

$= 10.79$

$\frac{b}{t} = 5.88 < \lambda_p = 10.79 \rightarrow\rightarrow\rightarrow No\ Local\ buckling$

- Webs of doubly symmetric I-shape sections:

Width to thickness ratio $\rightarrow\rightarrow \frac{h}{t_w} = \frac{183}{5.6} = 32.7$

Limiting width to thickness ratio $\rightarrow\rightarrow \lambda_p = 3.76\sqrt{\frac{E}{f_y}} = 3.76\sqrt{\frac{200 \times 1000}{248}}$

$= 106.78$

$\frac{b}{t} = 32.7 < \lambda_p = 106.78 \rightarrow\rightarrow\rightarrow No\ Local\ buckling$

The section is classified as compact section. Therefore, there will be no reduction in its moment capacity due to local buckling.

3.6 Check Lateral-Torsional Buckling

For continuous composite steel-concrete girders, lateral-torsional buckling may take place only in the bottom flange of steel section at the hogging moment zone where the flange is subjected to compression. Although, the top flange at mid-span is under compression, it is not susceptible to lateral-torsional buckling because it is laterally restrained by the concrete slab. Therefore, only one lateral bracing is needed at the interior support for the bottom

flange to prevent this buckling mode. The first plastic hinge will be formed at the interior support and it must have sufficient rotational capacity so that the second plastic hinge will form at the mid-span. AISC specifications [9] are used to check Lateral-torsional buckling for steel section, shown in Figure 3.9, ignoring the effect of concrete slab at hogging moment section.

$$A = 2 \times 8.5 \times 100 + 5.6 \times 183 = 2724.8\ mm^2$$

$$I_y = 2 \times \frac{8.5 \times 100^3}{12} + \frac{183 \times 5.6^3}{12} = 1419344.8\ mm^4$$

$$r_y = \sqrt{\frac{I_y}{A}} = \sqrt{\frac{1419344.8}{2724.8}} = 22.82\ mm$$

$$L_p = 1.76\, r_y \sqrt{\frac{E}{f_y}} = 1.76 \times 22.82 \times \sqrt{\frac{200 \times 1000}{248}} = 1140.56\ mm$$

$$L_{pd} = \left[0.12 - 0.076 \times \frac{M_1'}{M_2'}\right] \frac{E}{f_y}\ r_y$$

$$M_{mid} = \frac{M_1 + M_2}{2} \rightarrow\rightarrow\rightarrow M_1' = M_1 = -91.8\ kN.m$$

$$L_{pd} = \left[0.12 - 0.076 \times \frac{M_1'}{M_2}\right] \frac{E}{f_y}\ r_y = \left[0.12 - 0.076 \times \frac{-91.8}{109.7}\right] \times \frac{200 \times 1000}{248} \times 22.82$$

$$= 3378.8\ mm$$

$L_b = 1250\ mm < L_{pd}$, the section has enough rotational capacity to form the second plastic hinge under the concentrated load.

3.7 Design of Plates

According to AISC specifications [9], steel plates may be needed over supports or beneath concentrated forces to prevent web local yielding and web local crippling.

- **Web local yielding**

The nominal strength, Rn, shall be determined as follows:

a) When the concentrated force to be resisted is applied at a distance from the member end that is greater than the depth of the member, d,

$$\Phi Rn = \Phi f_{yw}\, t_w(5k + l_b) = 1 \times 248 \times 5.6 \times (5 \times 8.5 + l_b) = 322.4 * 10^3 N$$

$$l_b = 190\ mm$$

b) When the concentrated force to be resisted is applied at a distance from the member end that is less than or equal to the depth of the member, d,

$$\Phi Rn = \Phi f_{yw}\, t_w(2.5k + l_b) = 1 \times 248 \times 5.6 \times (2.5 \times 8.5 + l_b)$$

$$= 87.76 * 10^3 N$$

$$l_b = 42\ mm$$

- **Web local crippling**

The nominal strength, Rn, shall be determined as follows:

a) When the concentrated force to be resisted is applied at a distance from the member end that is greater than or equal to d/2,

$$\Phi Rn = 0.75 \times 0.8 \times t_w^2 \times \left(1 + 3\left(\frac{l_b}{d}\right)\left(\frac{t_w}{t_f}\right)^{1.5}\right) \times \sqrt{\frac{E\ f_{yw} t_f}{t_w}}$$

$$= 0.75 \times 0.8 \times 5.6^2 \times \left(1 + 3\left(\frac{l_b}{200}\right)\left(\frac{5.6}{8.5}\right)^{1.5}\right) \times \sqrt{\frac{200000 \times 248 \times 8.5}{5.6}}$$

$$= 322.4 * 10^3 N$$

$$l_b = 122\ mm$$

b) When the concentrated force to be resisted is applied at a distance from the member end that is less than d/2,

$$\Phi Rn = 0.75 \times 0.4 \times t_w^2 \times \left(1 + 3\left(\frac{l_b}{d}\right)\left(\frac{t_w}{t_f}\right)^{1.5}\right) \times \sqrt{\frac{E\ f_{yw} t_f}{t_w}}$$

$$= 0.75 \times 0.4 \times 5.6^2 \times \left(1 + 3\left(\frac{l_b}{200}\right)\left(\frac{5.6}{8.5}\right)^{1.5}\right) \times \sqrt{\frac{200000 \times 248 \times 8.5}{5.6}}$$

$$= 87.76 * 10^3 N$$

$$l_b = 10\ mm$$

Use PL100 × 200 × 8.5 over interior support

Use PL100 × 100 × 8.5 over exterior support

3.8 Design of Transverse Stiffeners

Stiffeners are required to resist compressive concentrated forces and designed in accordance with the requirements of section J4.4 in AISC specifications [9]. The effective column height (KL) is taken as 0.75h. The effective web width (b_w) is taken as either $25t_w$ for interior locations or $12t_w$ for locations near the end of a beam. The geometric properties of the pair of stiffeners are shown in Figure 3.10.

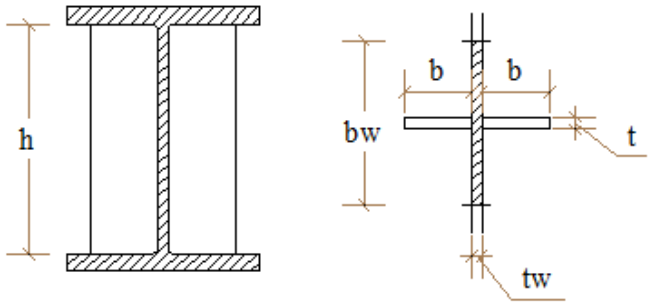

Figure 3.10: Detailed dimensions of transverse stiffeners.

Transverse stiffeners 2PL 8.5 × 47.2 × 183 are used against the compressive force at the interior and exterior supports.

Check local bucking in accordance to AISC specifications [9] table B4.1 (a)

$$\frac{b}{t} = \frac{47.2}{8.5} = 5.55 \leq 1.4\sqrt{\frac{E}{f_y}} = 1.49\sqrt{\frac{200000}{248}} = 42.3 \rightarrow No\ LB$$

Check overall buckling in accordance to AISC specifications [9] table B4.1 (a)

At the interior support

$h = 183\ mm$

$KL = 0.75h = 0.75 * 183 = 137.25\ mm$

$b_w = 25t_w = 25 * 5.6 = 140\ mm$

$A_g = 2bt + t_w b_w = 2 * 47.2 * 8.5 + 5.6 * 140 = 1586.4\ mm^2$

$$I = \frac{t(2b + t_w)^3}{12} + \frac{(b_w - t)t_w^3}{12} = \frac{8.5 * (2 * 47.2 + 5.6)^3}{12} + \frac{(140\ - 8.5) * 5.6^3}{12}$$

$$= 710258\ mm^4$$

$$r = \sqrt{\frac{I}{A_g}} = \sqrt{\frac{710258}{1586.4}} = 21.2\ mm$$

$$\frac{KL}{r} = \frac{137.25}{21.2} = 6.47 \leq 25$$

$$\Phi Pn = 0.9\, F_y A_g = 0.9 * 248 * 1586.4 = 354084\ N = 354\ KN \geq 322.4\ KN$$

At the exterior support (2PL 8.5 × 47.2 × 183)

$$b_w = 12t_w = 12 * 5.6 = 67.2\ mm$$

$$A_g = 2bt + t_w b_w = 2 * 47.2 * 8.5 + 5.6 * 67.2 = 1178.72\ mm^2$$

$$I = \frac{t(2b + t_w)^3}{12} + \frac{(b_w - t)t_w^3}{12} = \frac{8.5 * (2 * 47.2 + 5.6)^3}{12} + \frac{(67.2 - 8.5) * 5.6^3}{12}$$

$$= 709192\ mm^4$$

$$r = \sqrt{\frac{I}{A_g}} = \sqrt{\frac{709192}{1178.72}} = 24.5\ mm$$

$$\frac{KL}{r} = \frac{137.25}{24.5} = 5.6 \leq 25$$

$$\Phi Pn = 0.9\, F_y A_g = 0.9 * 248 * 1178.72 = 263090\ N = 263\ kN \geq 87.76\ kN$$

At the exterior support (2PL 5.6 × 47.2 × 183)

$$b_w = 12t_w = 12 * 5.6 = 67.2\ mm$$

$$A_g = 2bt + t_w b_w = 2 * 47.2 * 5.6 + 5.6 * 67.2 = 904.96\ mm^2$$

$$I = \frac{t(2b + t_w)^3}{12} + \frac{(b_w - t)t_w^3}{12} = \frac{5.6 * (2 * 47.2 + 5.6)^3}{12} + \frac{(67.2 - 5.6) * 5.6^3}{12}$$

$$= 467568\ mm^4$$

$$r = \sqrt{\frac{I}{A_g}} = \sqrt{\frac{467568}{904.96}} = 22.7\ mm$$

$$\frac{KL}{r} = \frac{137.25}{22.7} = 2.5 \leq 25$$

$$\Phi Pn = 0.9\, F_y A_g = 0.9 * 248 * 904.96 = 201987\ N = 202\ kN \geq 87.76\ kN$$

CHAPTER FOUR

EXPERIMENTAL PROGRAM

4.1 Introduction

Two-span continuous composite steel-concrete girders were tested experimentally during this research. The brief description of all experimental tests is included in this chapter. Experimental investigation of the mechanical properties of materials and composite girders are illustrated in the following sections. The experimental investigation includes the following:

1. Mechanical Properties of Materials
    I. NC and UHPC
    II. Structural steel and reinforcement steel
    III. Capacity of shear stud
2. Testing of the continuous composite girders

4.2 Mechanical Properties of Materials

Mechanical properties of materials are identified according to the international specifications or standards (ASTM and Eurocode-4) [16, 18, 19, 55-58]. All materials which were used in the construction and fabrication of the composite girders were tested to evaluate their mechanical properties.

4.2.1 Concrete (NC & UHPC)

The mix design for both NC and UHPC used in casting the slabs of the four girders are given in Table 4.1. Four tests (Compression test, splitting tensile test, direct tension test and four points bend test) were conducted experimentally to identify the mechanical properties of both the NC and the UHPC according to ASTM specifications [19, 55-57]. In addition, the stress-strain relations were determined experimentally for both the NC and the UHPC. These relations and the mechanical properties will be used in the numerical modeling of the continuous composite girders, as presented in CHAPTER Six.

Table 4.1: The mix design for NC and UHPC.

NC		UHPC [10]	
Mix component	Weight (Kg/m^3)	Mix component	Weight (Kg/m^3)
Portland Cement	345	Portland Cement	900
Water	217.3	Water	168
Coarse Aggregate	1074	Fine Sand	980
Fine Aggregate	725.6	Superplasticizer	40.3
		Steel Fibers	157
		Micro-Silica	220

4.2.1.1 Compression Test

The compressive strength test was conducted according to ASTM (C39) [55] specifications to determine the mechanical properties and the stress-strain curves of both the NC and the UHPC. Cylindrical specimens of a 75-mm diameter and 150-mm height (Height to diameter ratio is 2) were taken randomly from the NC and the UHPC mixes, as shown in Figure 4.1 and Figure 4.2, respectively. Once the specimens hardened, they were demolded (Figure 4.3 and Figure 4.4) and left for curing in an environment similar to that the composite girders were exposed to for 28 days. The cylindrical specimens were capped by sulfur to make the surface level to avoid stress concentration. Longitudinal and transverse strain gauges are used to measure normal strain in both directions. Load was applied at a constant rate of 1.5 kN/s. Load cell was used to record load and displacement up to failure. Load set-up is shown in Figure 4.5. Compression failure is shown in Figure 4.6. The mechanical properties including the compressive strength, modulus of elasticity and Poisson's ratio of the NC and UHPC are given by Table 4.2. While, the compressive stress versus strain diagrams for the NC and the UHPC are shown in Figure 4.7 and Figure 4.8, respectively.

Figure 4.1: Fresh NC specimens for compression test.

Figure 4.2: Fresh UHPC specimens for compression test.

Figure 4.3: Hardened NC specimens for compression test.

Figure 4.4: Hardened UHPC specimens for compression test.

Figure 4.5: Experimental test set-up.

Figure 4.6: Compression failure in UHPC cylinder.

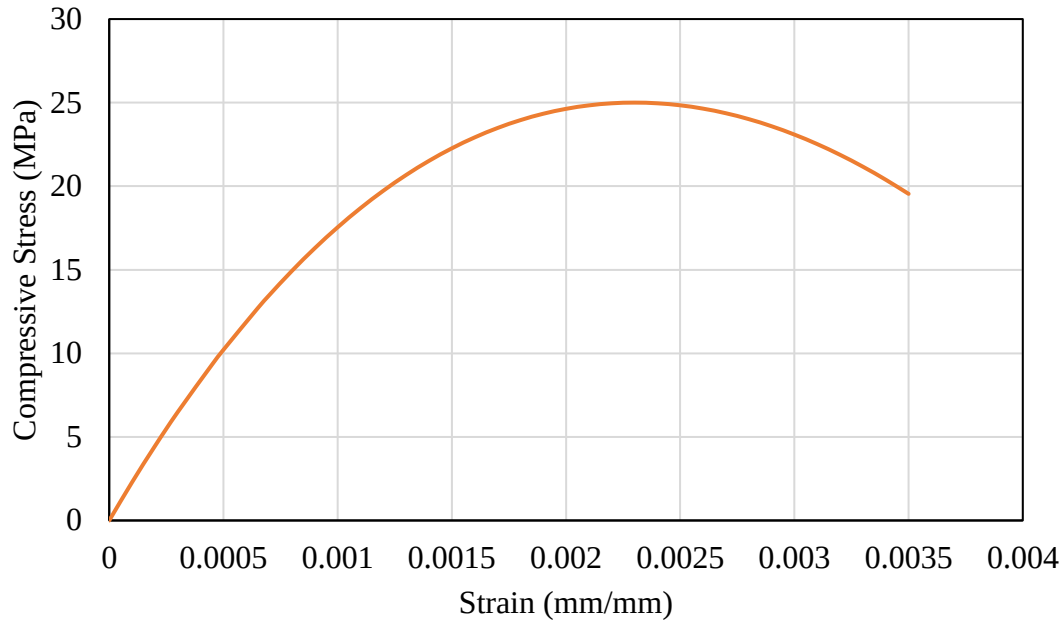

Figure 4.7: Compressive stress-strain diagram for NC.

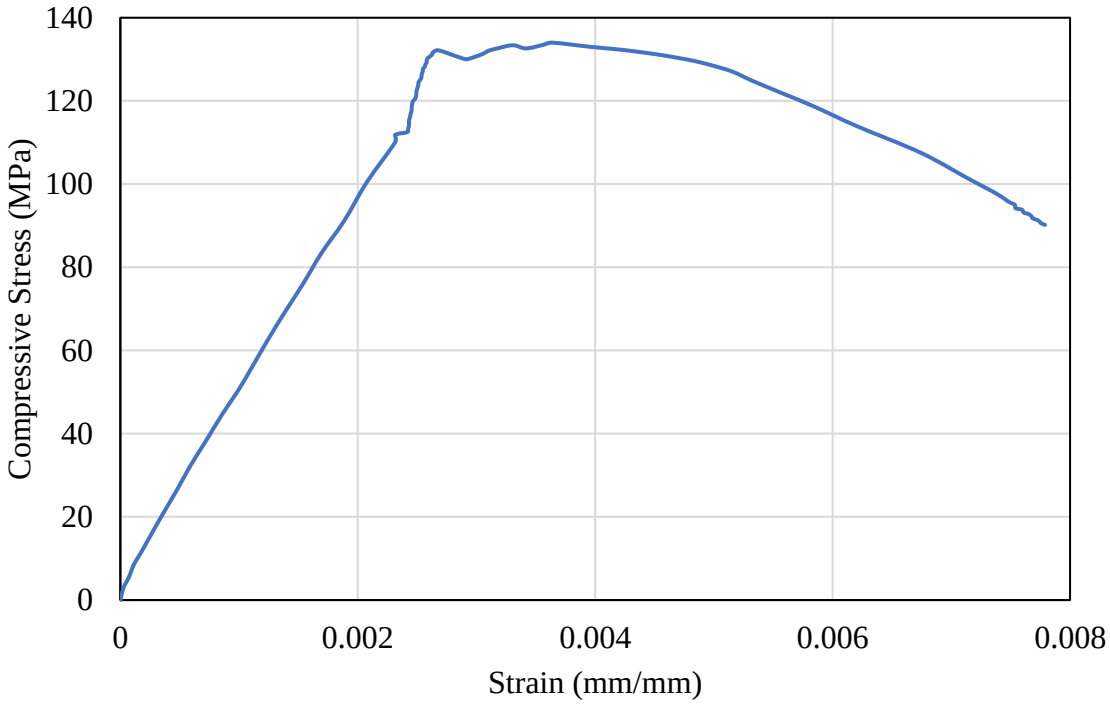

Figure 4.8: Compressive stress-strain diagram for UHPC.

Table 4.2: Mechanical properties of both NC & UHPC.

Mechanical Property	NC	UHPC
Compressive Strength (MPa)	25	134
Poisson's Ratio (ν)	0.17	0.16
Young's Modulus (MPa)	20283	47,000

4.2.1.2 Splitting Tensile Test

This test was conducted according to ASTM (C496) specifications [56]. Cylindrical samples (150 mm X 300 mm) were prepared and tested to evaluate the splitting tensile strength of both the NC and the UHPC. This test assesses only the indirect tensile capacity of the NC & the UHPC. Test set-up is shown in Figure 4.9. Load was applied at a constant rate of 0.5 KN/s. Failure plane due to splitting test is shown in Figure 4.10. Table 4.3 summarizes test results for both the NC and the UHPC. Tensile strength is evaluated using equation Eq. (4.1) as follow

$$f(\text{MPa}) = \frac{2\,P}{\pi\,L\,D} \qquad (4.1)$$

where P = maximum load (N) applied to the specimen;

L= length of specimen (mm); and

D= diameter of specimen (mm).

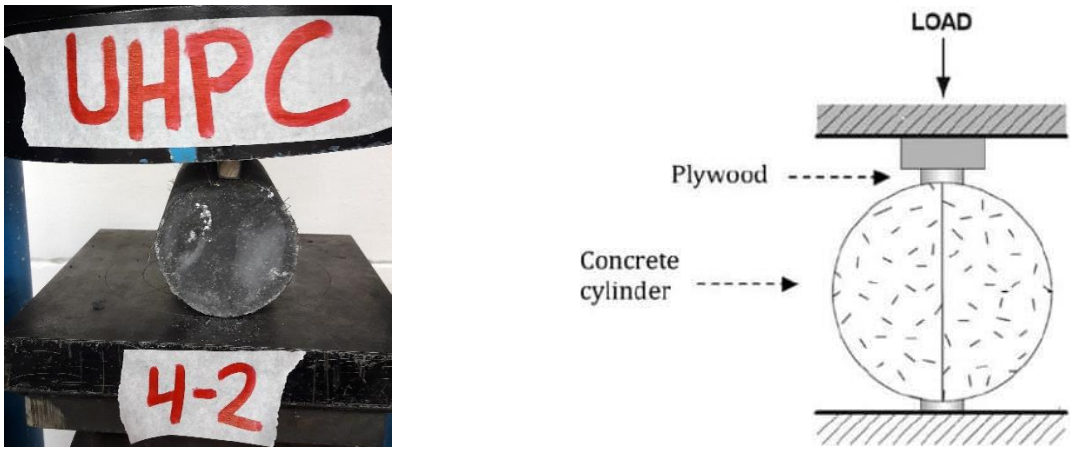

Figure 4.9: Splitting tensile test set-up.

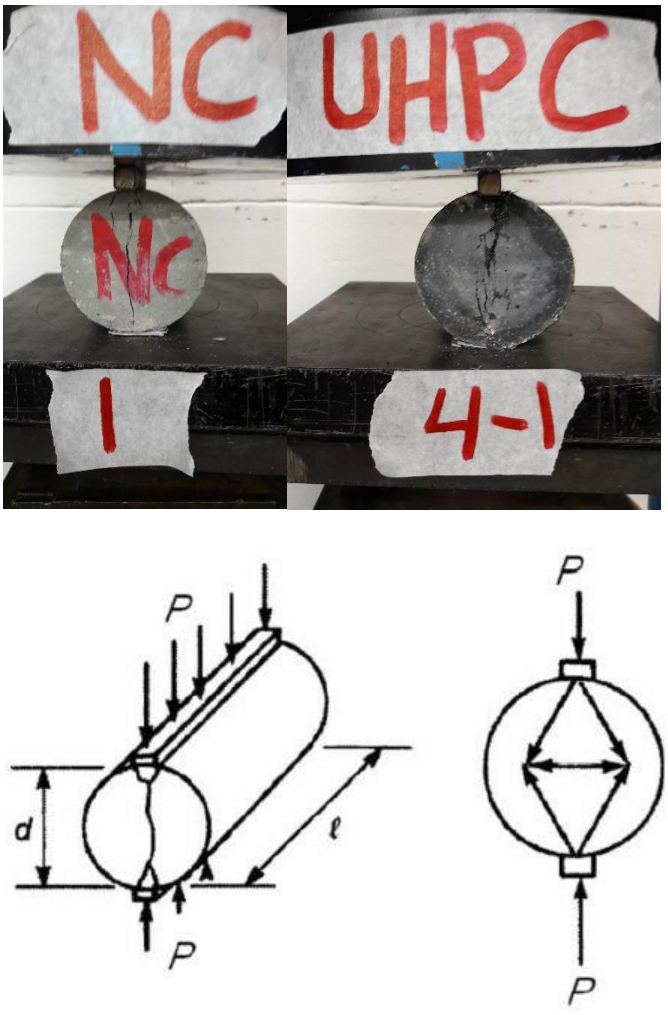

Figure 4.10: Failure of samples by splitting due to applied load.

Table 4.3: Summary of splitting tension test results for NC and UHPC.

Sample #	Maximum Applied Force (kN)		Indirect Tensile Strength (MPa)	
	NC	UHPC	NC	UHPC
1	28.4	310.7	1.61	17.58
2	29	279	1.64	15.79
3	27.5	299.3	1.56	16.94
Average strength=			1.60	16.77

4.2.1.3 Four Points Bend Test

In this test the force was applied by means of two loading pins with a distance between them equal to a half of the distance between the supporting pins, as shown in Figure 4.11. This test was conducted according to ASTM (C293) [57] specifications. The specimens of 40 mm X 40 mm cross-section and 160 mm length were prepared and tested to evaluate the flexural strength of both the NC and the UHPC, as shown in Figure 4.12. Flexural cracks appeared at the bottom of concrete prisms at the location of maximum moment, as shown in Figure 4.13.This test mainly evaluates the flexural strength or modulus of rupture which is tabulated in Table 4.4. Flexural strength is evaluated using Eq. (4.2) as follow

$$f(MPa) = \frac{3\,P\,a}{b\,d^2} \qquad (4.2)$$

where P = maximum load (N) applied to the specimen;

b= width of specimen (mm);

d= thickness of specimen (mm); and

a = distance between the supporting and loading pins.

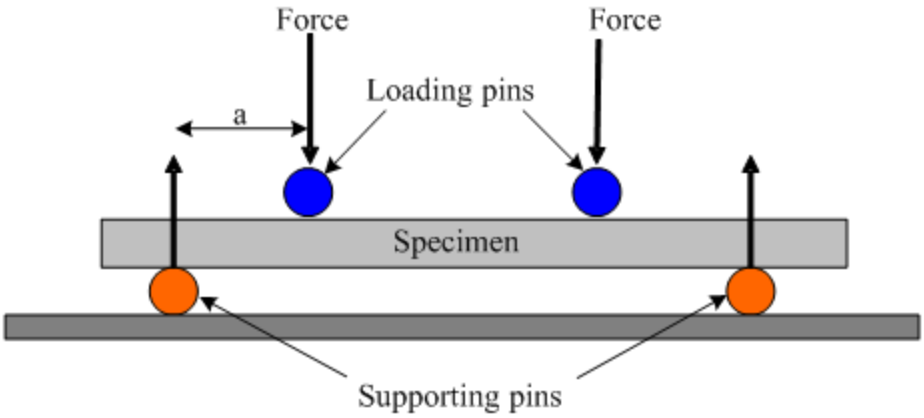

Figure 4.11: Schematic diagram of flexural strength test (four points bend test).

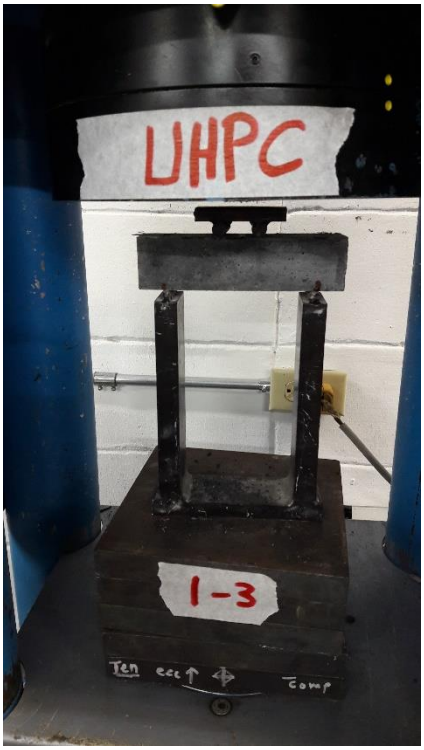

Figure 4.12: Flexural strength test set-up.

Figure 4.13: Flexural failure of UHPC prism.

Table 4.4: Summary of flexural strength test results for NC and UHPC.

Sample #	Maximum Applied Force (kN)		Flexural Strength (MPa)	
	NC	UHPC	NC	UHPC
1	2.01	14.5	4.24	30.59
2	2.07	12.7	4.37	26.79
3	2.00	12.7	4.22	26.79
	Average Flexural Strength=		4.28	28.00

4.2.1.4 Direct Tension Test

Direct tension test was carried out on dog-bone specimens to investigate UHPC behavior under tension. The shape of the tested specimens is shown in Figure 4.14 (a), while the test set-up is given by Figure 4.14 (b). The stress-strain curve for the UHPC under tension is shown in Figure 4.15. In the case of the NC, once the modulus of rupture, f_r, was determined, as presented in section 4.2.1.3, the full tensile behavior of the NC was obtained by assuming that the behavior of NC under tension is linear elastic up to the cracking of the concrete at f_r. Thereafter, the linear softening part was obtained as given by Bossio et al. [59] and shown in Figure 4.16.

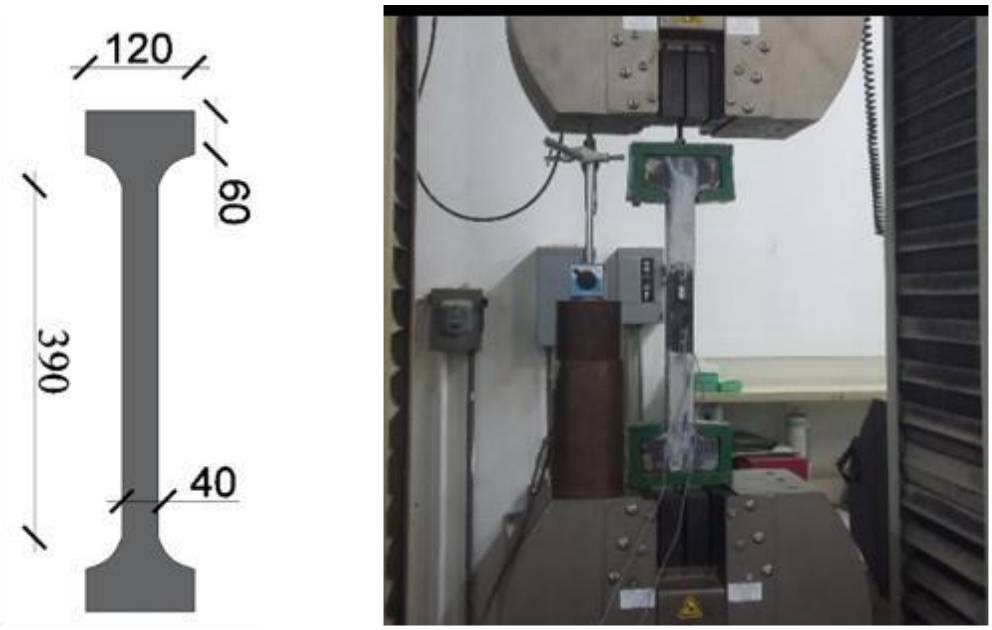

(a) Specimen shape. (b) Test set-up.

Figure 4.14: Direct tension test for the UHPC: (a) Specimen shape; (b) Test set-up.

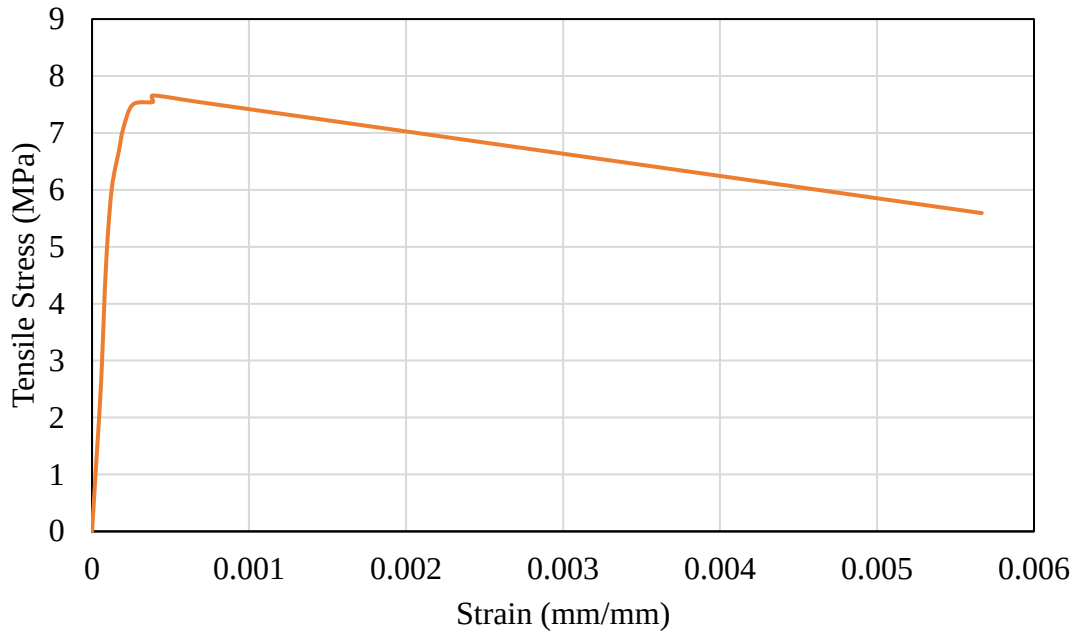

Figure 4.15: Tensile stress-strain relationship for UHPC.

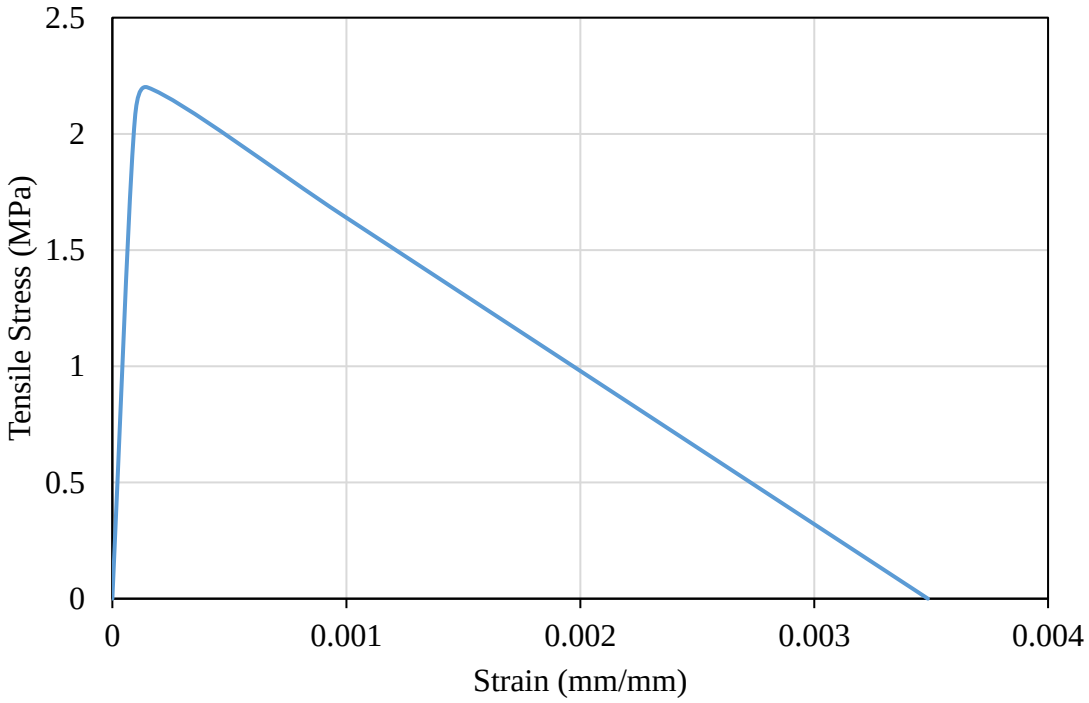

Figure 4.16: Tensile stress-strain relationship for NC.

4.2.2 Structural Steel and Reinforcement Steel

Tension test was conducted for both the structural steel section and the reinforcement bars to evaluate their mechanical properties and stress versus strain diagrams. Steel coupons were prepared for testing of structural steel according to ASTM (E8M-04) [58] specifications, as shown in Figure 4.17 (a). Longitudinal and transverse strain gauges were used to measure the instantaneous longitudinal and lateral strains corresponding to the applied load. The tensile stress versus strain was obtained for both structural steel section and the reinforcement steel, as shown in Figure 4.18 and Figure 4.19, respectively. Table 4.5 shows the mechanical properties (yield strength, ultimate strength, Poisson's ratio and Young's modulus) of both the structural steel and the reinforcements. Necking and ductile failure of steel samples were observed and shown in Figure 4.17 (b) & (c), respectively. The obtained mechanical properties and the tensile stress versus strain curves were used in the numerical modeling of the continuous composite girders, as presented in CHAPTER Six.

(a) Steel coupon (b) Necking of steel bar (c) Ductile failure

Figure 4.17: Direct tension test: (a) Steel coupon obtained from the structural steel section; (b) Necking of reinforcement bar; (c) Ductile failure in steel coupon.

Table 4.5: Mechanical properties of both structural steel section and reinforcement steel.

Mechanical Property	Structural steel	Reinforcement steel
Yield Strength (MPa)	306	555
Ultimate Strength (MPa)	425	585
Poisson's Ratio (ν)	0.27	0.3
Young's Modulus (GPa)	193	171

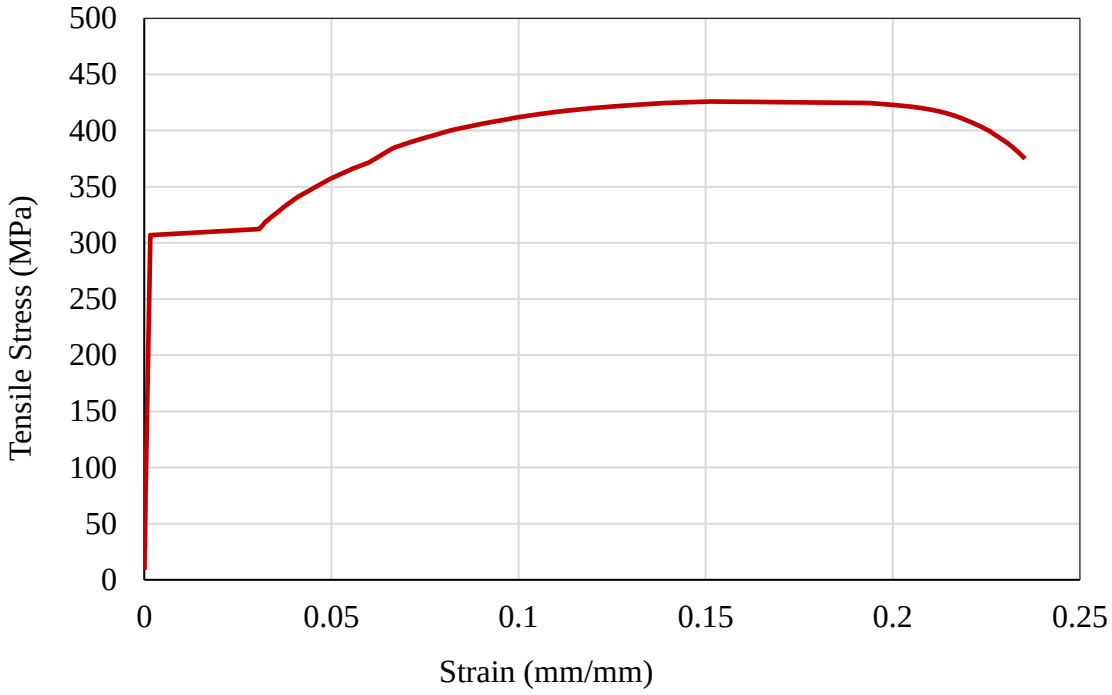

Figure 4.18: Tensile stress-strain relationship for structural steel beam.

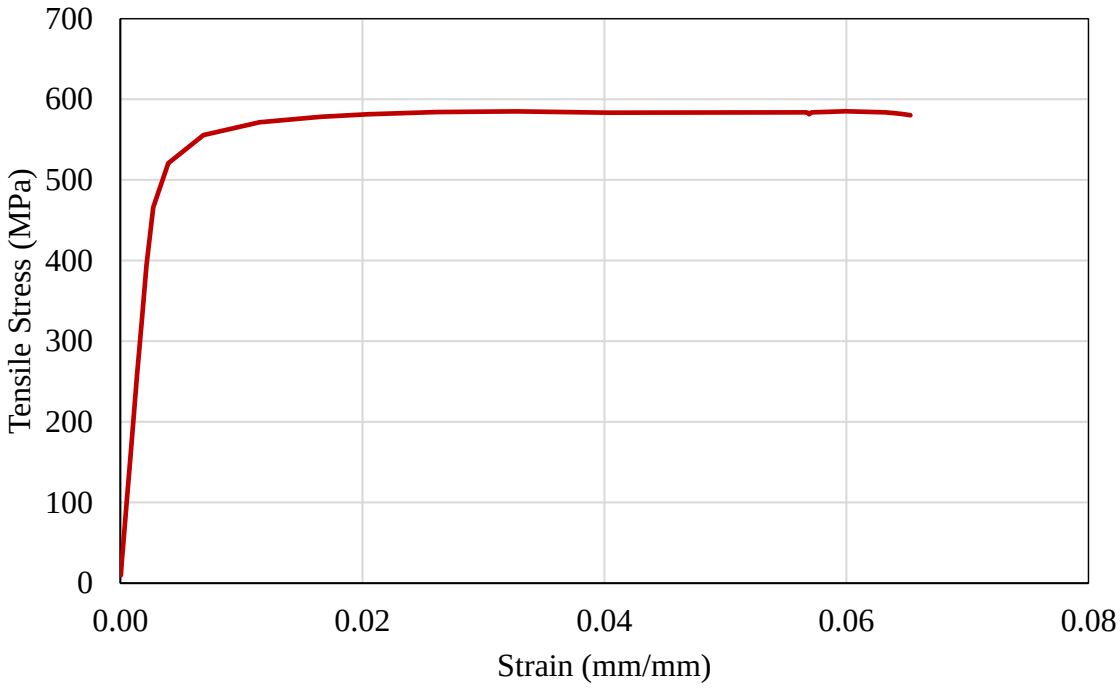

Figure 4.19: Tensile stress-strain relationship for reinforcement steel.

4.2.3 Shear Capacity of Shear Connectors

The shear strength of shear studs can be evaluated experimentally using the push-out test according to Eurocode-4 [16] specifications. Eurocode-4 provides the complete details of the standard push-out test including the dimensions of the specimen, steel section and reinforcement bars. In this work, shear studs embedded in NC and UHPC slabs were investigated experimentally to assess the behavior of the shear studs embedded in different concrete slabs. Six push-out test specimens were prepared and tested to evaluate the capacity of the shear studs embedded in UHPC slab. Three samples with stud spacing of 127 mm and the other three with stud spacing of 228 mm. In addition, another six specimens of the same dimensions and studs spacing were prepared to investigate the behavior of studs embedded in NC slab.

The schematic diagram of the push-out test and the detailed dimensions of the test's specimens are shown in Figure 4.20. Load is applied on the top end of steel section, linear variable differential transducer (LVDT) was utilized to measure the slip between the steel section and the concrete slab, as shown in Figure 4.21. The results showed that the load-slip behaviors of the studs for the two spacing are identical. Therefore, the average load versus the slip between the concrete slab and the steel beam is demonstrated in Figure 4.22. In addition, the capacity of shear studs embedded in UHPC slab was governed by the shear failure in the welding material of shear studs, as shown in Figure 4.23. While for studs embedded in NC slab, studs' capacity is governed by bearing failure in NC slab.

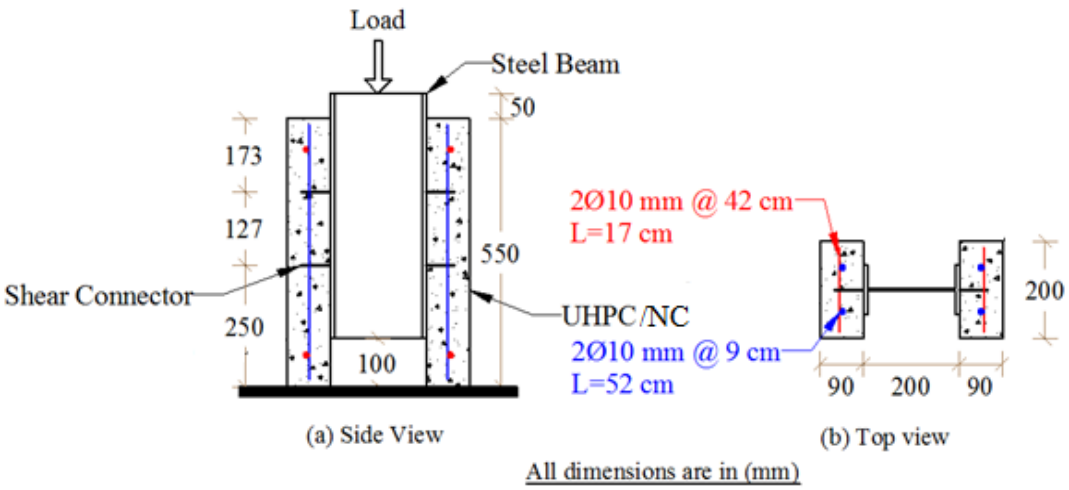

Figure 4.20: Schematic diagram for the push-out test and detailed dimensions of a typical specimen.

Figure 4.21: Experimental push-out test's set-up.

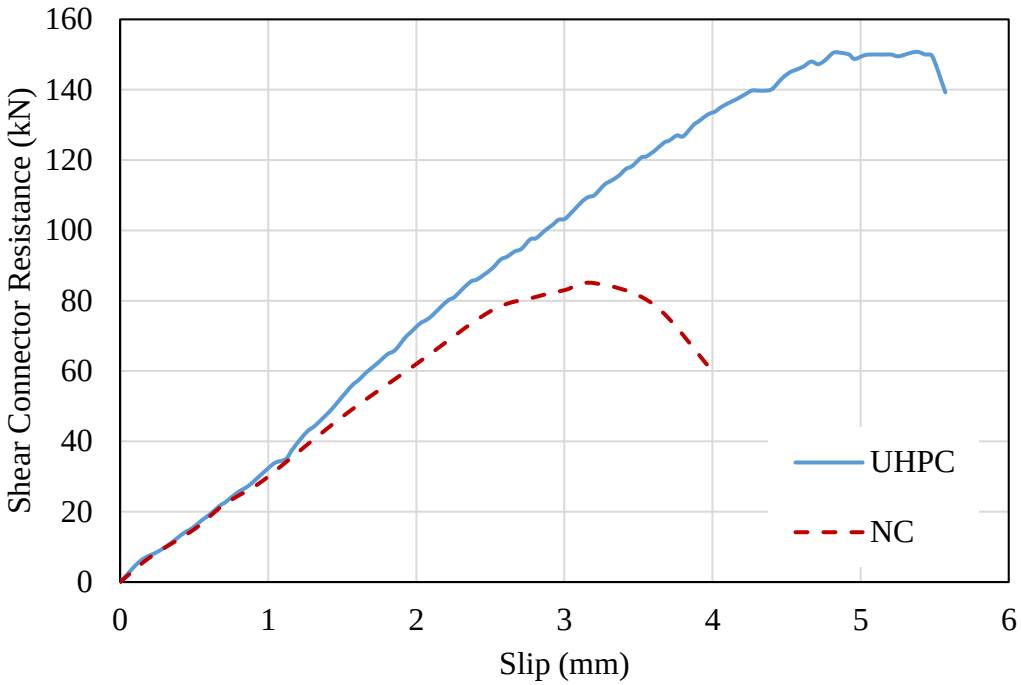

Figure 4.22: Experimental load-slip curve obtained from standard push-out test.

Figure 4.23: Shear Failure in the welding material.

4.3 Full-Scale Continuous Composite Girders Testing

This section presents the work needed prior to the experimental testing of the composite girders. It consists of the preparation and instrumentation of the composite girders and the test set-up.

4.3.1 Preparations and Instrumentations of Girders

This section illustrates the preparation of the steel sections, wooden formwork, holding reinforcements within the formwork and then casting both UHPC and NC slabs. In addition, it includes all instruments that used to perform the experimental testing of composite girders.

4.3.1.1 Preparation of Steel Girders

Hot-rolled steel beams were brought from the industry and then fabricated to form the steel beams with the required dimensions. The typical cross section of the steel beams is shown in Figure 4.24. Length of each beam is 5.10 m. Transverse stiffeners of a full height were installed using welding over each support, as per the design specifications shown in section 3.8, to prevent local failure in the web. Shear connectors of a 19 mm-diameter were installed utilizing welding to the top of steel flange at the proper spacing, as designed in section 3.3. Two different shear studs spacing were used at the hogging moment zone to represent full and partial composite action between the steel beam and concrete slab. Figure 4.25 shows the steel beam along with the shear studs' spacing. Fabricated steel beams with the installed studs are shown in Figure 4.26.

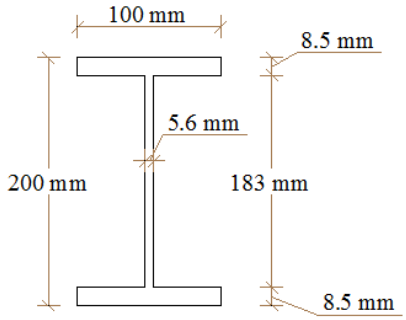

Figure 4.24: Typical cross section of the steel beam.

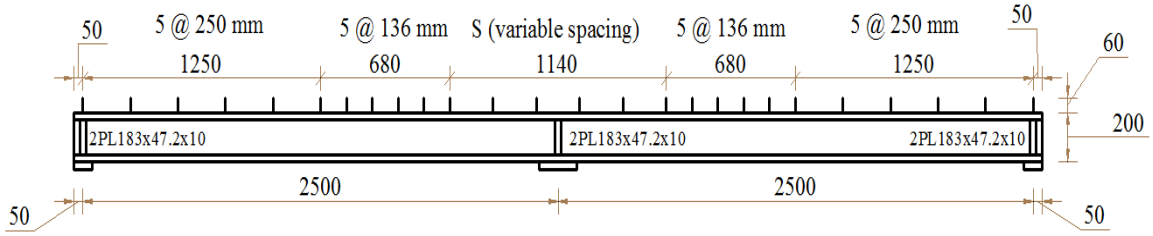

Figure 4.25: Steel beam's side view along with shear studs' spacing.

Figure 4.26: Fabricated steel beams with shear studs welded to the top flange.

4.3.1.2 Finalizing the Composite Girders

After finalizing steel beams, they were put on a level ground to start the wooden formwork. Plywood sheets were used to form the formwork for the toping slab. Minimum shrinkage and temperature reinforcements are provided into the slab in the longitudinal and transverse directions, as per the design requirements shown in Figure 4.27. The fabricated steel beams with the installed wooden formwork and slab reinforcements are shown Figure 4.28.

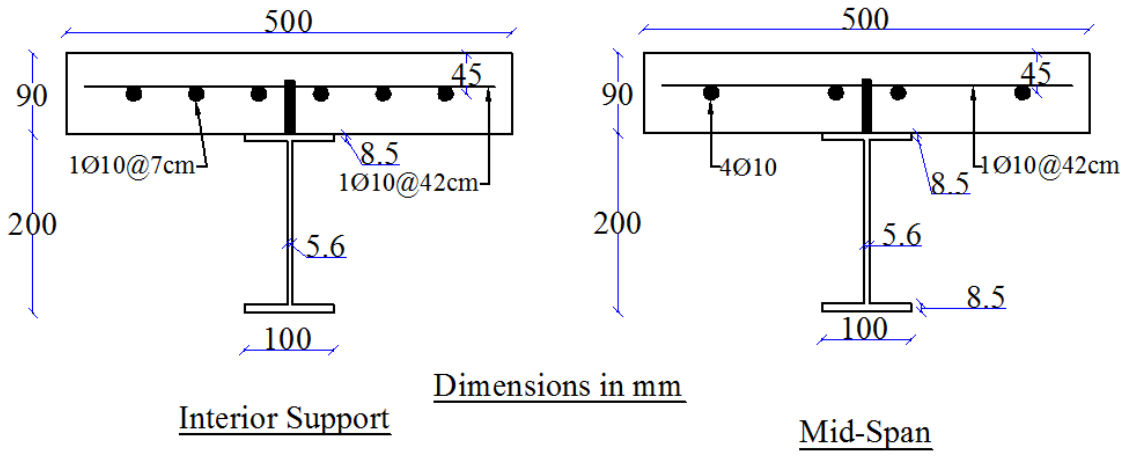

Figure 4.27: Composite girder's cross sections at both mid-span and interior support.

Figure 4.28: Steel beams with the installed wooden formwork and slab reinforcements.

Some strain gauges were used before casting NC and UHPC. These strain gauges were installed on the slab reinforcements, top of steel flange over the interior support and at each mid-span, as shown in Figure 4.29. Waterproofing was used to protect the strain gauges.

Figure 4.29: Strain gauges on the top of steel flange and reinforcements before casting concrete slab.

Concrete casting was performed in two stages, first stage is UHPC at the hogging moment zone followed by NC at sagging moment zones, as shown in Figure 4.30 and Figure 4.31, respectively. During casting of concrete, concrete cylindrical specimens were taken for the purpose of measuring mechanical properties of both the NC and the UHPC, as presented in section 4.2. After concrete casting the concrete surfaces were kept moist with wet burlap for 28-days, as shown in Figure 4.32. Composite steel-concrete girders which are ready for experimental testing are shown in Figure 4.33.

Figure 4.30: Casting of UHPC at hogging moment zone.

Figure 4.31: Casting of NC at sagging moment zone.

Figure 4.32: Curing of concrete using wet burlap for 28-days.

Figure 4.33: The prepared composite steel-concrete girders.

4.3.1.3 Strain Gauges and LVDT's

Strain gauges were needed to measure normal strain in NC, UHPC, steel section and steel reinforcements. Part of the strain gauges was impeded in concrete and they were used before casting concrete, as presented in section 4.3.1.2. The rest of strain gauges were used prior to testing of composite girders. Thirty-nine strain gauges were utilized for each composite girder to measure the normal strain at different locations. The strain gauges were labeled, as illustrated in Figure 4.34 to avoid conflict. Two LVDTs were used to measure the deflection at each mid-span.

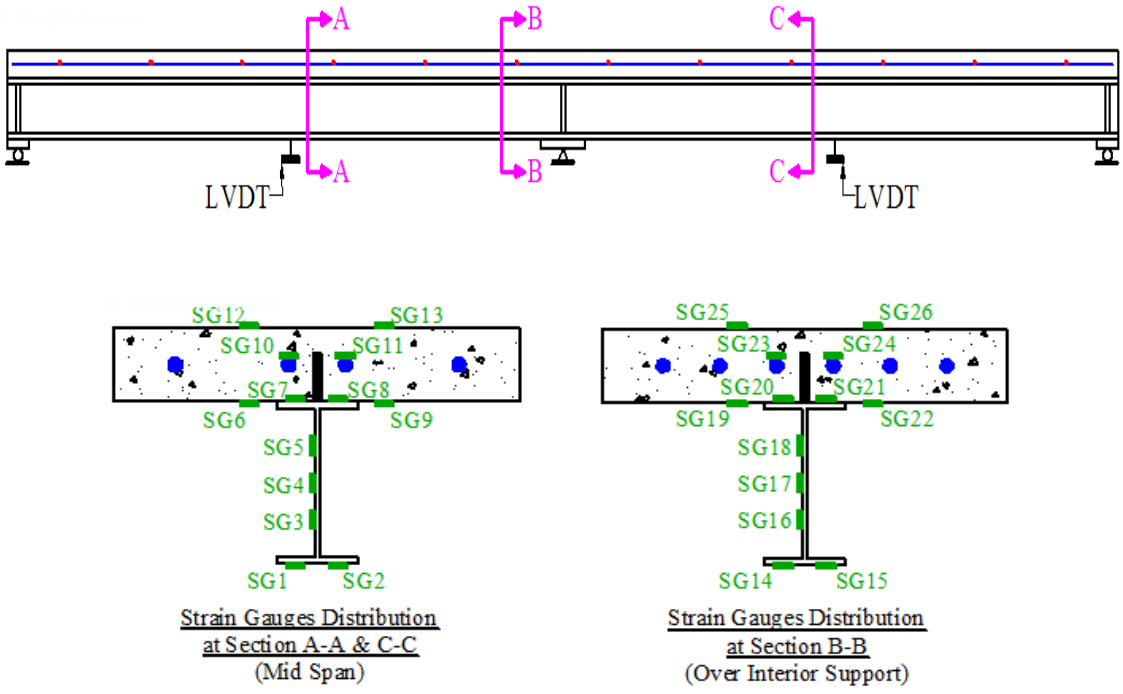

Figure 4.34: Locations and labels of strain gauges and LVDTs.

4.3.2 Testing Set-up

The composite girders were tested experimentally under a five-point bending test. Roller supports at both ends and the mid length were used. A lateral support was provided over the interior support to prevent lateral-torsional buckling of the compression flange. This support was provided from both sides by a steel beam which was placed between the compression flange and the reaction frame, as shown in Figure 4.35. The schematic and experimental test set-up are shown in Figure 4.36 and Figure 4.37, respectively.

Hydraulic jack, load cell and rigid beam to distribute jacking load to line loads at each mid-span were needed for the test set-up. Rigid beam was placed over the top of the concrete slab to transfer jacking load to concentrated line loads at each mid-span. The hydraulic jack was put over the center of the rigid beam and followed by the load cell, as shown in Figure 4.37.

The two-span composite girders were tested under monotonic loading at a rate of loading of 0.5 kN/s. Load was equally applied at the mid of each span as a concentrated line load at the top of the slab. Linear variable differential transducers (LVDTs) were placed at the mid of each span to measure the deflection. A displacement control data logger was used to record the load, the strains and the displacement through the load cell, strain gauges and LVDTs, respectively. The data logger was adjusted to record data at every 0.1-mm step. A white wash was applied over the surface of the UHPC slab to facilitate identifying the development of cracks.

Figure 4.35: Lateral bracing for the compression/bottom flange at interior support to prevent lateral-torsional buckling.

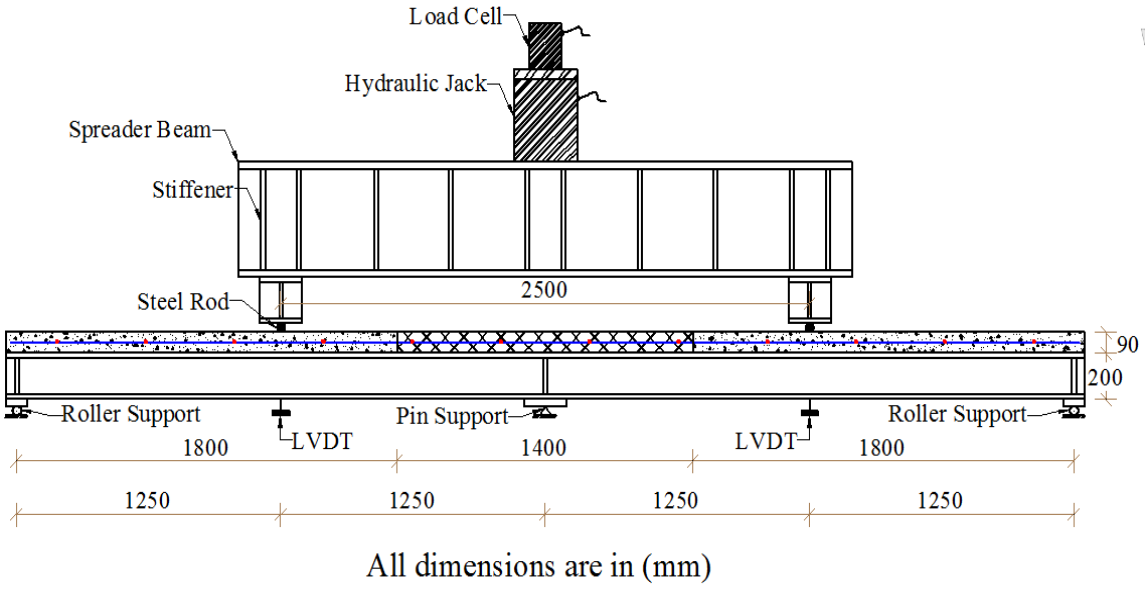

Figure 4.36: Schematic diagram for the test set-up.

Figure 4.37: Experimental test set-up.

Figure 4.38: Measuring deflection at mid-span by LVDT.

CHAPTER FIVE

EXPERIMENTAL RESULTS AND DISCUSSION

A total of four two-span composite girders were prepared and tested experimentally to evaluate the effectiveness of the UHPC slab and the degree of shear connection at the hogging moment zone on the behavior of the composite girders. All girders have the same thickness (90-mm) of NC and the same shear studs' spacing at sagging moment zone, as shown in Figure 5.1. The dimensions of both NC and UHPC are shown in Figure 5.2. At the hogging moment zone, girders (G1, G2 and G3) have same stud spacing of 127 mm, whereas girder G4 has stud spacing of 228 mm. At the hogging moment zone, only girder G3 slab was cast in two stages. The bottom 45 mm thickness of the slab was NC and top 45 mm thickness of the slab was UHPC. Table 5.1 summarizes the studs' spacing and the thickness of the NC and the UHPC at the hogging moment zone for the four girders. Figure 5.3 and Figure 5.4 illustrate the hogging moment region along with the considered variables.

The two-span continuous girders were tested under equal point loads applied at the mid of each span, as shown in Figure 5.5. The results obtained from the experimental investigation are briefly discussed in the following sections. Results include load versus mid-span deflection curves, cracking and yielding loads, strain distribution, ultimate moment capacity and failure mode.

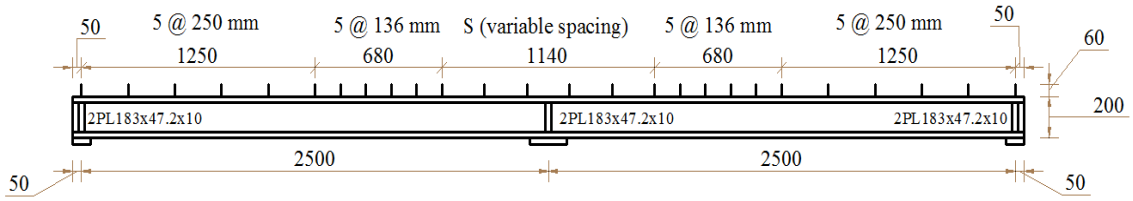

Figure 5.1: Detailed dimensions of the fabricated steel girder along with shear studs' spacing.

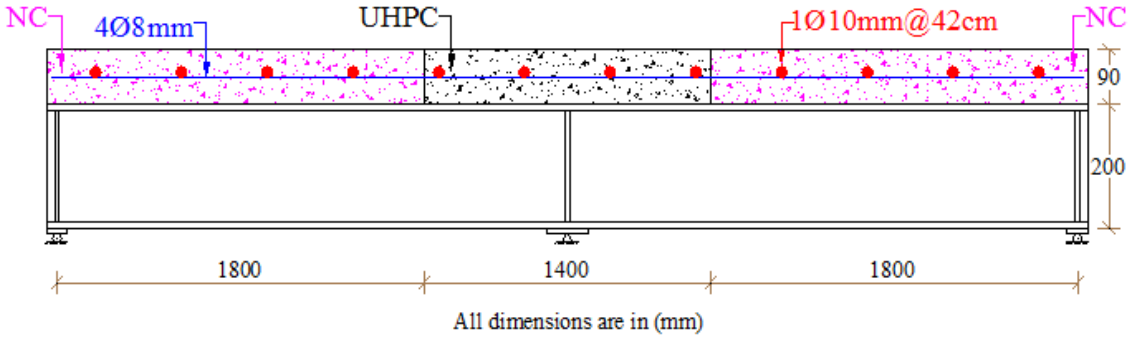

Figure 5.2: Detailed dimensions of the composite steel-concrete girder.

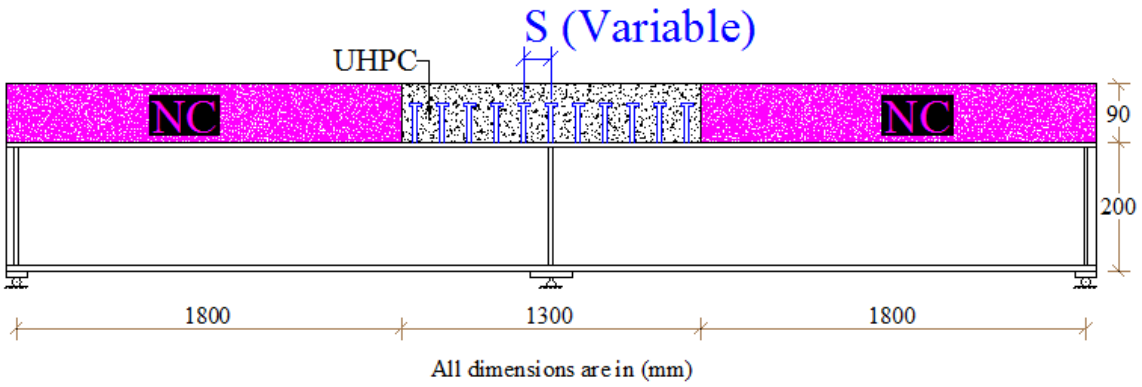

Figure 5.3: Varying the spacing between shear connectors at hogging moment zone.

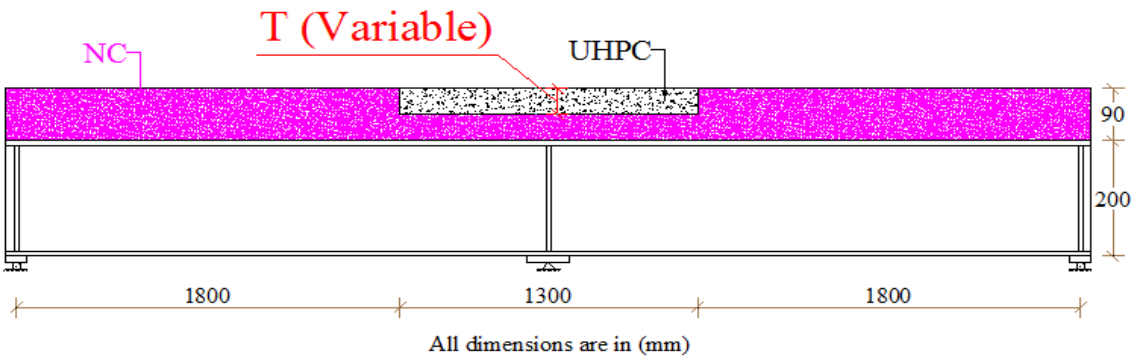

Figure 5.4: Varying the UHPC slab thickness at hogging moment zone.

Table 5.1: Studs' spacing and thickness of NC & UHPC at hogging moment zone.

Girder No.	Stud Spacing (mm)	UHPC Thickness (mm)	NC Thickness (mm)
G1	127	0	90
G2	127	90	0
G3	127	45	45
G4	228	90	0

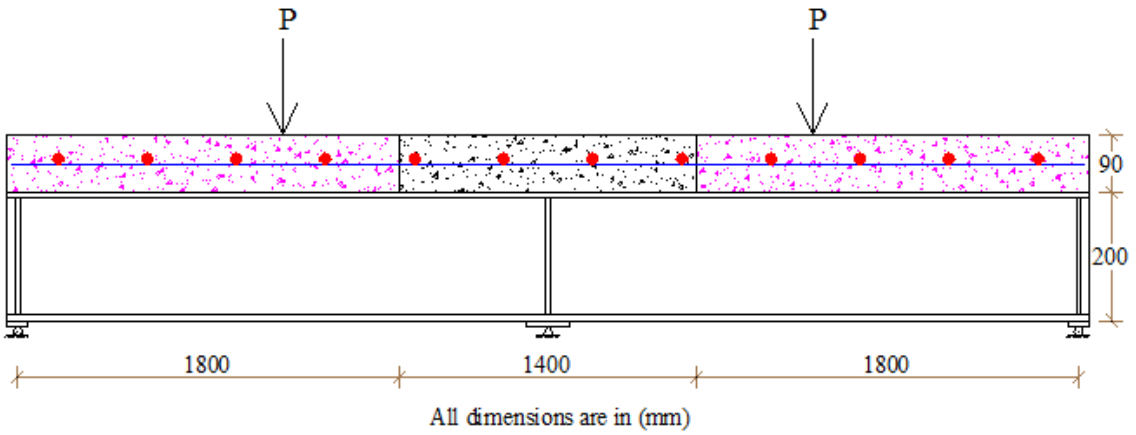

Figure 5.5: Equal point loads applied at the mid of each span.

5.1 Behavior of Continuous Composite Girders

The overall behavior of the composite girders is represented by the load-displacement curves, as shown in Figure 5.6. It is composed of two parts: (a) linear behavior, (b) nonlinear behavior. The linear behavior of the girders was observed at the early stage of loading where all materials were behaving within the linear-elastic region. The elastic stiffness, toughness, ductility and ultimate capacity of girders are important performance indexes which can be evaluated from the load-deflection curves. The elastic stiffness is defined as the load increment corresponds to the unit of deflection. The stiffness of girders was evaluated and shown in Table 5.2 along with the percentage increase in stiffness compared to girder G1. It is demonstrated that the girders exhibited different levels of elastic stiffness. Girder G2 has the highest stiffness because of the full degree of shear connection and full UHPC thickness at the hogging moment zone; whereas the stiffness of girders G4 and G3 is lower than G2 due to the partial degree of shear connection and the partial thickness of the UHPC slab at the hogging moment zone, respectively. It can be concluded that the full degree of shear connection and full UHPC thickness at the hogging moment zone significantly enhanced the elastic stiffness of composite girders.

Toughness is the ability of a girder to absorb energy and plastically deform without fracturing. A girder should withstand both high stresses and high strains. Generally, strength indicates how much force the girder can support, while toughness indicates how much energy a girder can absorb before rupturing. Toughness of a girder is defined as the area under the load-deflection curves. As illustrated in Figure 5.6, girder G2 has the highest

toughness compared to the other girders (G1, G3 and G4) due to the full thickness of UHPC slab at hogging moment zone.

Ductility of a girder is the ability of the beam to deform beyond its yielding point without significant strength loss. It can be expressed in terms of displacement, rotation, or curvature ratios of the maximum useable deformation to that at yield. It is observed that the ductility of composite girders is affected by the UHPC thickness and degree of shear connection at hogging moment zone. Girders G1 and G2 have the lowest and highest ductility, respectively, as shown in Figure 5.6. The lowest ductility of girder G1 is due to the brittleness of the NC slab at the hogging moment zone, whereas Girder G2 has the highest ductility due to the large ductility of the UHPC slab at the hogging moment zone. The UHPC has a large degree of ductility compared to the NC because of the use of small-size steel fibers. Girder G3 has a lower ductility compared to G2 because its concrete slab was cast with half depth UHPC at hogging moment zone. Although girder G4 has full UHPC thickness at hogging moment zone, a reduction in its ductility is noticed because of the partial degree of shear connection at hogging moment zone.

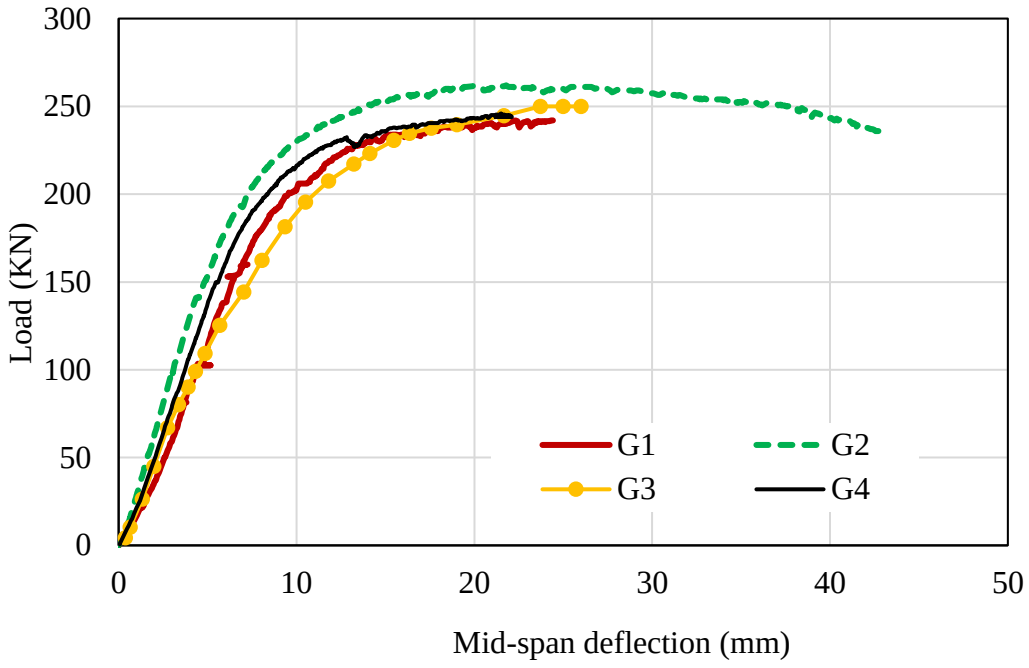

Figure 5.6: Load-displacement curves obtained from experimental testing.

For the ultimate stage, the obtained ultimate strength for the girders is summarized in Table 5.2. It is shown that the maximum improvement in ultimate capacity is 8% for girder G2 compared to G1 due to its full degree of shear connection and full UHPC thickness at hogging zone. The slight variation in the ultimate load was due to the fact that all girders failed due to the shear-compression failure in the NC slab at the mid-span, as shown in Figure 5.7. The neutral axis at the mid-span section gradually shifted upward within the NC slab causing an increase in the compressive stress on the NC. Crushing failure in the NC at the mid-span took place at the instant the stress on the top of the slab exceeded 0.85 fc'.

Table 5.2: Stiffness of continuous composite girders along with ultimate capacity.

Girder	Stiffness (kN/mm)	Percentage Increase	Ultimate load (Pu) (kN)
G1	22	-	242
G2	34	55%	262
G3	22.5	2%	250
G4	27	23%	247

Regarding the hogging moment zone, the developed cracks in the concrete slab are shown in Figure 5.8 for all of girders. It is shown that the NC slab of girder G1 over the interior support cracked and lost its action before reaching the ultimate. While, fine cracks were developed in UHPC slab of G2 due to its full degree of shear connection and full UHPC thickness at hogging zone. In regards to G3, the UHPC layer over the interior support lost its action at an early stage of loading at the instant when it cracked and delaminated, as shown in Figure 5.8. This can be attributed to the inadequate shear connection at the interface between the NC and UHPC layers to prevent debonding. This premature failure limited the full utilization of the UHPC slab to maintain the composite action for the higher load. For girder G4, its cracks are wider than that of G2 due to its partial degree of shear connection at hogging zone.

Figure 5.7: Shear-compression failure at mid-span.

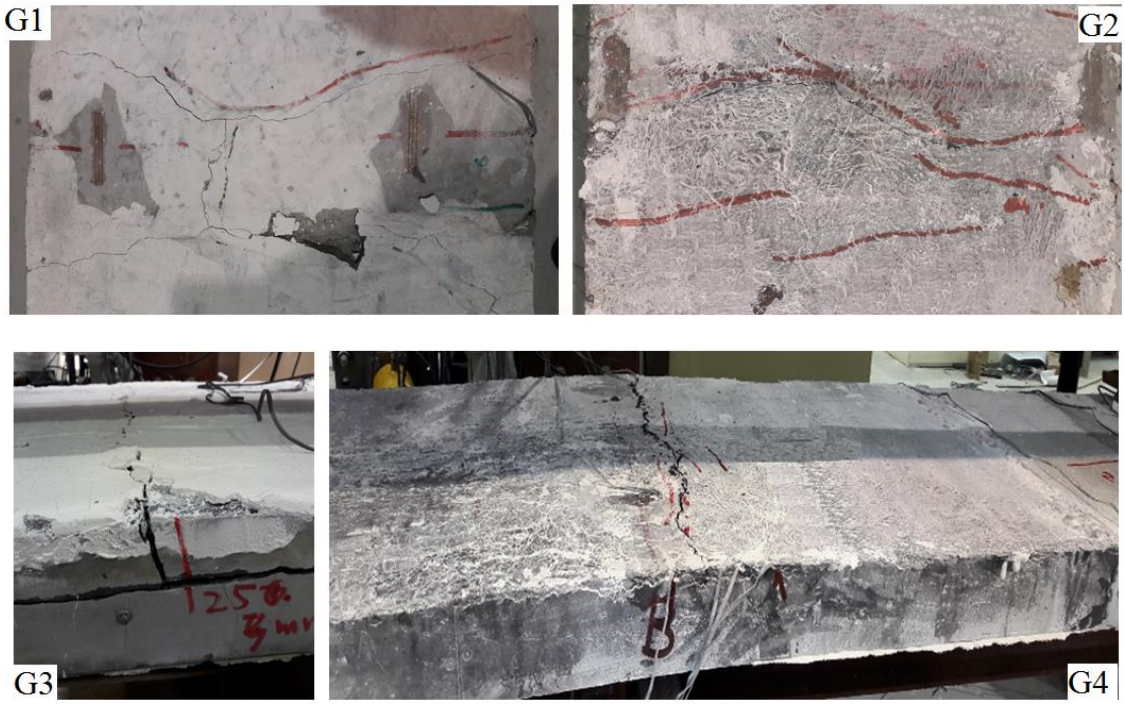

Figure 5.8: Developed cracks in concrete slab over the interior support for all girders at failure stage.

5.2 Maximum Service Load and Composite Action at Hogging Moment Zone

5.2.1 Maximum Service Load

The maximum service load of continuous composite girders is controlled by either cracking or yielding loads. The smaller between cracking and yielding loads governs the service load limit. The cracking load (P_{cr}) is defined as the load at which the first crack initiates in the concrete slab over the interior support. While, yielding load (P_y) is the load at which yielding of the bottom flanges of the steel section at mid-span occurs. The values of cracking and yielding loads are summarized in Table 5.3 along with the maximum service load. It was observed that the first crack in the two-span girders occurred transversely across the concrete slab over the interior support and subsequent cracks were developed immediately adjacent to the first crack.

The service load limit of girder G1 was controlled by cracking of concrete; whereas it was governed by yielding of steel for the girders (G2, G3 and G4). This is attributed to the effectiveness of the UHPC in resisting the initiation and propagation of the cracks at early stage of loading. It was noticed that girder G2 had the greatest service load compared to G1 because it had full degree of shear connection and full UHPC thickness at hogging zone. Although girder G4 had full thickness of UHPC at hogging zone, its service load is lower than G2 because it had partial degree of shear connection at hogging moment zone. For girder G3, its service load is lower than that of G2 because of the partial UHPC thickness at hogging zone. Slight enhancement was obtained in the service load due to the

variation in the degree of shear connection and UHPC thickness at hogging zone. It is because of service load was controlled by yielding of the steel at mid-span section which is identical for all girders.

5.2.2 Composite Action at Hogging Moment Zone

The ratio of cracking load to yielding load, λ, is taken as the indicator of the loading level up to which composite action is maintained at the hogging moment zone under service load. The higher values of λ would indicate higher load level to cause cracking of the slab. The values of P_{cr} and P_y, recorded from test observations, are shown in Table 5.3 along with λ values.

The value of λ is higher than one for girders (G2, G3 and G4), as shown in Table 5.3. This clearly confirms the effectiveness of the UHPC slab in maintaining the composite action at the hogging moment zone at a load much higher than the upper service load limit. Whereas girder G1 has λ value less than one which indicates that it lost its composite action early due to the poor resistance of NC to tensile stresses. Girder G3 has a λ value close to one which represents a satisfactory UHPC slab thickness necessary to maintain the composite action at hogging moment zone under the service load. Therefore, it can be concluded that using half-depth UHPC slab thickness at hogging moment zone is sufficient to achieve the desired performance of the continuous composite girders.

Table 5.3: Summary of experimental cracking, yielding and maximum service loads.

Girder	P_{cr} (kN)	P_y (kN)	Maximum Service Load (kN)	Service Load Limit State	$\lambda = P_{cr}/P_y$
G1	57	171	57	Cracking	0.33
G2	247	188	188	Yielding	1.31
G3	186	175	175	Yielding	1.06
G4	215	179	179	Yielding	1.20

5.3 Strain Distribution

The strain distribution at the interior support section for the girders (G2 and G4) at a service load of 50-kN is shown in Figure 5.9. Two straight lines were used to fit the strain within the concrete slab and the steel section. It was noticed that the two straight lines are not collinear. This is attributed to the relative slip at the interface between the concrete slab and the steel beam. It is demonstrated from Figure 5.9 that girder G4 has a higher slip than G2 at the interior support section because it has a partial degree of shear connection. Although girder G2 has full degree of shear connection at hogging zone, it has a little slip due to the ductility and deformation of shear connectors. Moreover, girder G4 experienced higher rotation than G2 over the interior support because of its partial degree of shear connection at hogging moment zone. Regarding the ultimate stage, the strain measurements at the mid-span and the interior support sections of the four girders are given by Figure 5.10 and Figure 5.11, respectively. These strain values will be used to evaluate the bending moment capacity (Section5.4) for the two sections to predict the theoretical failure load based on plastic analysis (Section5.5).

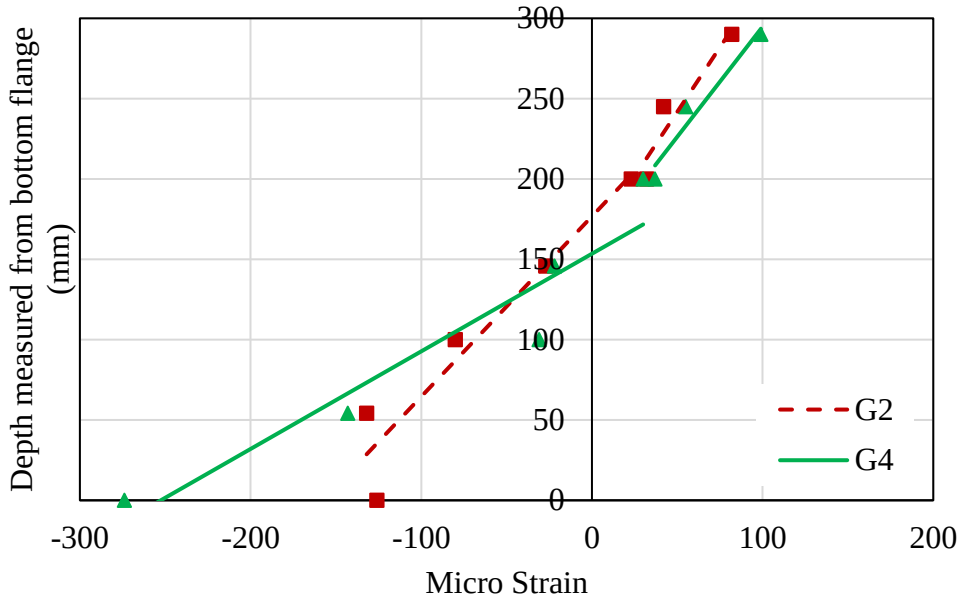

Figure 5.9: Experimental strain distribution over interior support section within the service condition.

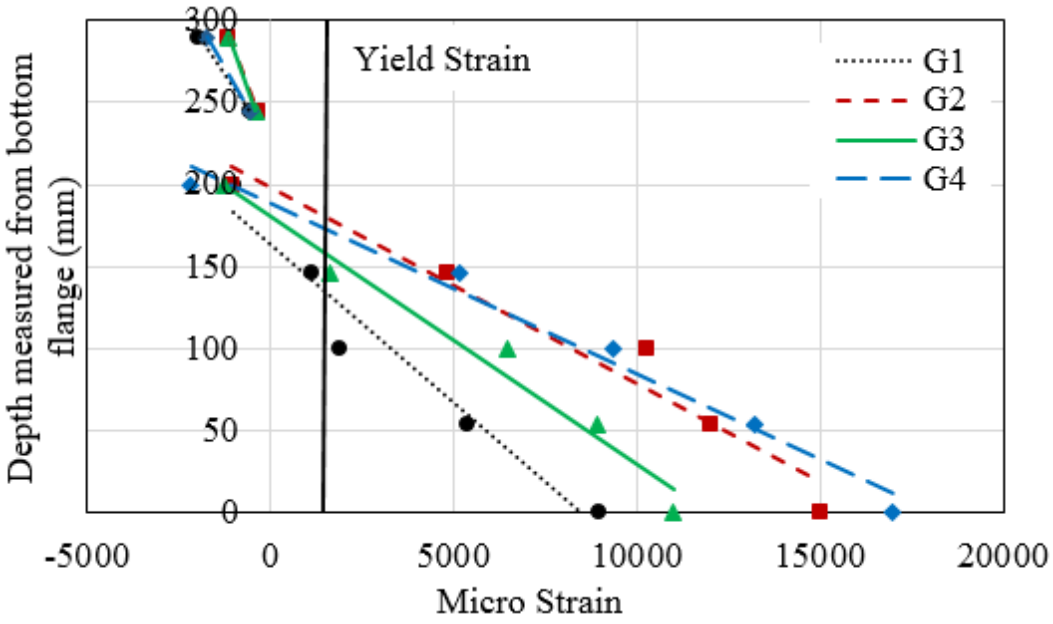

Figure 5.10: Experimental strain distribution at mid-span section at ultimate stage.

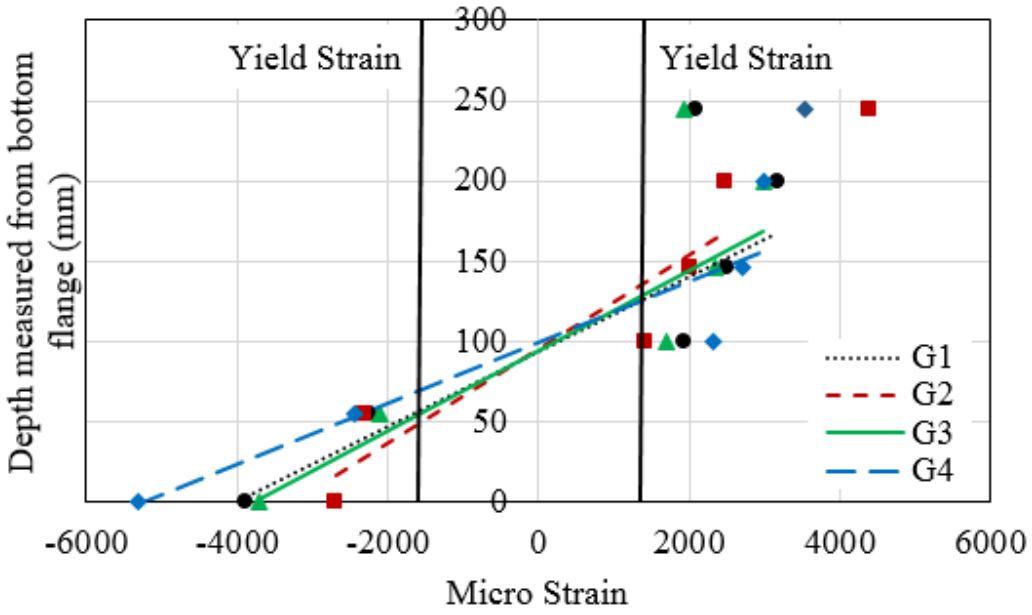

Figure 5.11: Experimental strain distribution over interior support section at ultimate stage.

5.4 Ultimate Moment Capacity

Based on the measured strain, the moment capacities of the girders at positive moment locations (M^*_{+ve}) and negative moment locations (M^*_{-ve}) were calculated and listed in Table 5.4.

Theoretical values for the girder's ultimate positive and negative moment capacities were evaluated as follows, assuming the stress distributions shown in Figure 5.12 and Figure 5.13, which corresponded to the elastic-plastic behavior of the steel without strain hardening:

$$\bar{M}_{+ve} = C_{sr} \times d_1 + C_{cc} \times d_2 + T_s \times d_3 \quad (5.1)$$

$$\bar{M}_{-ve} = T_{sr} \times d_1 + C_s \times d_3 + T_s \times d_4 \quad (5.2)$$

$$\bar{M}_{-ve} = T_{sr} \times d_1 + T_{UHPC} \times d_2 + C_s \times d_3 + T_s \times d_4 \quad (5.3)$$

where C_{sr}= the compressive force in the reinforcements steel;

C_{cc} = the compressive force in the NC slab;

C_s = the compressive force in the steel section;

T_{sr} = the tensile force in the reinforcement steel;

T_s = the tensile force in the steel section; and

T_{UHPC} = the tensile force in the UHPC slab.

Eq. (5.2) is used to evaluate the ultimate moment capacity with no UHPC at the hogging zone. While Eq. (5.3) includes the contribution of the UHPC slab in the hogging moment capacity. Theoretical values for $\bar{M}_{+ve}$ and $\bar{M}_{-ve}$ are shown in Table 5.4.

It is concluded that the ultimate moment capacities (M^*_{+ve} & M^*_{-ve}) evaluated based on the experimental strain measurements (Figure 5.10 and Figure 5.11) are higher than the theoretical values ($\bar{M}_{+ve}$ & $\bar{M}_{-ve}$), as demonstrated in Table 5.4. This can be attributed to ignoring the material strain-hardening behavior in the theoretical approach.

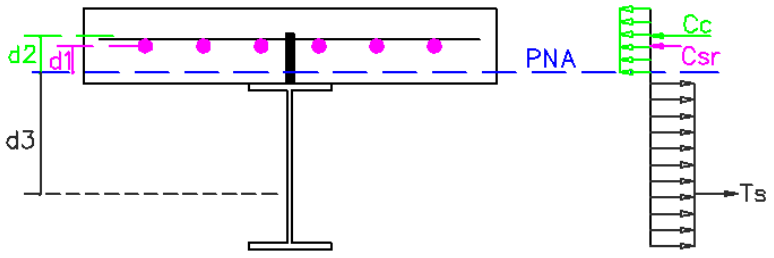

Figure 5.12: Stress distribution at sagging moment section at ultimate condition.

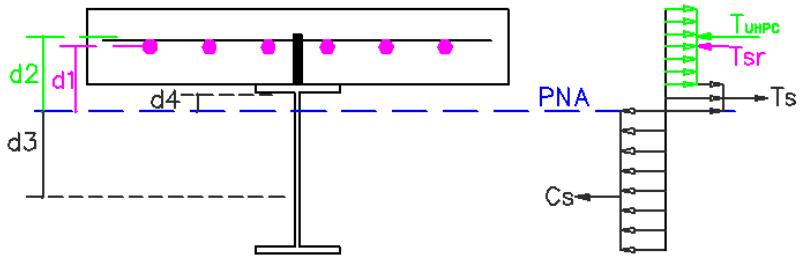

Figure 5.13: Stress distribution at hogging moment section at ultimate condition.

5.5 Plastic Analysis

Plastic analysis is used to predict the flexural failure load for the two-span continuous composite girders. The theoretical value of the load (P_f) necessary to cause failure in the composite girders is given as:

$$P_f = \left[\frac{2(2\alpha+1)}{L}\right] M_{-ve} \qquad (5.4)$$

where L = the span length;

M_{-ve} = the hogging moment capacity; and

α = the ratio between the sagging and the hogging moment capacity.

The evaluated failure loads (P_f^*) based on the experimental strain measurements and the theoretical failure loads ($\overline{P}_f$) assuming elastic-perfect plastic material behavior are summarized in Table 5.4 along with the experimental failure loads (P_u). Table 5.4 demonstrates that the predicted ultimate loads ($\overline{P}_f$, P_f^*) calculated using Eq. (5.4) are lower than the actual failure load (P_u) obtained from the experimental testing. Plastic analysis underestimates the failure load and leads to safe and reasonable load expectation. The

obtained failure load ($\bar{P}_f$) based on the elastic-plastic material is lower than that (P_f^*) obtained using experimental strain measurements due to ignoring the material strain hardening.

Table 5.4: Expected moment capacities at sagging & hogging moment zones with the corresponding failure loads.

Girder	P_u (kN)	M^*_{+ve} (kN.m)	M^*_{-ve} (kN.m)	α	P_f^* (kN)	P_f^*/P_u	$\bar{M}_{+ve}$ (kN.m)	$\bar{M}_{-ve}$ (kN.m)	α	$\bar{P}_f$ (kN)	$\bar{P}_f/P_u$
G1	242	111.8	71.8	1.557	236.3	98%	109.01	71.63	1.522	231.7	96%
G2	262	117.9	89.2	1.322	260	99%	109.01	96.02	1.135	251.2	96%
G3	250	112.5	78.6	1.431	242.9	97%	109.01	76.72	1.421	235.8	94%
G4	247	110.5	84.6	1.306	244.5	99%	109.01	75.8	1.438	235.1	95%

CHAPTER SIX

FINITE ELEMENT MODELING OF COMPOSITE GIRDERS

6.1 Introduction

Finite element (FE) modeling is another technique for investigating the behavior of new structural elements such as continuous composite girders. It is a powerful method capable of predicting the behavior of girders including load-displacement curves, cracking load, yielding load and mode of failure. FE modeling assumes that the materials used in modeling of composite girders are perfectly homogeneous. Therefore, its results depend mainly on the accuracy of the assumptions. The size of elements affects the results as well. The commercially available FE software (ABAQUS) [17] was used to model the continuous composite girders. The developed model included material and geometrical nonlinearities.

A 3D FE model of the continuous composite girders with UHPC slab at hogging moment zone was developed utilizing ABAQUS software [17]. The developed model was validated with the obtained experimental results. The suitable mesh and interface contact were used to predict the actual behavior of the composite girders.

The verified model was utilized to investigate the effectiveness of the UHPC slab to maintain the composite action at hogging moment zone. In addition, a parametric study was performed to evaluate the effects of the degree of shear connection, thickness and length of UHPC slab at hogging moment zone on the behavior of continuous composite girders.

6.2 Modeling of Continuous Composite Girders with UHPC Slab

A brief description of FE modeling of the two-span continuous composite girders with UHPC slab at hogging moment zone is presented in this section. The four girders, presented in CHAPTER Five, were modeled for the purpose of validation of the developed models. The validated model was modified to investigate the behavior of composite girders with different degrees of shear connection, and thicknesses and lengths of UHPC slab at hogging moment zone.

6.2.1 Geometry and Elements Types

The continuous composite girder is composed of different components such as NC slab, UHPC slab, I-beam, reinforcement bars, transverse stiffeners, bearing plates over supports and under the applied load and shear studs. Those components were modeled as 3-D element with their actual size except the reinforcements which were modeled as truss elements. Types of elements are the eight-node linear brick element (C3D8R) which was used to model the solid elements, and the two-node linear 3-D truss (T3D2) element which was utilized for the longitudinal and transverse slab reinforcements. All components were assembled together to form the complete continuous composite girder with its actual dimensions. Figure 6.1 shows the assembled composite steel-concrete girder.

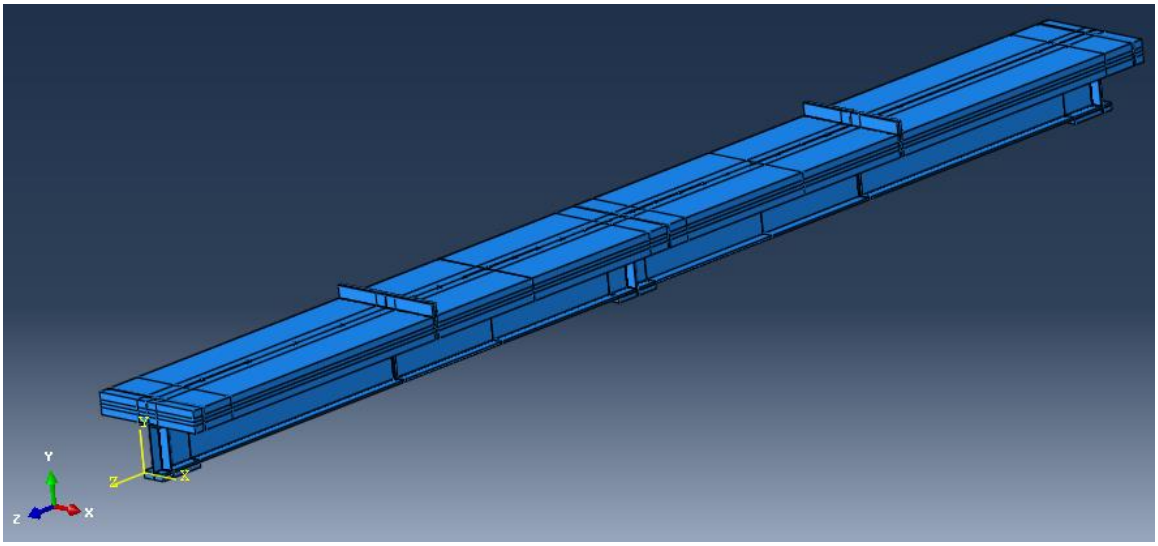

Figure 6.1: The developed 3D FE model.

6.2.2 Materials Modeling

The assembled continuous composite girders are composed of different parts of different material properties such as NC, UHPC, slab reinforcements and structural steel. Material models are explained briefly in the following subsections.

6.2.2.1 NC and UHPC

The behavior of quasi-brittle of NC and UHPC can be simulated by many conceptual models available in the literature, which include discrete crack model, smeared crack model and concrete damage plasticity model (CDP). In this study, the CDP model as developed by Lubliner et al. [60] and extended by Lee and Fenves [61] was utilized to simulate the behavior of concrete in both tension and compression. ABAQUS was used to model the behavior of composite girders based on material input parameters of NC and UHPC. The experimentally obtained stress-strain curves, presented in section 4.2.1, were used in modeling of both NC and UHPC.

The input of CDP model is the stress-inelastic strain shown in Figure 6.2 to Figure 6.5 and the parameters shown in Table 6.1. The linear elastic part was modeled by the Young's modulus (E) and the Poisson's ratio (ν).

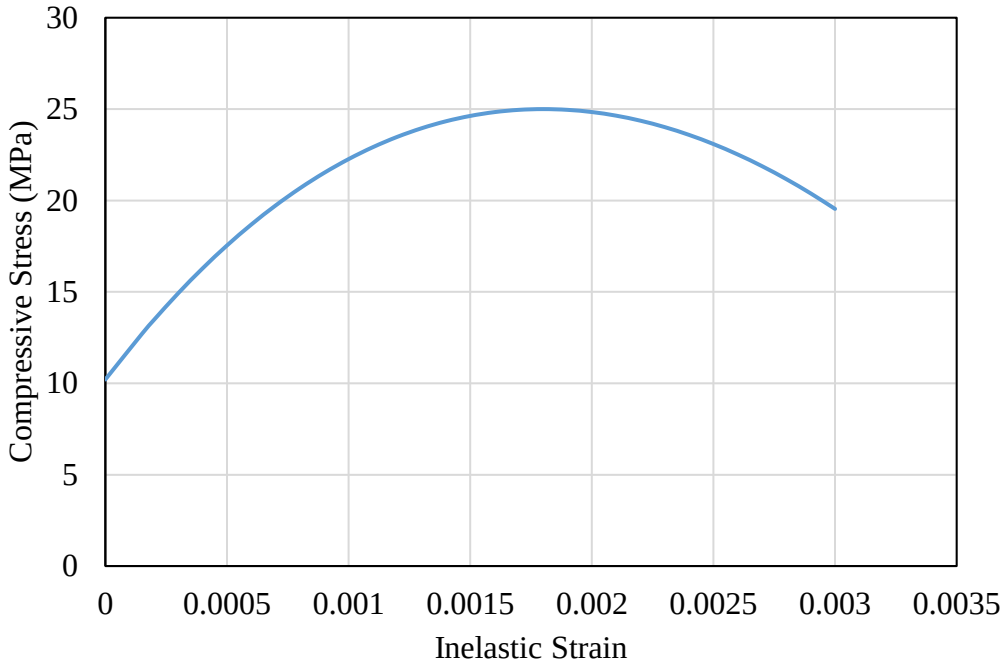

Figure 6.2: Compressive stress-inelastic strain relationship for NC.

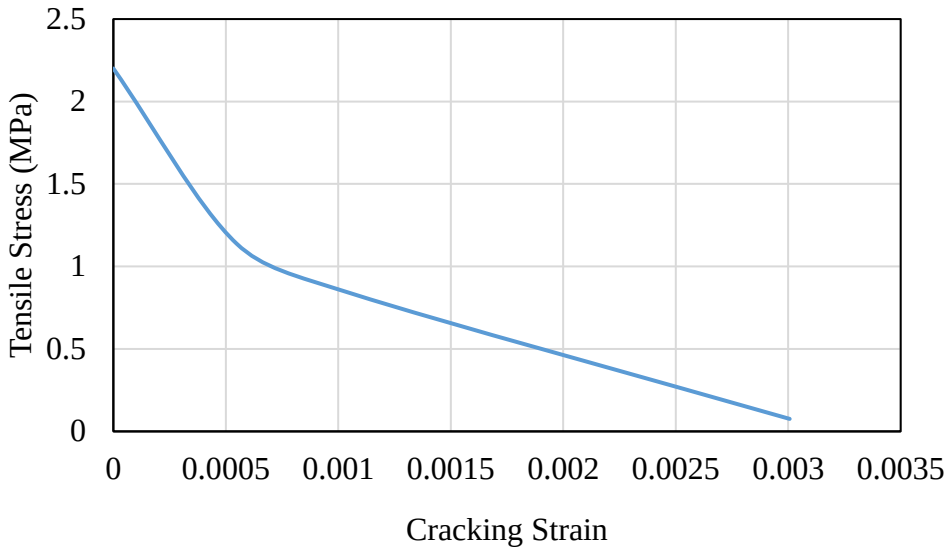

Figure 6.3: Tensile stress-cracking strain relationship for NC.

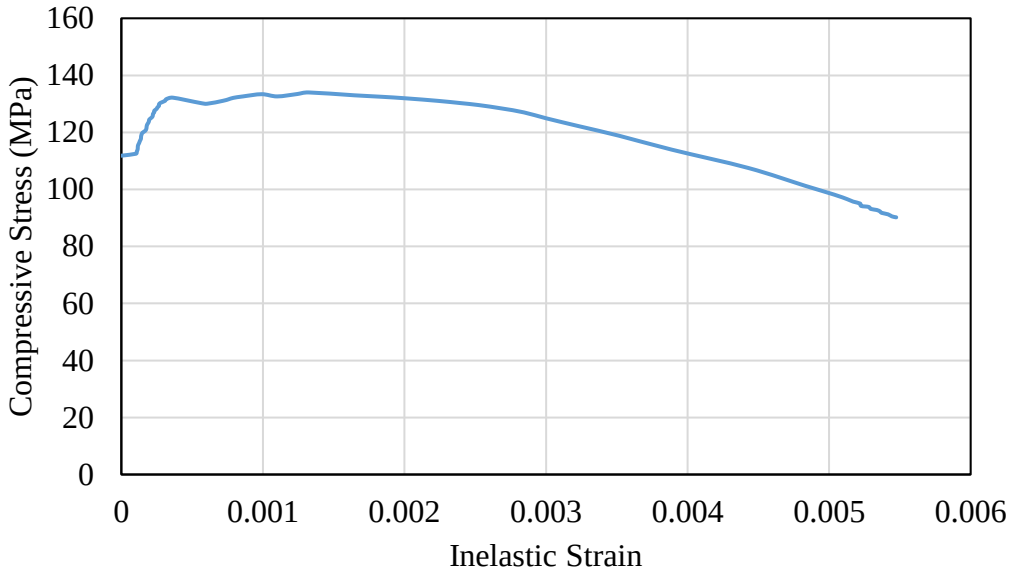

Figure 6.4: Compressive stress-inelastic strain relationship for UHPC.

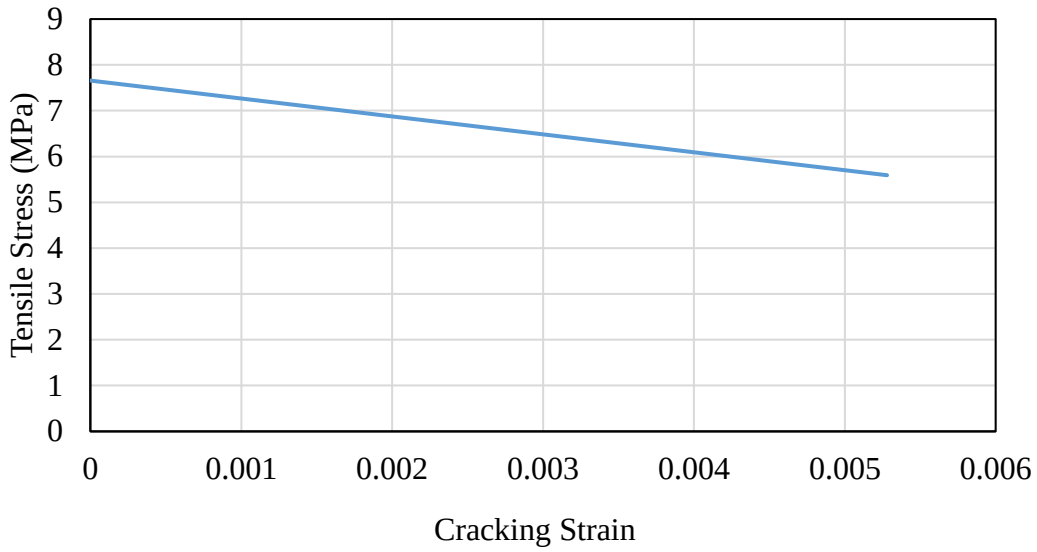

Figure 6.5: Tensile stress-cracking strain relationship for UHPC.

Table 6.1: Input parameters for the CDP model.

	Density	Young's Modulus	Poisson's Ratio	Dilatation Angle	Eccentricity	F_{bo}/f_{co}	K	Viscosity parameter
NC	2.45E-6	20283	0.199	36	0.1	1.16	0.67	0
UHPC	2.50E-6	47000	0.16	36	0.1	1.16	0.67	0

Concrete damage parameters d_c and d_t that were used to simulate the cracking in compression and tension, respectively are proposed by (Birtel and Mark 2006 [62]) and given by Eqs. (6.1) & (6.2).

$$d_c = 1 - \frac{f_c\, E_c^{-1}}{\varepsilon_c^{pl}\left(\frac{1}{b_c}-1\right)+f_c\, E_c^{-1}} \qquad (6.1)$$

where d_c = Concrete compression damage parameter;

f_c = Compressive stress;

E_c = Modulus of elasticity of concrete;

ε_c^{pl} = Plastic strain corresponding to compressive strength; and

b_c = Constant ranges $0 < b_c < 1$.

$$d_t = 1 - \frac{f_t E_c^{-1}}{\varepsilon_t^{pl}\left(\frac{1}{b_t} - 1\right) + f_t E_c^{-1}} \quad (6.2)$$

where d_t = Concrete tension damage parameter;

f_t = Tensile stress;

E_c = Modulus of elasticity of concrete;

ε_t^{pl} = Plastic strain corresponding to Tensile strength; and

b_t = Constant ranges $0 < b_t < 1$.

6.2.2.2 Structural steel and Reinforcement Steel

Structural steel and steel reinforcements were modeled utilizing isotropic plasticity model. The two materials were modeled as elastic-plastic material including material strain hardening. The elastic behavior was represented by the Young's modulus (E) and Poisson's ratio (ν). While, the full stress-inelastic strain curve was used to model the nonlinear/plastic behavior. Table 6.2 summarizes the mechanical properties of different steel materials. Figure 6.6 and Figure 6.7 show the stress versus inelastic strain relationship for structural steel and steel reinforcements, respectively.

Table 6.2: Summary of the mechanical properties of the structural steel and reinforcement steel.

Mechanical Property	Structural steel	Reinforcement steel
Yield Strength (MPa)	306	555
Ultimate Strength (MPa)	425	585
Poisson's Ratio (ν)	0.27	0.3
Young's Modulus (GPa)	193	171

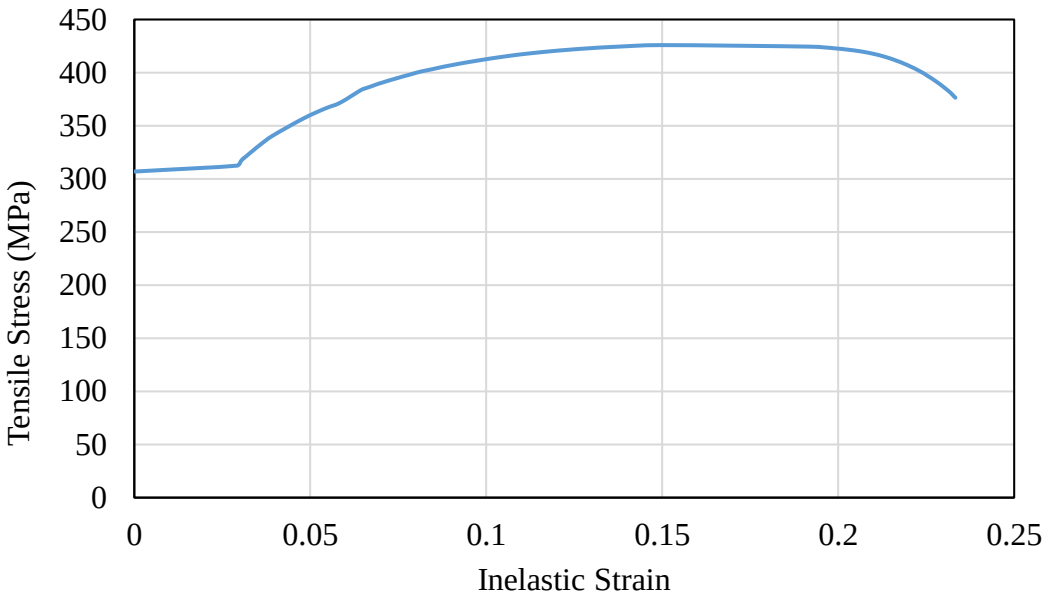

Figure 6.6: Tensile stress-inelastic strain relationship for structural steel.

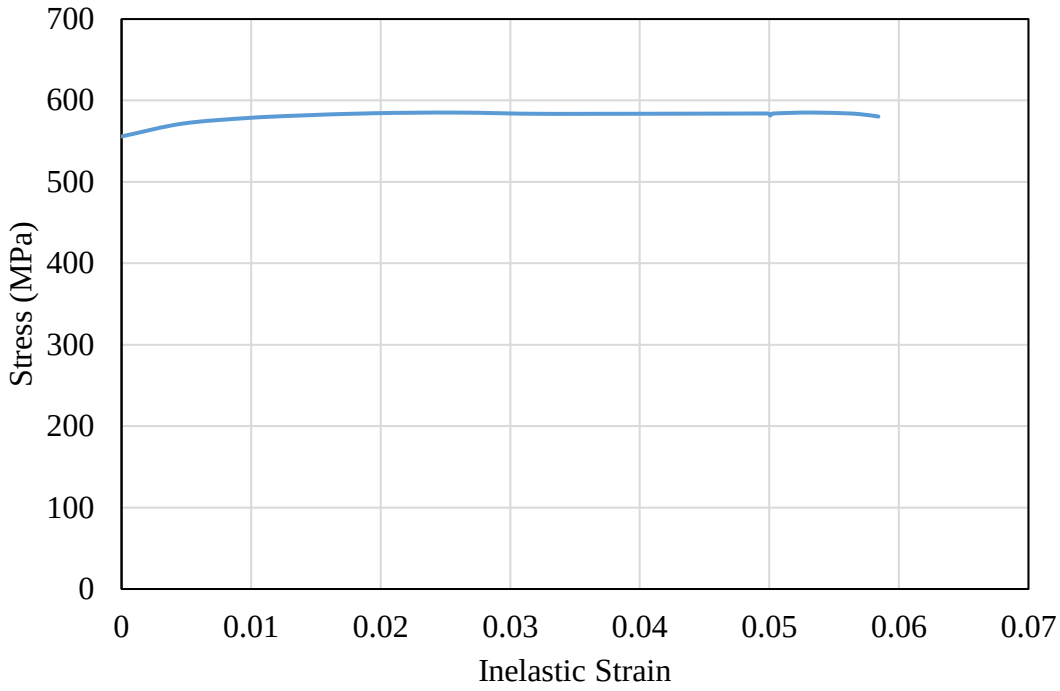

Figure 6.7: Tensile stress-inelastic strain relationship for reinforcement steel.

6.2.3 Modeling of Contact Region

The assembled model contains many components which contact each other forming the interfacial zones. The interaction between the components was modeled using surface to surface contact. Different surface to surface models were used to simulate the interaction between reinforcements-concrete slab, shear connectors-concrete slab, shear connectors-steel beam and stiffeners-steel beam.

Tied contact was used to model the surface interaction between shear connectors and stiffeners with steel beam. It was used to simulate the perfect bond between contacted elements. The welded connections between steel beam with shear studs and transverse stiffeners are considered as perfect bond because failure in welding material was not possible to take place.

For the contact between steel reinforcements and concrete slab, embedded contact was used to specify an element or a group of elements that lie embedded in a group of host elements whose response is used to constrain the translational degrees of freedom of the embedded nodes (i.e., nodes of embedded elements). The reinforcements were modeled as the embedded elements while the concrete slab was the host region.

Regarding the contact between shear studs and concrete slab, normal behavior and friction behavior models were used to simulate the interaction between the different elements. The normal behavior with hard contact was used in the normal direction to avoid penetration of shear connectors into the concrete slab, while friction behavior with 0.2-coefficient of friction was utilized in the tangential direction. Also, normal and friction models were used to simulate the friction between NC and UHPC layers at hogging zone with 0.4-coefficient of friction. Friction behavior is used at the interfacial regions where relative slip is possible to take place.

6.2.4 Model Meshing

Meshing of the assembled model is sensitive and requires special attention. The developed model was partitioned and discretized into small elements. Cell partitions was used to divide the irregular parts. Adequate attention was paid in the development of hexahedral mesh. Accuracy of the results depends upon the FE mesh. Therefore, different mesh sizes were tried through the mesh sensitivity analysis prior to converging the final FE mesh shown in Figure 6.8.

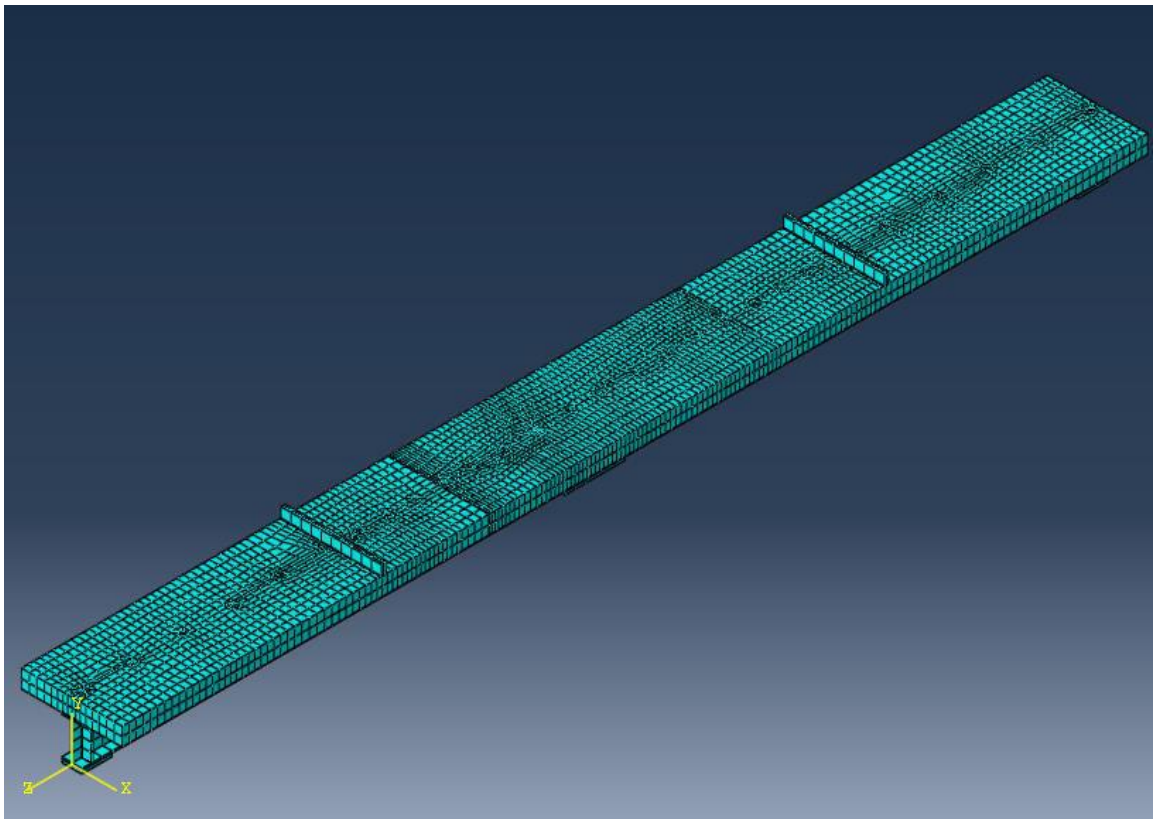

Figure 6.8: Meshing of the developed model of the composite girder.

6.2.5 Boundary Condition and Loading

The concentrated loading has been applied at the mid span as an equivalent pressure over steel plates. The steel plates cover the full width of the concrete slab. Steel plates were used under the applied loads and over the supports to avoid stress concentration in concrete slab and bottom flange of steel beam, respectively. Roller supports at both end of the specimen and rocker at the interior support were used to avoid rigid body motion. Figure 6.9 shows the applied loads at mid-spans and assigned supports.

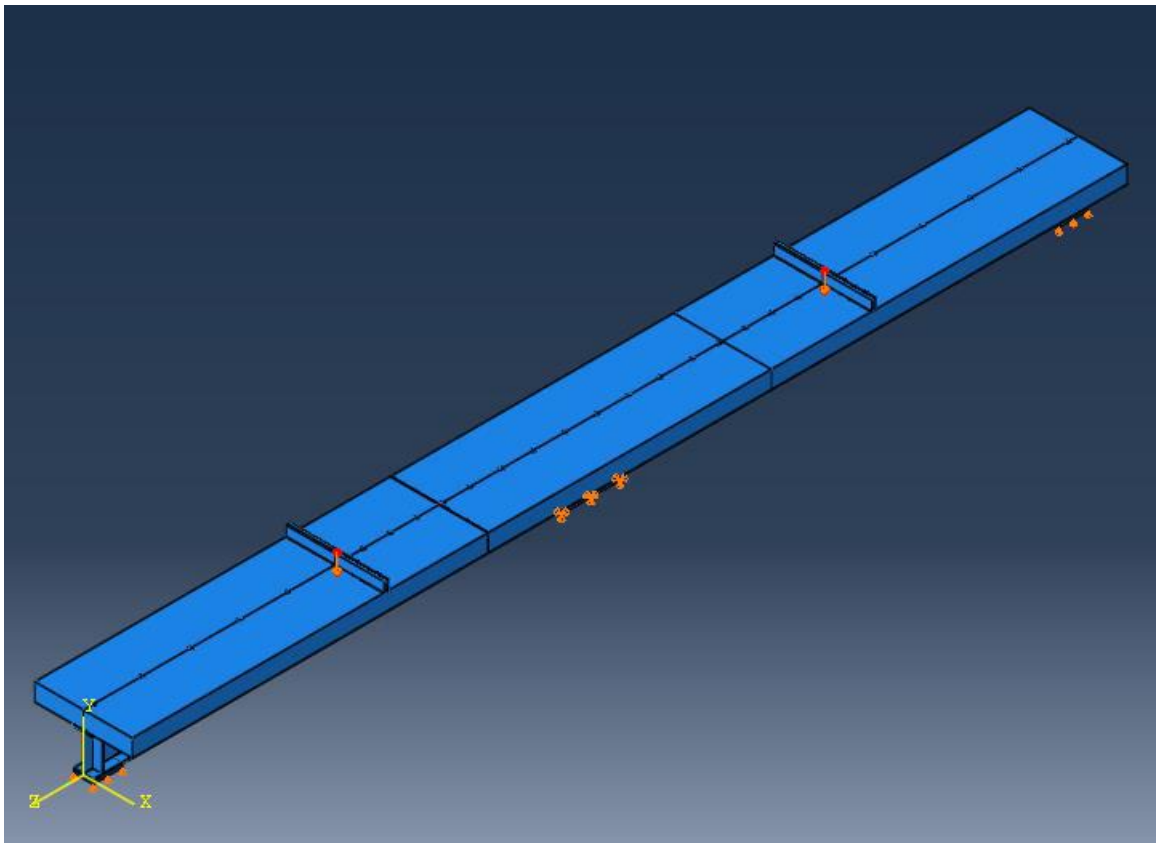

Figure 6.9: Assigned boundary conditions and applied load.

6.3 Validation of the Model

The developed FE model was validated with the results obtained from the experimental testing of the two-span continuous composite girders with UHPC slab at hogging moment zone. The obtained results from the experimental investigation were presented in CHAPTER Five. The experimental load versus mid-span deflection curves, ultimate load, cracking of concrete at hogging moment zone, yielding of steel flange at mid-span and failure mode were utilized to validate the developed FE model. Following subsections present the FE validation.

6.3.1 Load-Deflection Validation

The load versus mid-span deflection curves obtained numerically were compared with the experimental curves, as shown Figure 6.10 to Figure 6.13. Generally, the numerical load-deflection curves showed a good agreement with the experimental ones. The numerical curves had relatively higher stiffness than the experimental ones. The numerically predicted ultimate load was very close to that obtained experimentally. Table 6.3 shows that the maximum percentage difference between the experimental and numerical ultimate loads is 3%.

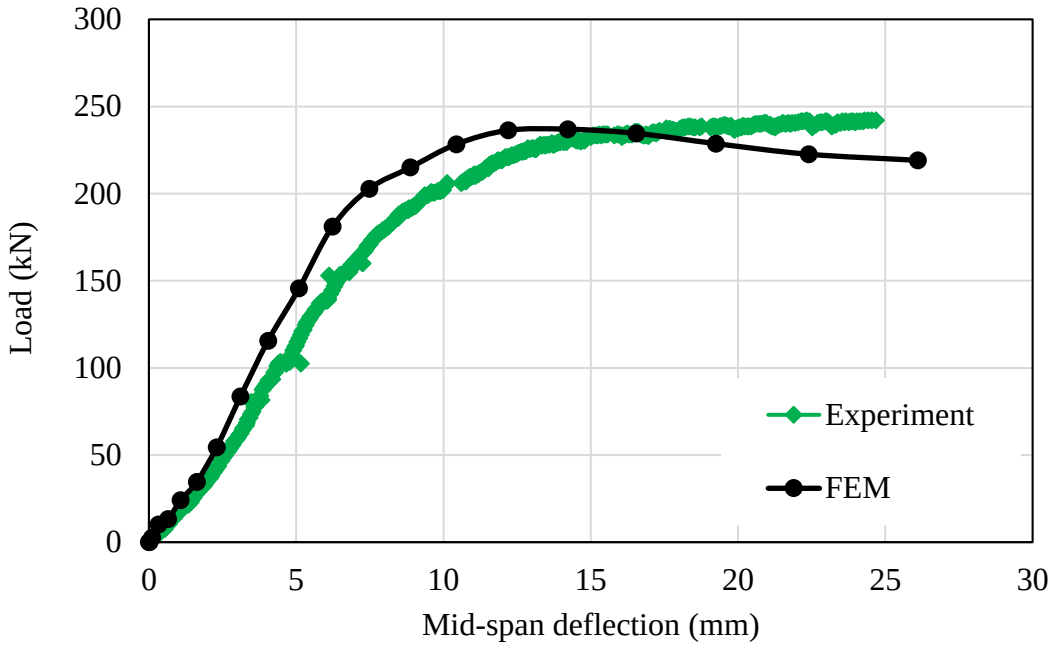

Figure 6.10: Load-displacement curve for girder G1.

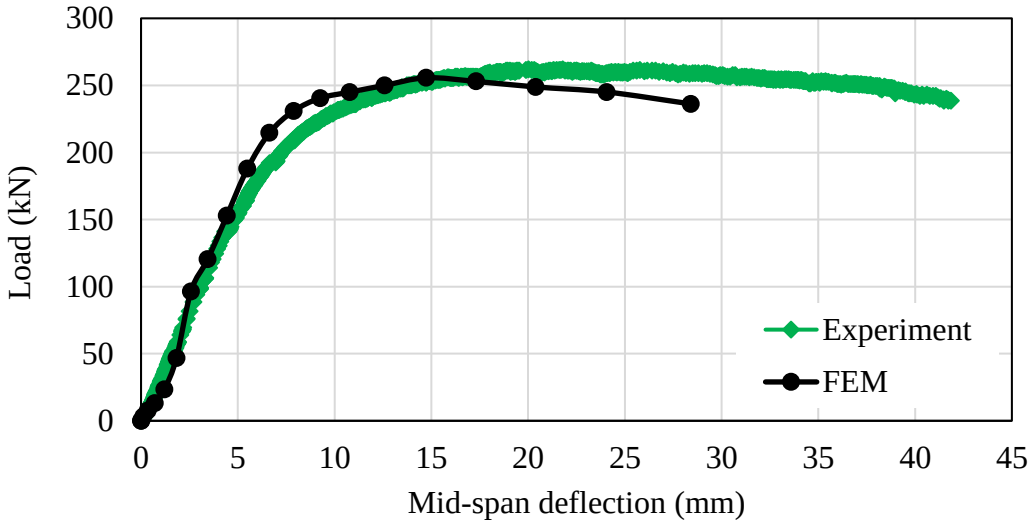

Figure 6.11: Load-displacement curve for girder G2.

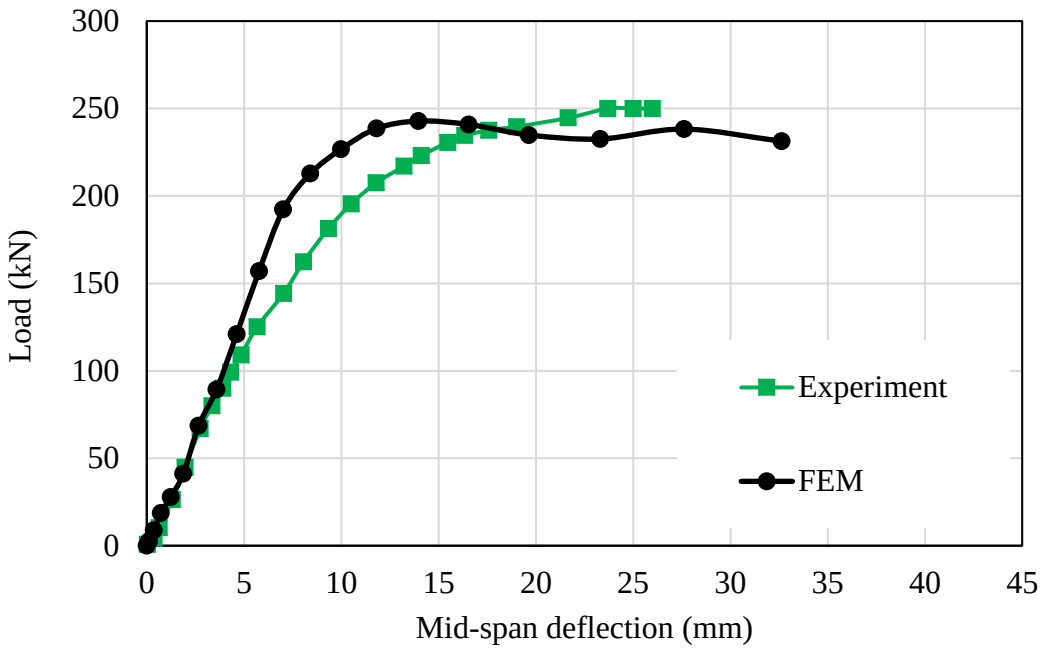

Figure 6.12: Load-displacement curve for girder G3.

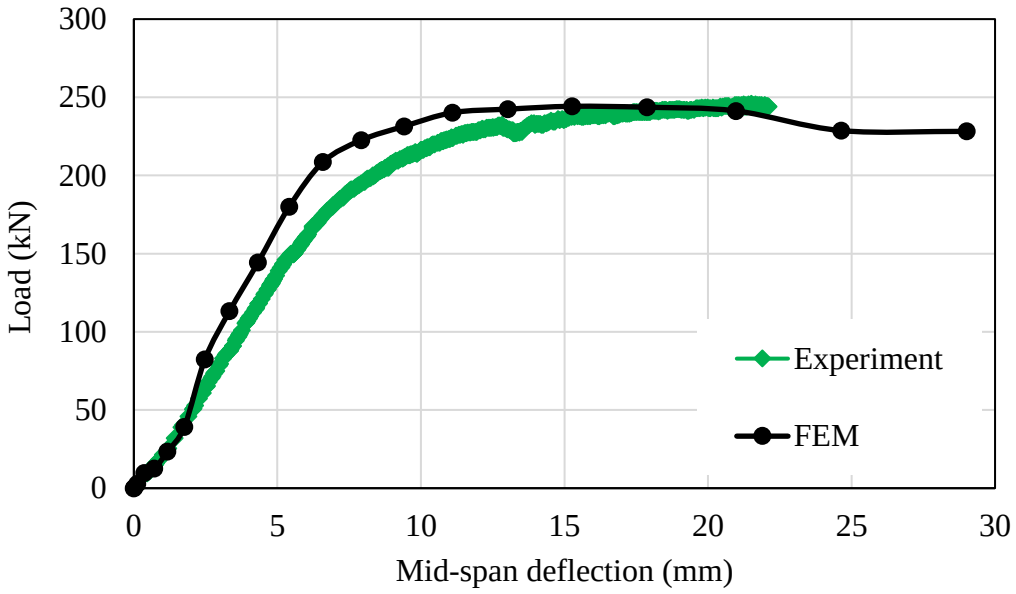

Figure 6.13: Load-displacement curve for girder G4.

Table 6.3: Experimental and numerical ultimate loads.

Girder	P_u (kN)		% Difference
	Exp.	FE	
G1	242	237	2%
G2	262	255.7	2%
G3	250	242.5	3%
G4	247	244	1%

6.3.2 Concrete Cracking & Steel Yielding Validation

The developed FE model was validated through the prediction of cracking and yielding loads. Finite element analysis utilizing concrete damage plasticity model was capable of capturing most of the developed cracks within the concrete slab. Transverse cracks at the UHPC slab and longitudinal cracks along the line of shear studs were captured. FE results showed the ability of the developed model in identifying the experimental cracks. Transverse cracks were observed experimentally and numerically within UHPC slab and shown in Figure 6.14 and Figure 6.15, respectively. In addition, longitudinal cracks were also noticed experimentally and numerically along the line of shear studs, as shown in Figure 6.16 and Figure 6.17, respectively. The numerical and experimental cracking loads are compared and shown in Table 6.4. The maximum difference between experimental and numerical cracking loads is 4%. It is obvious that the developed model was accurate enough in predicting the cracking load.

Figure 6.14: Experimentally observed cracks in UHPC slab at hogging moment zone.

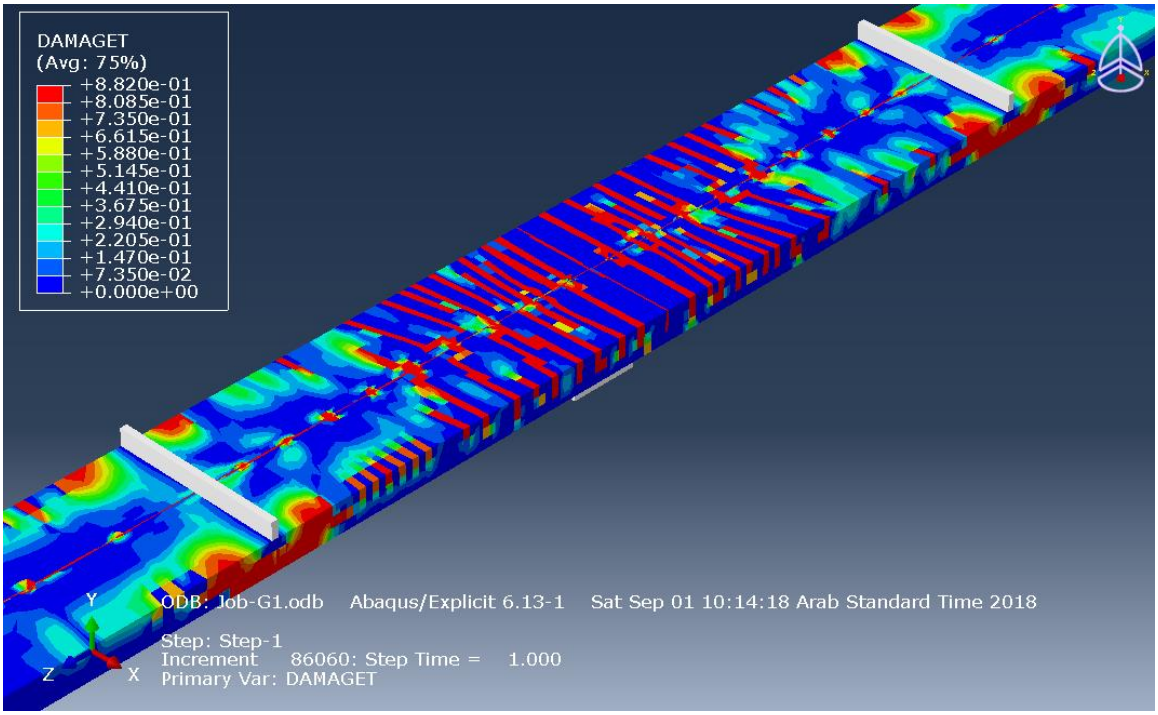

Figure 6.15: Numerically observed cracks in UHPC slab at hogging moment zone.

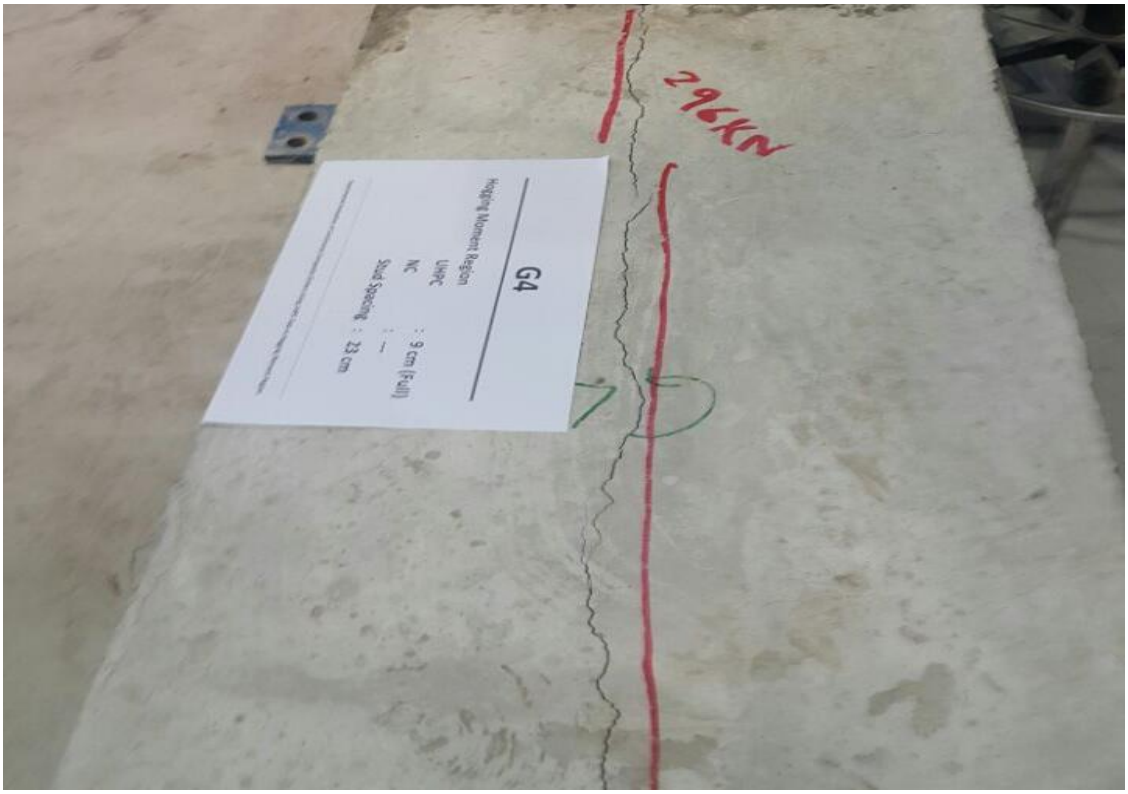

Figure 6.16: Longitudinal cracks observed experimentally along the line of shear studs.

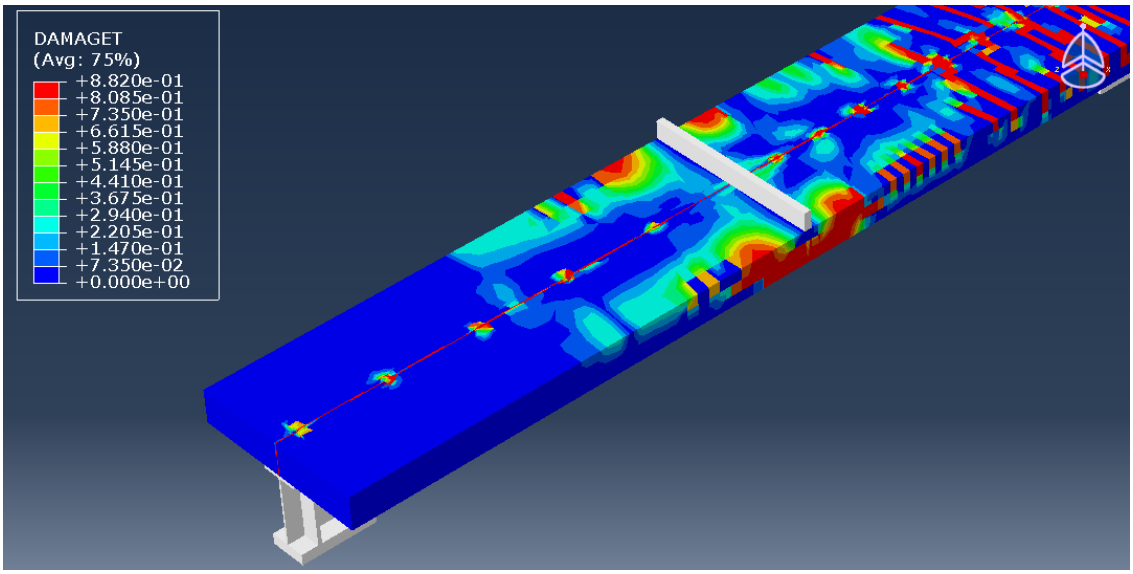

Figure 6.17: Longitudinal cracks observed numerically along the line of shear studs.

The FE model evaluated the load at which yielding started at the bottom steel flange at mid-span. The numerical results proved the efficiency of the model in predicting the yielding load. The experimental and numerical yielding loads were compared and given in Table 6.4. The comparison showed that the difference between experimental and numerical yielding loads is 1%.

Table 6.4: Comparison of cracking and yielding loads.

Girder	Cracking Load (kN)			Yielding Load (kN)		
	Exp.	FEM	% Diff.	Exp.	FEM	% Diff.
G1	57	55	4%	171	169	1%
G2	247	243	2%	188	187	1%
G3	186	181	3%	175	173	1%
G4	215	208	3%	179	178	1%

6.3.3 Failure mode Validation

Ultimate failure of the four girders tested experimentally was due to shear-compression failure mode at the mid-span, as shown in Figure 6.18. This mode of failure was captured by the developed FE model. Figure 6.18 and Figure 6.19 show the experimental and numerical shear-compression failure at mid-span, respectively. This mode of failure took place because NC reached the crushing strain leading to ultimate failure.

The validated model is powerful in predicting the behavior of continuous composite girders. It can be used to perform a parametric study to investigate the effects of different variables on the behavior of continuous composite girders.

Figure 6.18: Shear-compression failure at mid-span (Experimental).

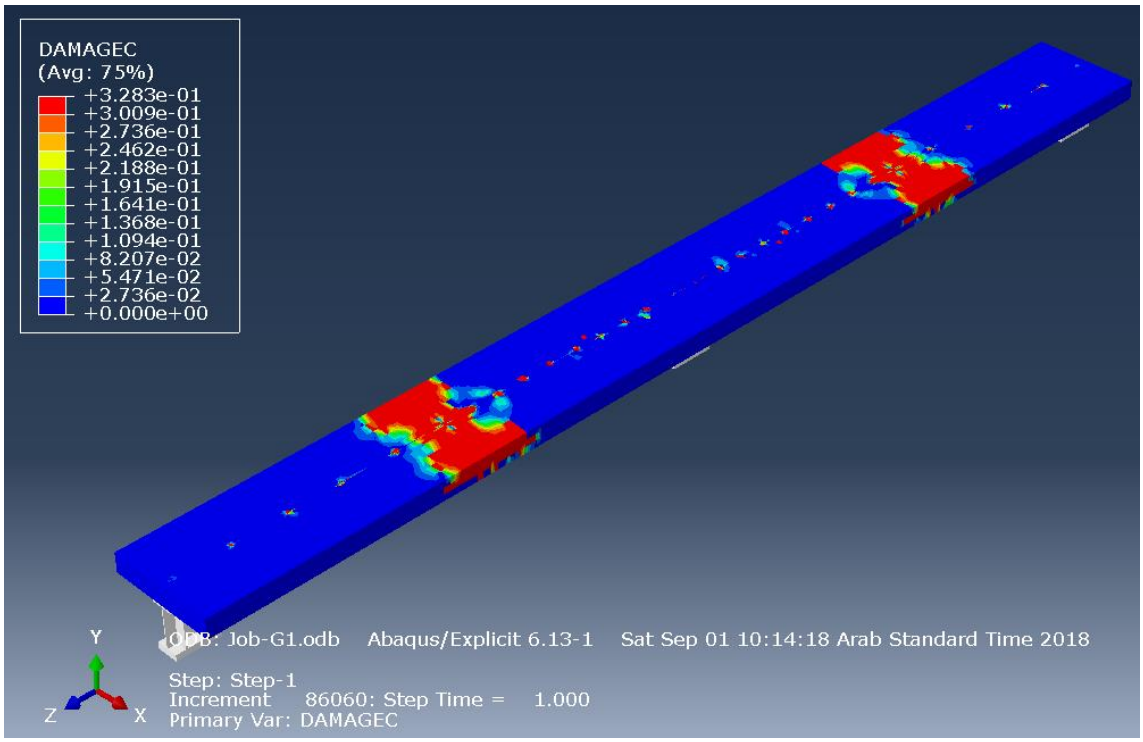

Figure 6.19: Shear-compression failure at mid-span (FE).

6.4 Parametric Study

A series of systematic changes were made to hogging moment zone for the two-span continuous composite girder, shown in Figure 6.20, to demonstrate the effect of such parametric changes on the behavior of continuous composite girders. Three different variables were considered in this study including the spacing (S) between shear studs, thickness (T) and length (L) of UHPC slab at hogging moment zone, as shown in Figure 6.20. The validated FE model utilizing ABAQUS software [17] was employed to investigate the effects of these variables on the behavior of continuous composite girders as presented in the following subsections.

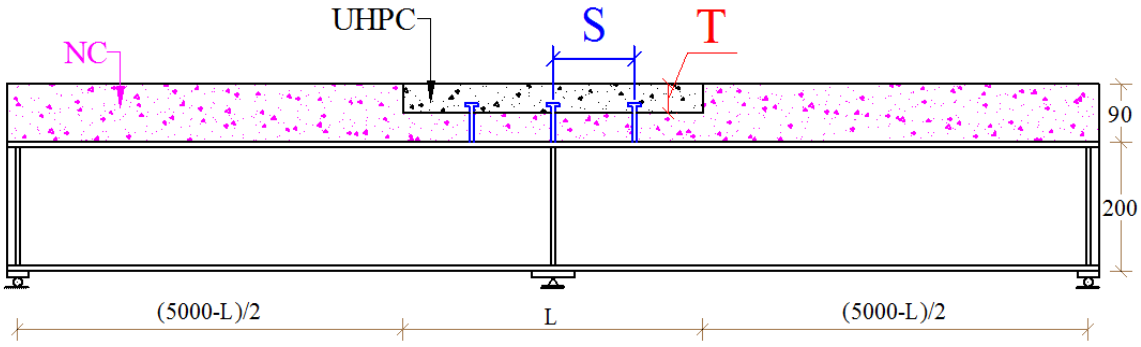

Figure 6.20: The three variables (S, T and L) considered at hogging moment zone.

6.4.1 Degree of Shear Connection

The effect of the shear connection at the hogging moment zone, shown in Figure 6.21, on the behavior of continuous composite girders was investigated considering six different studs spacing, as shown in Table 6.5. Besides the experimentally tested girders (G2 and G4), an additional four girders (G2-1, G2-2, G2-3 and G2-4) were modeled in the ABAQUS software. Girder G2 has a full degree of shear connection at the hogging zone. Girder G2-1 is considered to have a higher degree of shear connection than girder G2. Girders (G2-1, G2-2 and G2-3) are with partial shear connection levels.

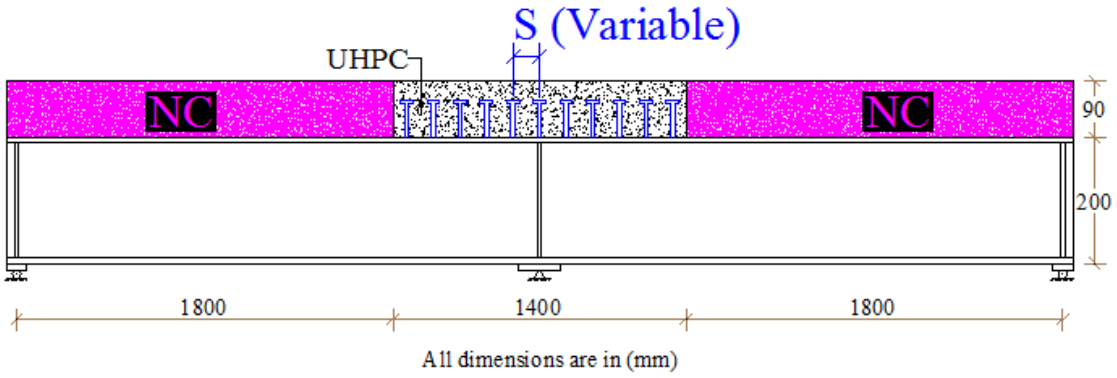

Figure 6.21: Varying the spacing between shear connectors at hogging moment zone.

Table 6.5: The considered degrees of shear connection at hogging moment zone.

Girder	Number of Studs @ Spacing mm
G2-1	12@103.6
G2	10@127
G2-2	8@163
G4	6@228
G2-3	4@380
G2-4	2@1140

Shear stud spacing slightly affected the ultimate capacity and stiffness of the composite girders, as illustrated in Figure 6.22. The interface slip between the top of the steel flange and the bottom of the UHPC slab versus loading for all girders are shown in Figure 6.23 and summarized in Table 6.6. It is obvious that the slip decreases with a higher degree of shear connection. The cracking load, yielding load and λ for all girders are given in Table 6.6. The values for λ decrease with a lower degree of shear connection. Girder G2-3 indicates that λ is close to one, which represents a satisfactory shear connection level to maintain the composite action at the hogging moment zone. Therefore, it can be concluded that the degree of shear connection at hogging moment zone can be taken as 50% of the full composite action to achieve the desired performance of the continuous composite girders.

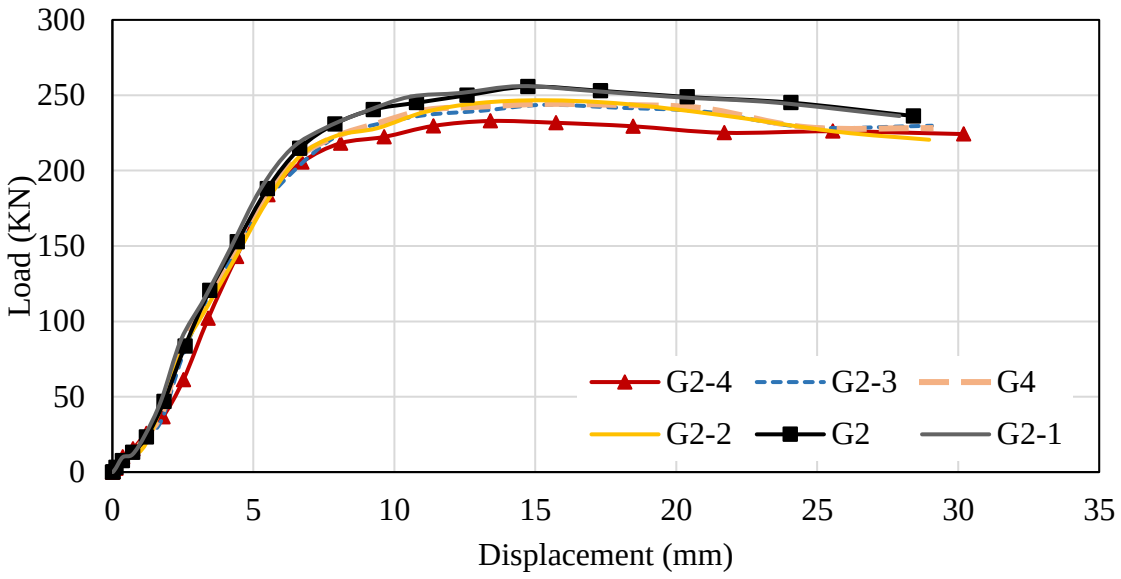

Figure 6.22: Load-displacement curves with different degrees of shear connection at hogging moment zone.

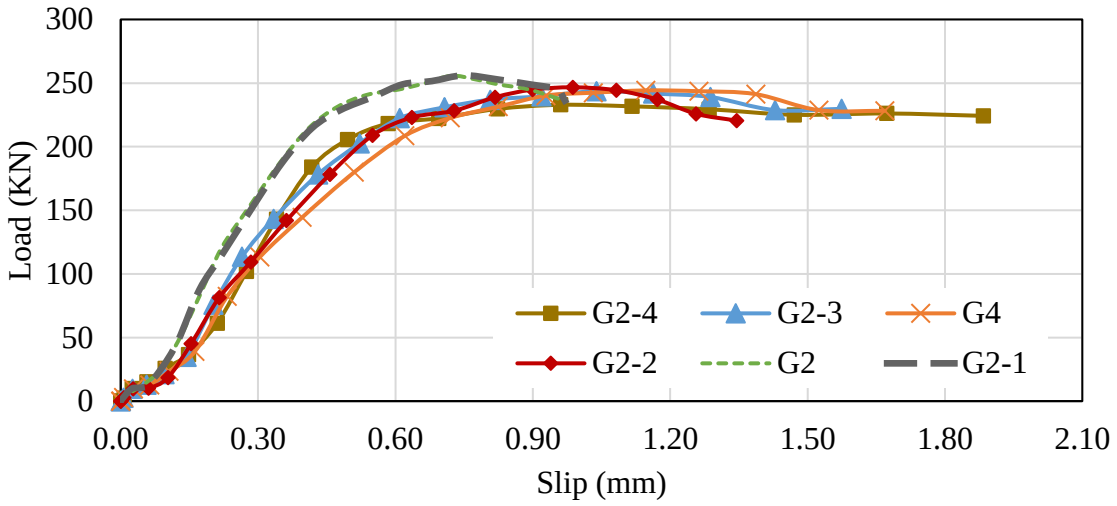

Figure 6.23: Load-slip curves with different degrees of shear connection at hogging moment zone.

Table 6.6: Interface slip, cracking and yielding loads corresponding to the different shear connections at hogging moment zone.

Girder	# of Stud @ Spacing mm	Interface Slip (mm)	P_{cr} (kN)	P_y (kN)	$\lambda=P_{cr}/P_y$
G2-1	12@103.6	0.97	243	187	1.30
G2	10@127	0.97	243	187	1.30
G2-2	8@163	1.35	227	184	1.23
G4	6@228	1.67	208	178	1.17
G2-3	**4@380**	**1.73**	**179**	**173**	**1.03**
G2-4	2@1140	1.88	154	171	0.90

6.4.2 Thickness of UHPC Slab

The effect of UHPC slab thickness, shown in Figure 6.24, at hogging moment was investigated numerically utilizing ABAQUS software. The study assumed two layers of concrete at hogging moment zone. The top layer is UHPC and the bottom one is NC. Besides the experimentally tested girders (G1, G2 and G3), an additional two girders (G1-1 and G1-2) were considered to investigate the effects of the UHPC thicknesses at the hogging moment zone, as shown in Table 6.7.

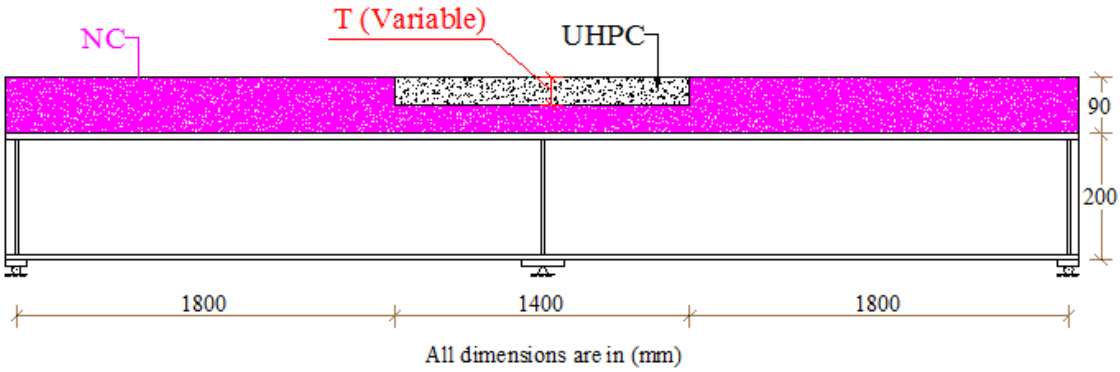

Figure 6.24: Varying the UHPC slab thickness at hogging moment zone.

Table 6.7: The considered thickness of UHPC at hogging moment zone.

Girder	UHPC Slab Thickness (mm)
G1	0 (90-mm NC)
G1-1	22.5
G3	45
G1-2	67.5
G2	90

The performance of girder G1-1 with a UHPC slab thickness equivalent to one quarter slab depth has not shown any improvement relative to the control girder G1, as shown in Figure 6.25 and Table 6.8. This is mainly attributed to the fact that shear studs do not penetrate the UHPC slab thickness. It is clearly shown in Figure 6.25 and Table 6.8 that as the UHPC slab thickness increases for girders (G3, G1-2 and G2), their performance improved in terms of the stiffness and λ values. Girder G3 with a UHPC slab thickness of half the depth of the slab gives a λ value close to one which represents a satisfactory UHPC slab thickness necessary to maintain the composite action at the hogging moment zone. Therefore, it can be concluded that using half depth UHPC slab thickness at hogging moment zone is sufficient to achieve the desired performance of the continuous composite girders.

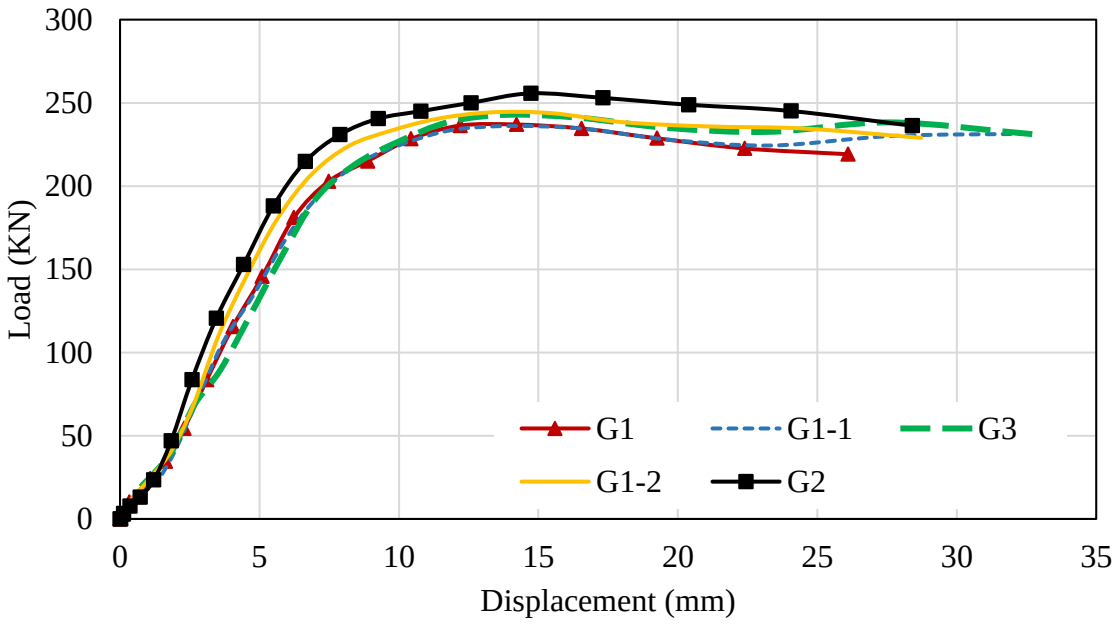

Figure 6.25: Load-displacement curves for girders with different UHPC thickness at hogging moment zone.

Table 6.8: Cracking, yielding and ultimate loads corresponding to UHPC thickness at hogging moment zone.

Girder	UHPC Slab Thickness (mm)	P_{cr} (kN)	P_y (kN)	λ	P_u (kN)
G1	0 (90-mm NC)	55	169	0.33	237
G1-1	22.5	55	169	0.33	236.1
G3	**45**	**181**	**173**	**1.05**	**242.9**
G1-2	67.5	219	181	1.21	244.3
G2	90	243	187	1.30	255.7

6.4.3 Length of UHPC Slab

The effect of the UHPC slab length at hogging moment zone, shown in Figure 6.26, was investigated numerically utilizing ABAQUS software. A half-depth UHPC slab thickness and a 50%-degree of shear connection were implemented at hogging moment zone to evaluate the proper UHPC slab length that is sufficient for all loading conditions. This study considers symmetrical and unsymmetrical loading conditions to evaluate the critical UHPC slab length necessary to maintain the composite action at hogging moment zone.

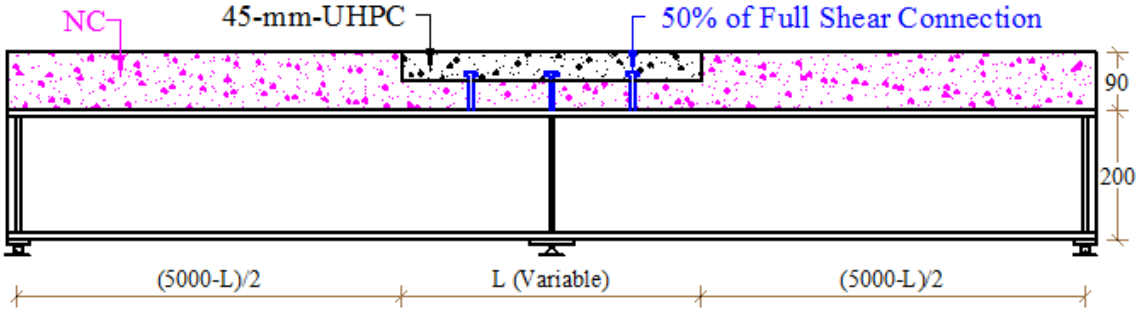

Figure 6.26: Varying the UHPC slab length at hogging moment zone.

The adequacy of the 1400-mm-length of UHPC slab to maintain the composite action at hogging moment zone was investigated for the symmetrical and unsymmetrical loading conditions shown in Figure 6.27 and Figure 6.28, respectively. These loading conditions are the most critical ones that require the largest length of UHPC slab. The results, summarized in Table 6.9, have shown that λ values are higher than one for all cases of loading, which indicate that the 1400-mm length is sufficient to maintain the composite action at hogging moment zone. Also, it is clearly shown that the symmetrical loading case 1, shown in Figure 6.27, is more critical than case 2 because it has a smaller value of λ.

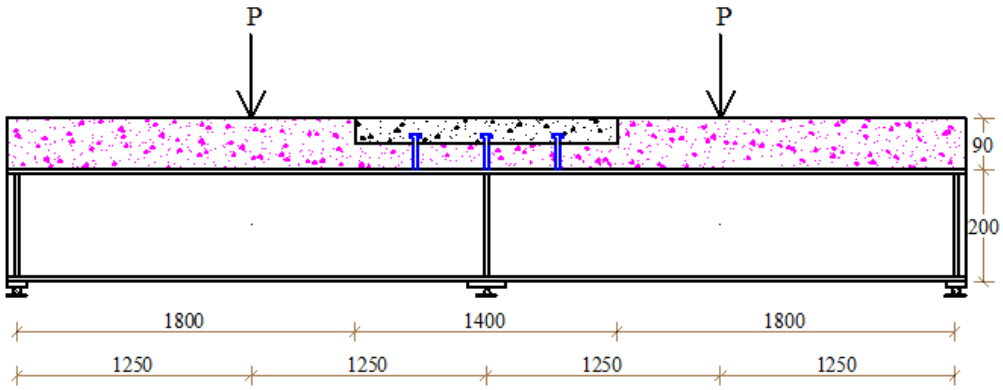

(a) Case 1: two-point loads applied at the mid of each span.

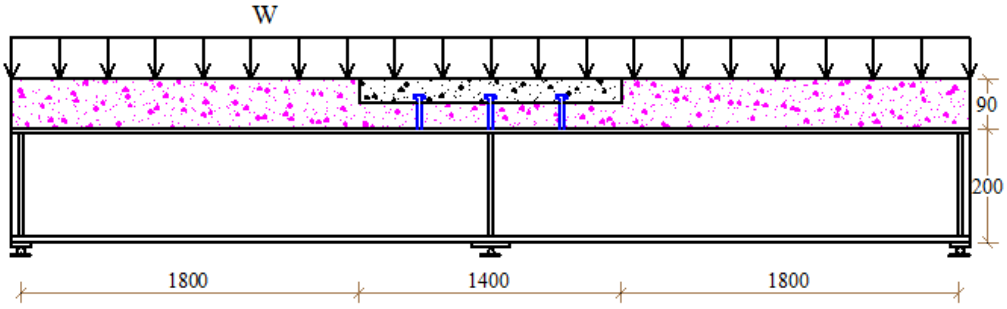

(b) Case 2: uniformly distributed load applied on the two spans.

Figure 6.27: Symmetrical loading conditions: (a) case 1; (b) case 2.

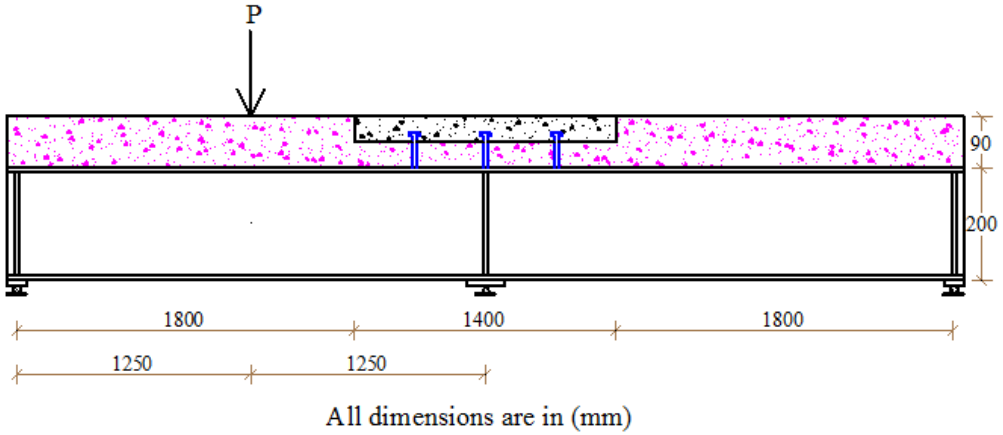

Figure 6.28: Unsymmetrical loading condition, case 3.

Table 6.9: Cracking, yielding and λ parameter for the three-critical cases of loading.

Loading Condition	UHPC Slab Length (mm)	Degree of Shear Connection	P_{cr} (kN)	P_y (kN)	λ
Case 1	1400	50%	180	163	1.11
Case 2	1400	50%	1290	992	1.30
Case 3	1400	50%	228	202	1.13

Besides, the effect of the variable UHPC slab length, shown in Figure 6.26, was investigated numerically utilizing ABAQUS software for the most critical case of loading shown in Figure 6.28. Six girders (G-L0, G-L300, G-L600, G-L900, G-L1200 and G-L1500) were considered to evaluate the critical length of the UHPC slab at the hogging moment zone, as shown in Table 6.10.

Table 6.10: Varying the length of UHPC slab at hogging moment zone.

Girder	UHPC Slab Length (mm)
G-L0	0 (Only NC)
G-L300	300
G-L600	600
G-L900	900
G-L1200	1200
G-L1500	1500

The overall behavior of the composite girders with different UHPC slab lengths at hogging moment zone is illustrated by load-deflection curves, as shown in Figure 6.29. It is demonstrated that the length of UHPC slab slightly affects the ultimate capacity and

stiffness of the composite girders, as shown in Figure 6.29 and Table 6.11. Also, insignificant variation in yielding load was obtained, as summarized in Table 6.11. However, significant enhancement in cracking loads was obtained as increasing the length of UHPC slab, as shown in Table 6.11. Also, it is noticed that cracks initiated in NC slab for girders (G-L0, G-L300 and G-L600) and in UHPC slab for girders (G-L900, G-L1200 and G-L1500). The performance of girder G-L1500 with a 1500-mm UHPC slab length has not shown any improvement relative to the girder G-L1200, as shown in Figure 6.29 and Table 6.11. While, it is clearly shown in Figure 6.29 and Table 6.11 that as the UHPC slab length increases for girders (G-L900, G-L1200, G-L1400), their performance improved in terms of the stiffness, cracking load and λ values. Girder G-L900 with a UHPC slab length of 900-mm gives a λ value close to one which represents a satisfactory UHPC slab length necessary to maintain the composite action at the hogging moment zone. Therefore, it can be concluded that the length of UHPC slab at hogging moment zone can be taken as 20% of the span length to achieve the desired performance of the continuous composite girders.

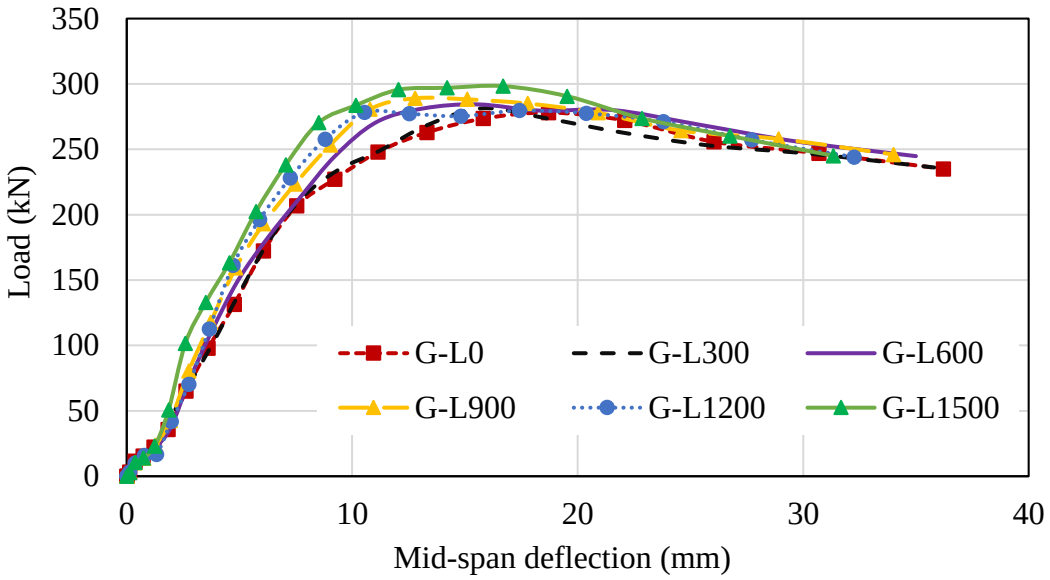

Figure 6.29: Load-displacement curves for girders with different UHPC length at hogging moment zone.

Table 6.11: Cracking, yielding and ultimate loads corresponding to different UHPC length at hogging moment zone.

Girder	UHPC Slab Length (mm)	Cracking of Concrete		Yielding of Steel		λ	P_u (kN)
		P_{cr} (kN)	Location	P_y (kN)	Location		
G-L0	0 (NC)	147	NC	175	Bottom flange at mid-span	0.84	278.1
G-L300	300	155		178		0.87	281.4
G-L600	600	166		182		0.91	284.4
G-L900	**900**	**197**		**184**		**1.07**	**289.0**
G-L1200	1200	228	UHPC	186		1.23	297.5
G-L1500	1500	238		202		1.18	298.3

CHAPTER SEVEN

ANALYTICAL EVALUATION OF COMPOSITE GIRDERS WITH UHPC SLAB

Experimental and FE evaluation of the behavior of continuous composite steel-concrete girders were carried out and presented in CHAPTER Four to CHAPTER Six, respectively. The experimental and FE results showed the effectiveness of UHPC slab to maintain the composite action at hogging moment zone and to improve the maximum service load. The use of UHPC at hogging moment improves the stiffness, cracking load and ultimate strength of composite girders. This chapter presents the analytical evaluation of cracking, yielding and ultimate loads. Some assumptions including material and geometry were made to simplify the analytical approach.

7.1 Assumptions

The analytical approach is performed based on several material and geometrical assumptions, as presented in sections 7.1.1 and 7.1.2.

7.1.1 Material Assumptions

Followings are the material assumptions made to simplify the analytical approach:

A) Elastic-perfect plastic behavior is used for reinforcement steel and steel section.

B) Compressive and tensile strength of steel is the yielding strength, f_y.

C) Compressive strength of NC & UHPC is considered as 0.85fc'.

D) Tensile strength of NC is ignored.

E) Tensile strength of UHPC is assumed constant and equal to direct tensile strength.

F) Full composite action between steel section and concrete slab.

7.1.2 Geometrical Assumptions

Geometrical assumptions were made to prevent all secondary mode of failures. These failures include local buckling in flanges and web, lateral-torsional buckling, web local yielding and crippling and shear failure. This section presents all secondary modes of failure that may take place in the two-span continuous composite girders.

7.1.2.1 Local Buckling in Flanges & Web

Local buckling may take place in the components of steel section which are under compression. The flanges or web of steel section may buckle locally prior reaching the yielding of steel section leading to a reduction in the capacity of the steel section. Therefore, this mode of failure should be prevented by satisfying width to thickness ratio of flanges and web. Based on width to thickness ratio and according to AISC specifications [9], steel sections are classified into three categories, as shown in Figure 7.1. This design approach assumes the section is compact.

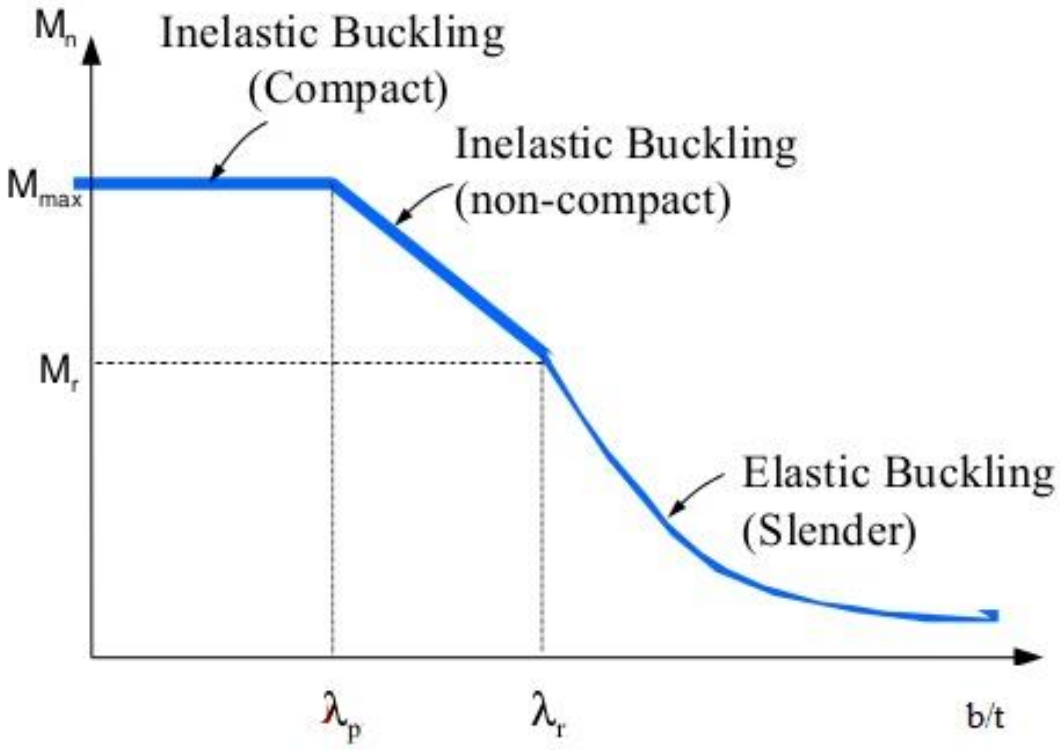

Figure 7.1: Classification of steel sections based on width to thickness ratio.

7.1.2.2 Lateral-Torsional Buckling

Lateral-torsional buckling may take place in the bottom flange of steel section at the hogging moment zone where the flange is unrestrained and subjected to compressive force. While this secondary failure will not take place in top flange of composite girders because of the continuous lateral support provided by the concrete slab. Therefore, lateral support is needed at the interior support only for the bottom flange to prevent this local failure. According to AISC specifications [9] and based on unbraced length, steel sections are classified into three categories, as shown in Figure 7.2. This design approach assumes the section is compact.

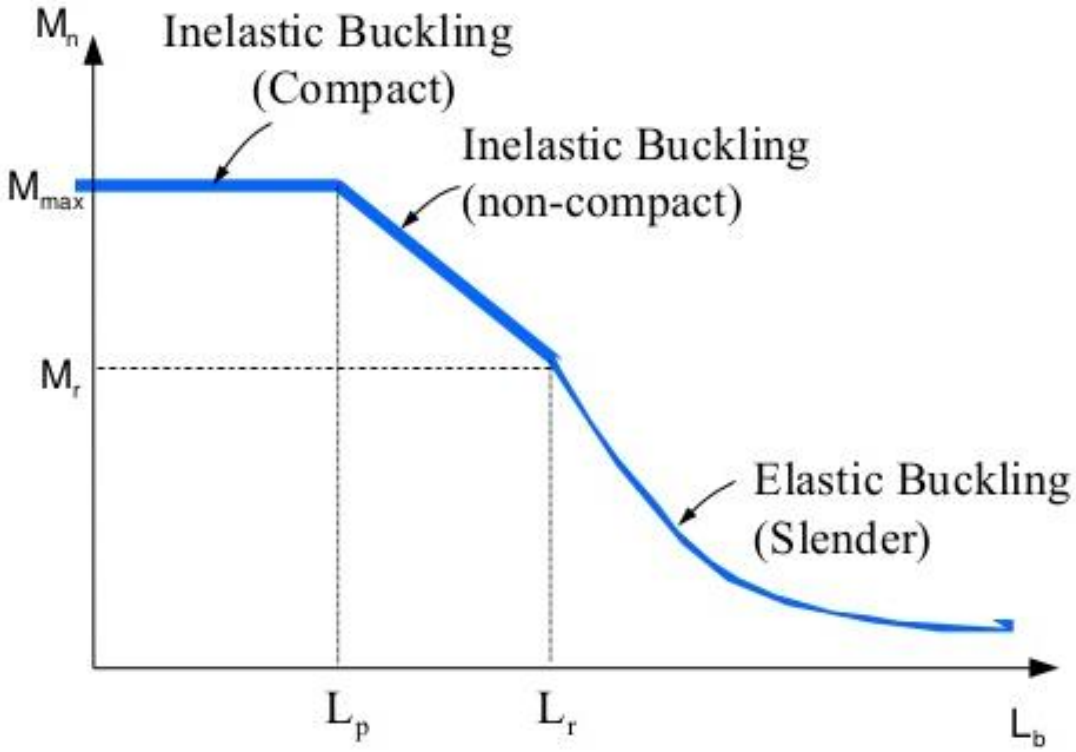

Figure 7.2: Classification of steel sections based on unbraced length.

7.1.2.3 Web Local Yielding & Crippling

Web local failures including yielding and crippling take place due to the high concentrated loads such as supports reactions. These secondary failures can be prevented by providing the adequate steel plates. These plates are used beneath the concentered forces.

7.1.2.4 Shear Failure

Shear strength of composite steel-concrete sections is evaluated based on the steel web only. Therefore, shear failure should be prevented by selecting the proper dimensions of web of steel section.

7.1.2.5 Stress Concentration

Stress concentrates in the regions where concentrated forces are applied over a very small area. For continuous composite girders, the regions above support and below applied loads are subjected to stress concentration failure. Therefore, steel plates of proper sizes should be provided to prevent this local failure.

7.2 Maximum Service Load

The elastic capacity of the continuous composite girders is controlled by three loading limits: (a) Cracking of concrete slab over interior support; (b) yielding of bottom flange at mid-span; and (c) yielding of bottom flange over interior support. The elastic load is defined as the maximum service load that can be applied before reaching cracking of concrete or yielding of steel section. Therefore, the maximum service load is the smallest between cracking and yielding loads. The elastic bending moment diagram, shown in Figure 7.3, is employed to evaluate the smallest among the three loading limits. The analytical evaluation of cracking and yielding loads is presented in sections 7.2.1 and 7.2.2, respectively.

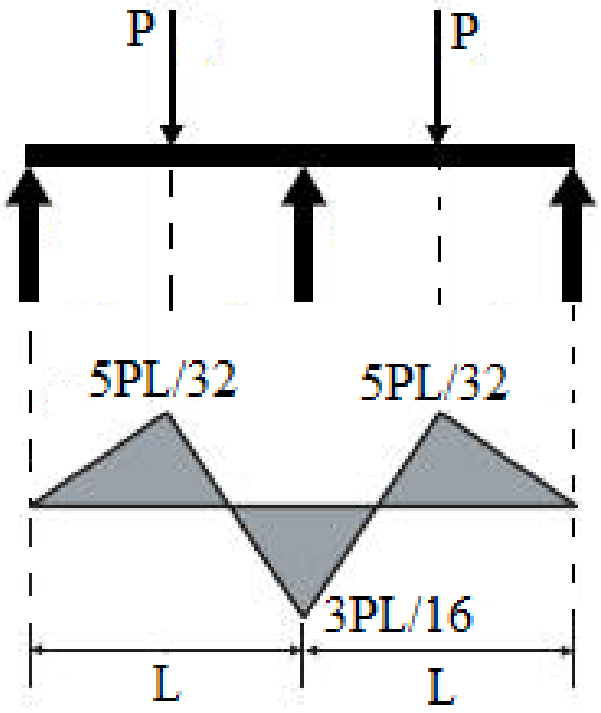

Figure 7.3: Elastic bending moment diagram.

7.2.1 Cracking load

Cracking load is evaluated based on the properties of the section at the interior support where concrete slab is under tension. Cracks begin when the tensile stress in UHPC slab at the extreme tension fiber reaches the modulus of rupture (f_r) of UHPC. The transformed section method, which transforms the composite beam into one made of a single material, is used to evaluate the cracking load following these steps:

A) Determine the modular ratios n_1 and n_2.

B) Transform UHPC and reinforcement steel to an equivalent structural steel area, as shown in Figure 7.4.

C) Evaluate the elastic/geometric centroid of the new transformed section to determine the distances y_t and y_b, as shown in Figure 7.4.

D) Evaluate second moment of inertia (I) about the elastic neutral axis.

E) Equate the modulus of rupture (f_r) of UHPC to the tensile stress in UHPC at the extreme tension fiber.

F) Solve for the cracking moment (M_{cr}) utilizing Eq. (7.1).

$$M_{cr} = \frac{n * I * f_r}{y_t} \qquad (7.1)$$

G) Utilizing elastic bending moment diagram to calculate the cracking load (P_{cr}) given in Eq. (7.2).

$$P_{cr} = \frac{16\ M_{cr}}{3\ L} \qquad (7.2)$$

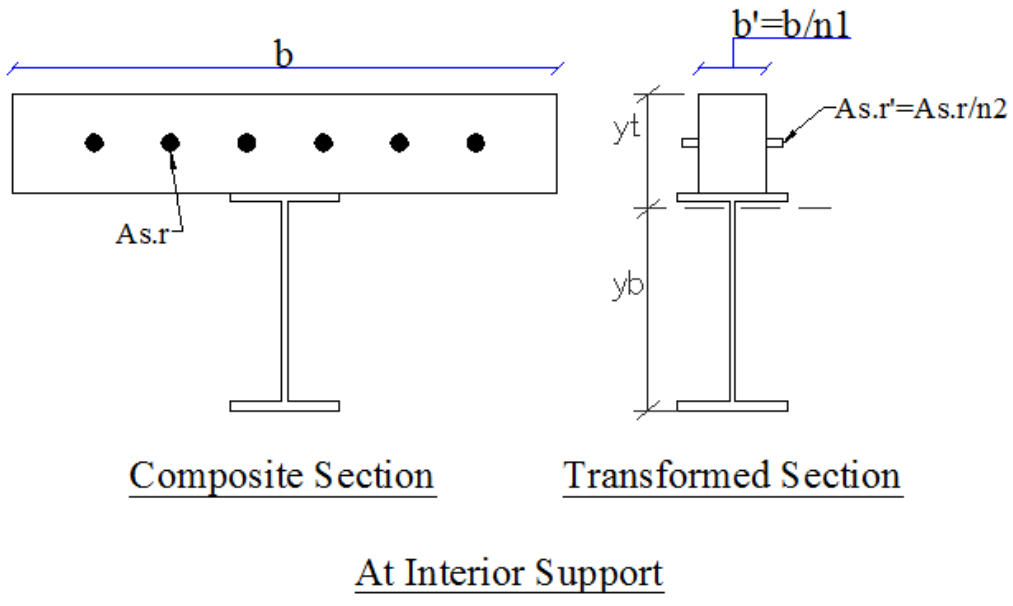

Figure 7.4: The transformation of the composite section at interior support into an equivalent homogenous section.

7.2.2 Yielding load

Yielding load is the load corresponding to yielding of bottom flange either at mid-span or interior support. It is evaluated utilizing a trial-and-error procedure to find the location of neutral axis that requires satisfying the equilibrium of forces. Yielding load is found by following these steps:

A) Assume a trial depth (y) for the elastic neutral axis at mid-span section.

B) Let the strain at the bottom flange to be the yielding strain (ε_y) of steel section.

C) Calculate the strain in reinforcement steel, top flange and concrete slab using strain compatibility condition.

D) Find the stress corresponding to the calculated strain.

E) Check the equilibrium of forces (C=T).

F) If the equilibrium of forces does not satisfy, then the depth (y) will be adjusted accordingly and all previous steps will be repeated.

G) If the equilibrium of forces does satisfy, the moment of all forces will be calculated

H) Repeat all previous steps for the section at the interior support.

I) Utilizing the elastic bending moments ($M_{+ve}=5P_y\ L\ /32$, $M_{-ve}=3P_yL/16$) to find the load corresponding to the yielding of both sections.

J) Yielding load is the smaller of the two forces and given in Eq. (7.3).

$$P_y = min\left(\frac{16\ M_{-ve}}{3\ L}\ \ or\ \ \frac{32\ M_{+ve}}{5\ L}\right) \qquad (7.3)$$

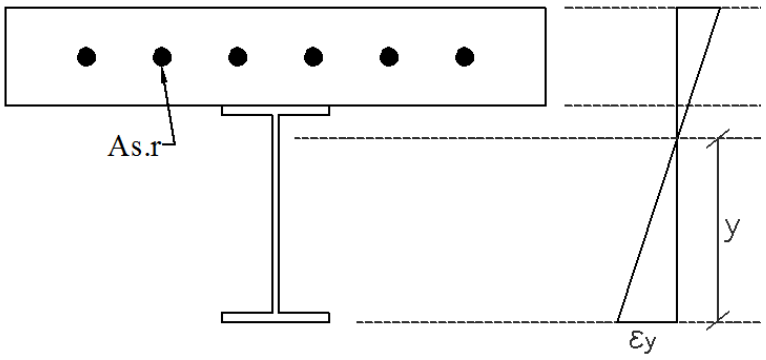

Figure 7.5: Strain distribution at yielding of bottom flange at either mid-span or interior support.

7.3 Ultimate Plastic Capacity

According to AISC specifications [9], design of continuous composite girders with NC slab at the hogging moment zone ignores the NC slab because NC cracks before reaching ultimate stage. Therefore, it was assumed that the steel section is either acts alone or compositely with the slab reinforcements. For Both assumptions, the steel section rotates enough to form the second plastic hinge at sagging moment section.

However, the use of UHPC at hogging moment zone increases the stiffness which restricts girders rotation over the support. Therefore, design of composite girders should allow full yielding of steel section at hogging moment zone prior to crushing of NC at sagging moment section or reaching local failures.

Plastic analysis is used to predict the ultimate load necessary to cause the flexural failure in the two-span continuous composite girder. Failure load is evaluated using virtual work method based of the possible failure mechanisms shown in Figure 7.6. Sections capacities

at mid-span and interior support are assumed as αM_p and M_p, respectively. The evaluated failure load (P_f) utilizing plastic analysis is given by Eq. (7.4).

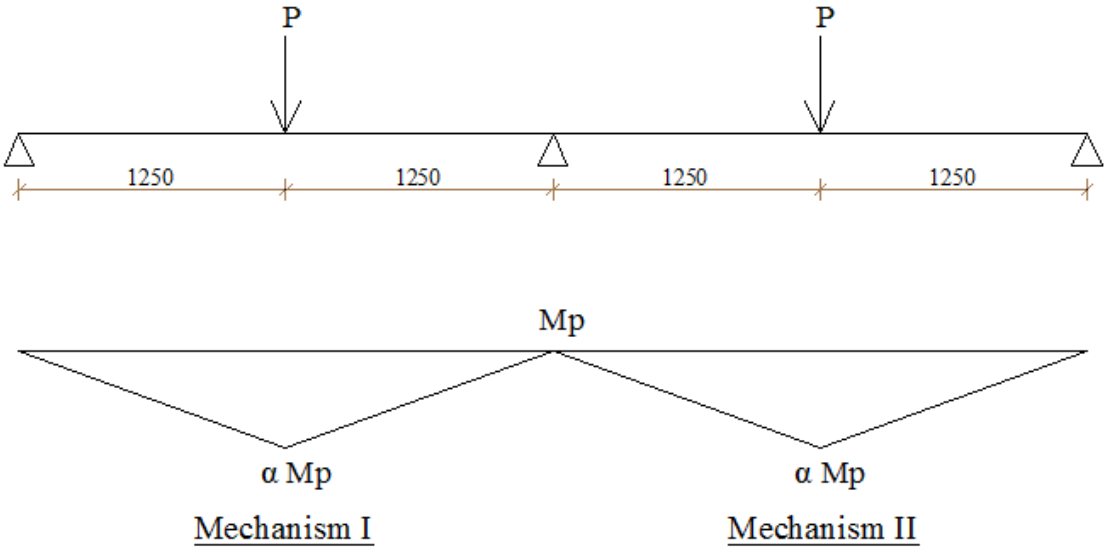

Figure 7.6: Failure mechanisms of the two-span continuous girder.

$$P_f = \left[\frac{2(2\alpha+1)}{L}\right] M_p \qquad (7.4)$$

Where M_p= negative moment capacity; and

α=ratio of the positive to negative moment capacities.

Theoretical values for the girder's ultimate positive and negative moment capacities, shown in Table 7.1, were evaluated assuming elastic-plastic behavior of the steel. Failure loads ($\overline{P}_f$) were evaluated utilizing Eq. (7.4) and summarized in Table 7.1. It is demonstrated that the predicted ultimate loads ($\overline{P}_f$) calculated using Eq. (7.4) are lower than the actual failure load (P_u) obtained from the experimental testing and numerical investigation. Therefore, it can be concluded that plastic analysis underestimates the failure load and leads to safe and reasonable load expectation.

Table 7.1: Experimental, numerical and analytical ultimate loads carrying capacity.

Girder	P_u (kN)		$\bar{M}_{+ve}$ (kN.m)	$\bar{M}_{-ve}$ (kN.m)	α	$\bar{P}_f$ (kN)	$\bar{P}_f/P_u$
	Exp.	FE					
G1	242	237	109.01	71.63	1.522	231.7	96%
G2	262	255.7	109.01	96.02	1.135	251.2	96%
G3	250	242.5	109.01	76.72	1.421	235.8	94%
G4	247	244	109.01	75.8	1.438	235.1	95%

CHAPTER EIGHT

CONCLUSIONS AND RECOMMENDATIONS

8.1 Conclusions

Based on the experimental and numerical evaluations for the use of UHPC slab at hogging moment zone, the following can be concluded:

1. The use of a UHPC slab at the hogging moment zone maintained the composite action at a load level much higher than the upper service load limit and greatly improved the stiffness leading to a reduction in mid-span deflection;

2. The ultimate load carrying capacity is slightly affected with the variation in the degree of shear connection, thickness and length of UHPC at the hogging moment zone;

3. Cracking load is significantly improved with the use of UHPC at hogging zone. Steel fibers provide a post-cracking tension resistance which resist the initiation and propagation of cracks;

4. The maximum service load is governed by yielding of steel beam rather than cracking of UHPC at hogging zone;

5. The predicted failure load using plastic analysis is a reasonable and safe estimate compared to the experimental failure load;

6. The analytical approach which assumes that materials behavior is elastic-perfectly plastic ignores the strain hardening part. This approach yields safe and reasonable results;

7. The degree of shear connection can be taken as 50% of full composite action at negative moment region to achieve the required performance of the continuous composite girders;

8. The use of half UHPC slab thickness at hogging moment zone is sufficient to achieve the desired performance of the continuous composite girders; and

9. The length of UHPC slab at hogging moment zone can be taken as 20% of the span length to achieve the desired performance of the continuous composite girders.

8.2 Recommendations

Following suggestions are recommended for future work:

1. Experimental evaluation of the use of UHPC slab at hogging moment zone under fatigue loading.

2. Experimental investigation of different shear connection techniques such as Perfo-Bond Strips (PBLs) or channel connectors on the behavior of composite girders.

3. Conduct a push-out test to study the behavior of shear studs embedded in UHPC slab with different stud's length and diameter.

REFERENCES

1. Wang, B., Q. Huang, and X. Liu, *Deterioration in strength of studs based on two-parameter fatigue failure criterion.* Steel and Composite Structures, 2017. **23**(2): p. 239-250.

2. Xiang, T., C. Yang, and G. Zhao, *Stochastic creep and shrinkage effect of steel-concrete composite beam.* Advances in Structural Engineering, 2015. **18**(8): p. 1129-1140.

3. Xing, Y., et al., *Experimental and numerical study on static behavior of elastic concrete-steel composite beams.* Journal of constructional steel research, 2016. **123**: p. 79-92.

4. Zhou, M., et al., *Shear stress calculation and distribution in variable cross sections of box girders with corrugated steel webs.* Journal of Structural Engineering, 2016. **142**(6): p. 04016022.

5. Thirumalaiselvi, A., et al., *Numerical evaluation of deformation capacity of laced steel-concrete composite beams under monotonic loading.* Steel Compos Struct, 2016. **20**(1): p. 167-184.

6. Vasdravellis, G. and B. Uy, *Shear strength and moment-shear interaction in steel-concrete composite beams.* Journal of Structural Engineering, 2014. **140**(11): p. 04014084.

7. Rodrigues, J.P.C. and L. Laím, *Experimental investigation on the structural response of T, T-block and T-Perfobond shear connectors at elevated temperatures.* Engineering structures, 2014. **75**: p. 299-314.

8. Zhan, Y., et al., *Interface behavior between steel and concrete connected by bonding.* Journal of Bridge Engineering, 2016. **21**(6): p. 04016026.

9. Manual, S.C., *American institute of steel construction.* Inc., Thirteenth Edition, First Print, 2005.

10. Hakeem, I.Y.A., *Characterization of an ultra-high performance concrete*, 2011, King Fahd University of Petroleum and Minerals (Saudi Arabia).

11. Titoum, M., M. Tehami, and B. Achour, *Effects of partial shear connection on the behavior of semi-continuous composite beams.* International Journal of Steel Structures, 2009. **9**(4): p. 301-313.

12. Queiroz, F., P. Vellasco, and D. Nethercot, *Finite element modelling of composite beams with full and partial shear connection.* Journal of constructional steel research, 2007. **63**(4): p. 505-521.

13. Loh, H., B. Uy, and M. Bradford, *The effects of partial shear connection in composite flush end plate joints Part II—Analytical study and design appraisal.* Journal of constructional steel research, 2006. **62**(4): p. 391-412.

14. Loh, H., B. Uy, and M. Bradford, *The effects of partial shear connection in composite flush end plate joints Part I—experimental study.* Journal of constructional steel research, 2006. **62**(4): p. 378-390.

15. Ban, H. and M.A. Bradford, *Flexural behaviour of composite beams with high strength steel.* Engineering structures, 2013. **56**: p. 1130-1141.

16. Standardization, E.C.f., *Eurocode 4: Design of Composite Steel and Concrete Structures*1994: CEN.

17. ABAQUS, C., *Analysis user's manual, Version 6.12*, 2012, ABAQUS.

18. Testing, A.S.f. and Materials. *Annual Book of ASTM Standards: Iron and Steel Products. Steel-Structural, Reinforcing, Pressure, Vessel, Railway*. 1983. Astm.

19. Concrete, A.I.C.C.o. and C. Aggregates, *Standard Test Method for Static Modulus of Elasticity and Poisson's Ratio of Concrete in Compression1*2014: ASTM International.

20. Moallem, M.R., *Flexural Redistribution in Ultra-High Performance Concrete Lab Specimens*, 2010, Ohio University.

21. Dugat, J., N. Roux, and G. Bernier, *Mechanical properties of reactive powder concretes.* Materials and structures, 1996. **29**(4): p. 233-240.

22. Gao, J., W. Sun, and K. Morino, *Mechanical properties of steel fiber-reinforced, high-strength, lightweight concrete.* Cement and Concrete Composites, 1997. **19**(4): p. 307-313.

23. Lubbers, A.R., *Bond performance between ultra-high performance concrete and prestressing strands*, 2003, Ohio University.

24. Perry, V. and D. Zakariasen, *First use of ultra-high performance concrete for an innovative train station canopy.* Concrete Technology Today, 2004. **25**(2): p. 1-2.

25. Song, P. and S. Hwang, *Mechanical properties of high-strength steel fiber-reinforced concrete.* Construction and Building Materials, 2004. **18**(9): p. 669-673.

26. Graybeal, B.A., *Characterization of the behavior of ultra-high performance concrete*, 2005.

27. Lukasik, J. *Concrete: A High-Techmaterial of the 21st Century*. in *8th Hitachi EU Science and Technology Forum*. 2005. Athens.

28. Brühwiler, E. and E. Denarié. *Rehabilitation of concrete structures using ultra-high performance fibre reinforced concrete*. in *Proceedings, UHPC-2008: the second international symposium on ultra-high performance concrete*. 2008.

29. Kang, S.-T., et al., *Tensile fracture properties of an Ultra High Performance Fiber Reinforced Concrete (UHPFRC) with steel fiber.* Composite Structures, 2010. **92**(1): p. 61-71.

30. Kang, S.-T. and J.-K. Kim, *The relation between fiber orientation and tensile behavior in an Ultra High Performance Fiber Reinforced Cementitious Composites (UHPFRCC).* Cement and Concrete Research, 2011. **41**(10): p. 1001-1014.

31. Shende, A., A. Pande, and M.G. Pathan, *Experimental study on steel fiber reinforced concrete for M-40 grade.* International Refereed Journal of Engineering and Science, 2012. **1**(1): p. 043-048.

32. Hassan, A., S. Jones, and G. Mahmud, *Experimental test methods to determine the uniaxial tensile and compressive behaviour of ultra high performance fibre reinforced concrete (UHPFRC).* Construction and Building Materials, 2012. **37**: p. 874-882.

33. Yoo, D.-Y., J.-H. Lee, and Y.-S. Yoon, *Effect of fiber content on mechanical and fracture properties of ultra high performance fiber reinforced cementitious composites.* Composite Structures, 2013. **106**: p. 742-753.

34. Yoo, D.-Y., S.-T. Kang, and Y.-S. Yoon, *Effect of fiber length and placement method on flexural behavior, tension-softening curve, and fiber distribution*

characteristics of UHPFRC. Construction and Building Materials, 2014. **64**: p. 67-81.

35. Yoo, D.Y., S.T. Kang, and Y.S. Yoon, *Erratum: Effect of fiber length and placement method on flexural behavior, tension-softening curve, and fiber distribution characteristics of UHPFRC (Construction and Building Materials (2014) 64 (67-81)).* Construction and Building Materials, 2014. **72**.

36. Wu, Z., et al., *Effects of steel fiber content and shape on mechanical properties of ultra high performance concrete.* Construction and Building Materials, 2016. **103**: p. 8-14.

37. Basu, P.K., A.M. Sharif, and N.U. Ahmed, *Partially prestressed continuous composite beams. I.* Journal of Structural Engineering, 1987. **113**(9): p. 1909-1925.

38. Basu, P.K., A.M. Sharif, and N.U. Ahmed, *Partially prestressed composite beams. II.* Journal of Structural Engineering, 1987. **113**(9): p. 1926-1938.

39. Elremaily, A. and S. Yehia. *Use of External Prestressing to Improve Load Capacity of Continuous Composite Steel Girders*. in *Structures Congress 2006: Structural Engineering and Public Safety*. 2006.

40. Chen, S., X. Wang, and Y. Jia, *A comparative study of continuous steel–concrete composite beams prestressed with external tendons: experimental investigation.* Journal of constructional steel research, 2009. **65**(7): p. 1480-1489.

41. Nie, J., et al., *Analytical and numerical modeling of prestressed continuous steel-concrete composite beams.* Journal of Structural Engineering, 2011. **137**(12): p. 1405-1418.

42. Lin, W. and T. Yoda, *Experimental and numerical study on mechanical behavior of composite girders under hogging moment.* International Journal of Advanced Steel Construction, 2013. **9**(4): p. 309-333.

43. Lin, W., et al., *Mechanical performance of steel-concrete composite beams subjected to a hogging moment.* Journal of Structural Engineering, 2013. **140**(1): p. 04013031.

44. Lin, W., T. Yoda, and N. Taniguchi, *Application of SFRC in steel–concrete composite beams subjected to hogging moment.* Journal of constructional steel research, 2014. **101**: p. 175-183.

45. Sharif, A.M., et al., *Use of CFRP to maintain composite action for continuous steel–concrete composite girders.* Journal of Composites for Construction, 2015. **20**(4): p. 04015088.

46. Samaaneh, M.A., et al., *Numerical investigation of continuous composite girders strengthened with CFRP*. Steel and Composite Structures, 2016. **21**(6): p. 1307-1325.

47. Fabbrocino, G. and M. Pecce. *Experimental tests on steel-concrete composite beams under negative bending*. in *3rd structural specialty conference of the Canadian society for civil engineering. London (Ontario)*. 2000.

48. Loh, H., B. Uy, and M. Bradford, *The effects of partial shear connection in the hogging moment regions of composite beams: Part I—Experimental study.* Journal of constructional steel research, 2004. **60**(6): p. 897-919.

49. Loh, H., B. Uy, and M. Bradford, *The effects of partial shear connection in the hogging moment regions of composite beams Part II—Analytical study.* Journal of constructional steel research, 2004. **60**(6): p. 921-962.

50. Nie, J., J. Fan, and C. Cai, *Experimental study of partially shear-connected composite beams with profiled sheeting.* Engineering structures, 2008. **30**(1): p. 1-12.

51. Husain, H.M., et al., *Behavior of composite steel-concrete beam subjected to negative bending.* Engineering and Technology Journal, 2009. **27**(1): p. 53-71.

52. LIN, W. and T. YODA, *Mechanical behaviour of composite girders subjected to hogging moment: Experimental study*. Journal of Japan Society of Civil Engineers, Ser. A1 (Structural Engineering & Earthquake Engineering (SE/EE)), 2011. **67**(3): p. 583-596.

53. Committee, A., A.C. Institute, and I.O.f. Standardization. *Building code requirements for structural concrete (ACI 318-08) and commentary*. 2008. American Concrete Institute.

54. AASHTO, L., *AASHTO LRFD bridge design specifications.* Transportation (Amst). American Association of State Highway and Transportation Officials, Inc.: Washington, DC, 2007.

55. Standard, A., *C39, 2005,"Standard Test Method for Compressive Strength of Cylindrical Concrete Specimens," ASTM International, West Conshohocken, PA, 2005, DOI: 10.1520/C0039_C0039M-05E01*.

56. Standard, A., *C496 / C496-M-17, 2017,"Standard Test Method for Splitting Tensile Strength of Cylindrical Concrete Specimens," ASTM International, West Conshohocken, PA, 2017*.

57. Standard, A., *C293, 2016,"Standard Test Method for Flexural Strength of Concrete," ASTM International, West Conshohocken, PA, 2017.*

58. Standard, A., *E8M-04, 2005,"Standard Test Methods for Tension Testing of Metallic Materials [Metric] (Withdrawn 2008)," ASTM International, West Conshohocken, PA, 2008.*

59. Bossio, A., et al., *Modeling of concrete cracking due to corrosion process of reinforcement bars.* Cement and Concrete Research, 2015. **71**: p. 78-92.

60. Lubliner, J., et al., *A plastic-damage model for concrete.* International Journal of solids and structures, 1989. **25**(3): p. 299-326.

61. Lee, J. and G.L. Fenves, *Plastic-damage model for cyclic loading of concrete structures.* Journal of engineering mechanics, 1998. **124**(8): p. 892-900.

62. Birtel, V. and P. Mark. *Parameterised finite element modelling of RC beam shear failure*. in *ABAQUS users' conference*. 2006.

VITAE

Name	:	Nizar Abdul-Hamid Yousef Assi
Nationality	:	Palestinian
Date of Birth	:	11/Jan/1990
Email	:	nizar97eng@gmail.com
Address	:	Ramallah, Palestine, T.L: +970 59 848 2798
Academic Background	:	Civil Engineering

- Graduated from Birzeit University with B.Sc. degree in civil engineering in 2012 with **Distinction grade (86%)**, Department of Civil Engineering, West Bank, Palestine. (Received Honor Awards in most semester in BS program)

- Received a **scholarship** from Hani Qaddumi Scholarship Foundation (HQSF) in Palestine to study the BS degree at Birzeit University in 2008.

- Received a **scholarship** from King Fahd University of Petroleum and Minerals (KFUPM) in 2011 to study the MS & PhD degrees at KFUPM.

- MS (Civil Engineering - Structure) from King Fahd University of Petroleum and Minerals (KFUPM), May 2015, **GPA (3.94/4)**

- PhD (Civil Engineering - Structure) from King Fahd University of Petroleum and Minerals (KFUPM), December 2018, **GPA (3.97/4)**